The copyright of this thesis vests in the author. No quotation from it or information derived from it is to be published without full acknowledgement of the source. The thesis is to be used for private study or non-commercial research purposes only.

Published by the University of Cape Town (UCT) in terms of the non-exclusive license granted to UCT by the author.

University of Cape Town

A Molecular Basis for the C-Domain Selectivity of Angiotensin-Converting Enzyme

Wendy Lee Kröger

Thesis presented for the Degree of

Doctor of Philosophy

in the Division of Medical Biochemistry
University of Cape Town

February 2009

Supervisor: Professor E. D. Sturrock

Declaration

I, Wendy Kröger, declare that this thesis is my own, unaided work (except where acknowledgements indicate otherwise). Neither the whole work not part thereof has been, is being, or is to be submitted for any degree or examination at any other university.

I empower the University of Cape Town to reproduce for the purpose of research either the whole or any part of the contents of this thesis, in any manner whatsoever.

Signature of candidate:_____

Signed on the _____ day of _____, 2009.

Abstract

Angiotensin-Converting Enzyme (ACE) plays an essential role in blood pressure regulation and ACE inhibitors are widely used to treat cardiovascular disease. Two isoforms exist, somatic ACE (sACE) consisting of two homologous domains, N- and C-domain, and testis ACE (tACE), corresponding to the C-domain of sACE. Despite a high degree of sequence identity, these two domains display marked differences in substrate and inhibitor specificity. Furthermore, the C-domain of ACE has been implicated to play a dominant role in blood pressure control. It has therefore been suggested that development of ACE inhibitor treatments that selectively block the C-domain will result in decreased side-effects compared to current therapies. Analysis of three-dimensional structures of tACE in complex with domain-specific inhibitors has enabled the identification of key active-site residues potentially playing a role in domain selectivity. To investigate the contribution of such residues, a series of C-domain mutants was generated containing single and multiple N-domain active-site substitutions. These constructs were used to characterise specific interactions using domain-selective inhibitors and fluorogenic peptides. Mutants tested with the fluorogenic peptides displayed minimal, if any, acquisition of N-domain-like catalytic properties. Of the single mutations, S_2 (F391Y, tACE numbering) and S_1 (V518T) pocket substitutions caused the largest decreases in affinity for the C-selective phosphinic inhibitor RXPA380 (34-fold) and keto-ACE derivatives (14-26 fold), respectively. The V379S mutation caused an unexpected increase in affinity (2-10 fold) for C-selective inhibitors containing a P_2' Trp that could be explained by the formation of a water-mediated hydrogen bond interaction resulting from rearrangement of inhibitor and protein side-chains within the S_2' pocket. Multiple mutants containing an N-domain-like S_2' pocket combined with the S_2 F391Y substitution (S_2'F) caused the most notable shift in K_i from that of tACE for the highly selective phosphinic inhibitors, RXPA380 (K_i's tACE = 69 nM; S_2'F = 5300 nM) and N-specific RXP407 (K_i's tACE = 2800 nM; S_2'F K_i = 16.1 nM). This work identifies key residues contributing to the domain selectivity of ACE, and highlights the complex combination of effects involved in this phenomenon. Furthermore, it provides useful insight for the further design of domain-selective inhibitors.

Acknowledgements

I would like to express my sincere appreciation to:

My supervisor, Prof Edward D. Sturrock, for his significant ($p<0.001$) contribution to my PhD project and thesis, as well as my professional development as a scientist. I would particularly like to thank you for creating an environment that has given me the freedom to develop my critical and analytical skills, even when this has frustrated me intensely. I feel I have benefited tremendously from this opportunity, and have thoroughly enjoyed this experience.

Dr Trudi O'Neill for her contribution to this work. This has included technical assistance, advice and training, as well as preparation of the non-S_2' and multiple tACE mutant pcDNA constructs. Your friendship and guidance, both in and out of the lab, have been of great value to me.

Sylva Schwager for the HPLC purification of the lis-W enatiomers, general technical assistance, and sharing her expertise on protein expression and purification. I would also like to thank you for your wonderful friendship and moral support.

Prof Vincent Dive for his kind contribution of the phosphinic inhibitors RXPA380 and RXP407, as well as his helpful advice on the inhibitor studies.

Dr Aloysius Nchinda for his contribution to this work. This has included the synthesis and purification of keto-ACE and its derivatives and the lisinopril-Trp analogue, as well as providing the docked model of tACE-Abz-LFK(Dnp)-OH.

Prof Adriana K. Carmona for generously providing all of the fluorogenic peptides used in the kinetic studies, and her helpful advice during the assay optimisation.

Ross Douglas for kindly providing the N-domain S357V mutant construct.

Dr Aman Mahajan for synthesising the lisinopril analogue, Lis-W.

To Prof Edward Sturrock, Dr Jean Watermeyer, Dr Adele Thomas, Dr Trudi O'Neill, Sylva Schwager and Nailah Conrad for their endless proof-reading of this thesis, and their extremely helpful and insightful comments and suggestions.

My colleagues within the Metalloprotease Group (past and present), Dr Trudi O'Neill, Dr Pierre Redelinghuys, Ross Douglas, Nailah Conrad, Ayesha Parker, Tony Chang, Dr Jean Watermeyer, Dr Adele Thomas, Colin Anthony, Itai Chitapi, Christopher Yates, Tanya Paquet, Kerry Gordon, Riyad Domingo, Dr Aloysius Nchinda, Dr Dawn Webber, Kate Larmuth, Henry Kambafwile and Raymond Moholisa, for their helpful technical assistance, advice and ideas, friendship and moral support. It has been an absolute pleasure working with you!

My friends both in and outside of UCT. Thanks for your amazing friendship, endless support, and constant supply of red wine, mojitos, G & T's and margarita jugs! I would not have made it without you guys!

My new sister-in-law, Michi. Thanks for the dinners, runs, brownies, wine, Miko sitting, and everything else you have done for me in the past two years. I could not ask for a more amazing sister, and don't know how I got through life before you arrived.

To Miko, maybe the craziest, but definitely the sweetest and most amazing dog in the world!

My parents, Bridget and Brian, and brother Raymond. I am so blessed to have such an amazing family, and do not believe I would have succeeded in this journey without you. Your love, friendship, support, encouragement and financial assistance have been absolutely invaluable to me.

The South African National Research Foundation, the Stella and Paul Loewenstein Charitable and Educational Trust, the Ernst and Ethel Erikson Trust and the University of Cape Town for funding this work.

Abbreviations

Abz	*o*-aminobenzoic acid
ACE	angiotensin-converting enzyme
ACE2	angiotensin-converting enzyme 2
ACN	acetonitrile
Ang I	angiotensin I
Ang II	angiotensin II
Ang III	angiotensin III
Ang(1-7)	angiotensin(1-7)
AT_1	angiotensin II type I receptor
AT_2	angiotensin II type II receptor
AT_4	angiotensin type IV receptor
B_1	kinin type I receptor
B_2	kinin type II receptor
BK	bradykinin
cAMP	cyclic adenosine monophosphate
cGMP	cyclic guanosine monophosphate
CHO-K1	Chinese hamster ovary K1
$CONH_2$	amidated C-termini
CPA	carboxypeptidase A
CPD	carboxypeptidase D
dH_2O	de-ionised H_2O
DMEM	Dulbecco's modified eagle's medium
DMSO	dimethyl sulphoxide
DNA	deoxyribonucleic acid
Dnp	2,4-dinitrophenyl
E. coli	*Escherichia coli*
EDTA	ethylenediaminetetraacetic acid
FAPGG	furylacryloyl-Phe-Gly-Gly
FCS	fetal calf serum
FRET	fluorescence resonance energy transfer
GnRH	gonadotropin-releasing hormone

HEPES	N-2-hydroxyethylpiperazine-N'-2-ethanesulphonic Acid
HHL	hippuryl-His-Leu
HL	His-L-Leu-L
HPLC	high-performance liquid chromatography
kAW	(5S)-5-[(N-benzoyl)-amino]-4-oxo-6-phenyl-hexanoyl-L-tryptophan
kAF	(5S)-5-[(N-benzoyl)-amino]-4-oxo-6-phenyl-hexanoyl-L-phenylalanine
KKS	kallikrein-kinin system
LB	Luria-Bertani
lis-W	lisinopril derivative with a P_2' Trp substituent
LPH	lactase-phlorizin hydrolase
PAL	peptidyl-α-hydroyglycine α-amidating lyase
PAM	peptidylglycine α-amidating monooxygenase
PBS	phosphate-buffered saline
PCR	polymerase chain reaction
PDB	protein data bank (http://www.rcsb.org/pdb)
PDE	phosphodiesterase
pGlu	pyroglutamic acid
PHM	peptidylglycine α-hydroxylating monooxygenase
RAS	renin-angiotensin system
RE	restriction endonuclease site
RXPA380	C-domain-specific phosphinic inhibitor
RXP407	N-domain-specific phosphinic inhibitor
S_2' fragment	the *Sph*I-*Eco*RI fragment of the tACEΔ6NJ gene
sACE	somatic angiotensin-converting enzyme
SDS-PAGE	sodium dodecylsulphate polyacrylamide gel electrophoresis
SDKP	*N*-acetyl-Ser-Asp-Lys-Pro
SI	stoichiometry of inhibition
tACE	testis angiotensin-converting enzyme
TBE	Tris-borate/EDTA buffer
TFA	trifluoroacetic acid
TM	transmembrane region
T_m	primer melting temperature
Z-FHL	Z-Phe-His-Leu

Table of Contents

Abstract i

Acknowledgements ii

Abbreviations iv

Chapter 1: Review of the Literature 1

1.1 The renin-angiotensin and kallikrein-kinin systems 2

1.2 ACE - a zinc metallopeptidase 5

1.2.1 The structures of tACE and the N-domain 8

1.2.2 Mechanism of substrate hydrolysis 11

1.2.3 ACE substrates 12

1.2.4 ACE inhibitors 14

1.3 Comparison of ACE with other two domain homologues 17

1.4 Domain selectivity of ACE 21

1.4.1 Rationale for domain-selective ACE inhibitor therapies 21

1.4.2 The molecular basis for domain selectivity of ACE 23

1.4.2.1 The S2 pocket 25

1.4.2.2 The S1 pocket 25

1.4.2.3 The S1' pocket 26

1.4.2.4 The S2' pocket 26

Hypothesis 28

Aim and objectives of this study 28

Chapter 2: Cloning and Mutagenesis of tACE Constructs 29

2.1 Introduction 30

2.2 Experimental procedure 31

2.2.1 Chemicals 31

2.2.2 Cloning..... 31

2.2.2.1 Vector insert ligations..... 32

2.2.2.2 Transformation of E. coli competent cells..... 32

2.2.2.3 Mini-preparation plasmid DNA Isolation..... 33

2.2.3 Sub-cloning of S2' fragment into pGEM-11Zf(+)..... 33

2.2.4 Site-directed mutagenesis..... 34

2.2.4.1 Stop codon insertion into pcDNA-tACEΔ36NJ..... 35

2.2.4.2 Conversion of S2' tACE residues to corresponding N-domain residues 36

2.2.4.3 S2, S1 and S1' pocket mutants..... 36

2.3 Results and discussion..... 37

2.3.1 Sub-cloning..... 37

2.3.2 Site-directed mutagenesis..... 38

2.3.2.1 Stop codon insertion into pcDNA-tACEΔ36NJ..... 38

2.3.2.2 Construction of active-site mutants..... 39

2.4 Summary..... 44

Chapter 3: Protein Expression, Purification and Substrate Hydrolysis of tACE Mutant Proteins 45

3.1 Introduction..... 46

3.2 Experimental procedure..... 46

3.2.1 Chemicals..... 46

3.2.2 Expression of constructs..... 47

3.2.3 HHL and Z-FHL assays..... 47

3.2.4 Isolation and purification of tACE modified derivatives..... 48

3.2.5 Isolation and purification of N-domain derivatives of sACE..... 48

3.2.6 Fluorogenic peptide assay..... 49

3.2.7 Active enzyme concentration determination..... 50

3.3 Results and discussion....50

3.3.1 Protein expression and purification....50

3.3.2 Active enzyme concentration determination....52

3.3.3 Hydrolysis of FRET peptides....54

3.3.3.1 Hydrolysis of Abz-LFK(Dnp)-OH....54

3.3.3.2 Hydrolysis of Abz-SDK(Dnp)P-OH....59

3.4 Summary....61

Chapter 4: Kinetic Characterisation of tACE Proteins **62**

4.1 Introduction....63

4.2 Experimental procedures....65

4.2.1 Chemicals....65

4.2.2 Preparation of Abz-FRK(Dnp)P-OH....65

4.2.3 Preparation of inhibitors....65

4.2.4 Purification of lis-W isomers....66

4.2.4 Fluorogenic assay....66

4.2.5 Inhibition assay....66

4.3 Results and discussion....67

4.3.1 Hydrolysis of Abz-FRK(Dnp)P-OH....67

4.3.2 Domain selectivity of the phosphinic inhibitors....69

4.3.3 Domain selectivity of keto-ACE and its derivatives....70

4.3.4 Domain selectivity of lisinopril and lis-W....72

4.3.5 Roles of tACE active-site residues in the selectivity of C-domain-selective inhibitors....74

4.3.5.1 Roles of S2 residues....74

4.3.5.2 Roles of S1 residues....77

4.3.5.3 Roles of S1' residues in lisinopril and lis-W binding....78

4.3.5.4 Roles of S2' residues in binding of inhibitors containing a P2' Trp or Phe..... 80

4.3.5.5 Effect of a combined N-domain S2' pocket and F391Y mutation on RXPA380 binding..... 83

4.3.6 Roles of tACE active-site residues in binding of the N-domain-selective inhibitor RXP407..... 85

4.4. Summary..... 86

Conclusions **88**

Appendix I **93**

Cloning and Mutagenesis..... 93

Restriction enzyme digests..... 93

Agarose gel electrophoresis..... 93

Preparation of E. coli JM109 competent cells using RbCl..... 93

Coding sequence of 3' end of pcDNA-tACEΔ36NJ with new stop codon..... 94

Original primers used for T282S and V380T mutations..... 94

Appendix II **95**

Substrate kinetics..... 95

Preparation of synthetic substrates..... 95

5.7 mM HHL working solution..... 95

1 mM Z-FHL working solution..... 95

Standard curve for fluorogenic peptide..... 95

References **96**

List of Figures

Figure 1.1.	The renin-angiotensin and kallikrein-kinin systems	3
Figure 1.2.	Diagrammatic representation of the ACE gene and protein products	6
Figure 1.3.	Protein sequence alignment of sACE N- and C-domains, and tACE	7
Figure 1.4.	The 3 dimensional structures of the ACE domains	9
Figure 1.5.	Lisinopril bound to the active-site of ACE	11
Figure 1.6.	The proposed mechanism of thermolysin substrate hydrolysis	12
Figure 1.7.	Some physiological substrates of ACE	13
Figure 1.8.	Some well known ACE inhibitors	16
Figure 1.9	Structural alignment of the crystal structure of CPD domain II to the model of CPD domain I	19
Figure 1.10	Stick representation of the CPD inhibitor GEMSA complexed to the active-site of domain II of CPD	20
Figure 2.1	Schematic representation of the tACEΔ36NJ coding	30
Figure 2.2	Strategy used to sub-clone tACEΔ36NJ into the pcDNA3.1(+) expression vector	32
Figure 2.3	Strategy used to sub-clone the tACE S_2' fragment into pGEM-Zf(+)	34
Figure 2.4	Scheme representing the *Dpn*I site-directed mutagenesis approach	35
Figure 2.5	Primer design for insertion of a stop codon into pcDNA-tACEΔ36NJ	36
Figure 2.6	Primer design for site-directed mutagenesis of S_2' mutants	37
Figure 2.7	Sub-cloning of S_2' fragment into pGEM-11Zf(+)	38
Figure 2.8	Stop codon was inserted into the pcDNAtACEΔ36NJ construct downstream of the tACE gene	39

Figure 2.9	The S_2' residues of interest were converted from C-domain to corresponding N-domain residues by site-directed mutagenesis, using a *Dpn*I PCR method	41
Figure 2.10	Representative gel of a Mg titration in a PCR reaction	42
Figure 2.11	The S_2' residues of interest were converted from C-domain to corresponding N-domain residues by site-directed mutagenesis, using a *Dpn*I PCR method	42
Figure 3.1	Representative SDS-PAGE (10 %) indicating purity of a selection of tACE mutants	51
Figure 3.2	Plot of percentage activity versus the molar ratio of inhibitor to enzyme	53
Figure 3.3	SDS-PAGE displaying A) V518T and B) S516N mutants stored under different conditions for one month	54
Figure 3.4	Stick representation of Abz-LFK(Dnp)-OH docked into the tACE active-site	57
Figure 3.5	Additional residues that may play a role in the C-domain specificity of Abz-LFK(Dnp)-OH	58
Figure 4.1	The *S*- and *R*-enantiomers of lis-W	65
Figure 4.2	Representative Dixon plot	67
Figure 4.3	Log scale comparison of the relative binding affinities of tACE active-site mutants for RXPA380 with that of wild-type tACE	70
Figure 4.4	Log scale comparison of the relative binding affinities of tACE active-site mutants for kAW and kAF, with that of wild-type tACE	72
Figure 4.5	Comparison of the relative binding affinities of tACE active-site mutants for lisinopril and lis-W with that of wild-type tACE	74
Figure 4.6	Stick representation of inhibitors A) RXPA380 B) kAW and C) kAF within the tACE active-site, aligned with the N-domain	76
Figure 4.7	Sphere representation of RXPA380 and N-domain Y369, the tACE F391 counterpart	77
Figure 4.8	Sphere representation of kAW and N-domain T496	78

Figure 4.9 Stick representation of lisinopril and lis-W within the active-site of tACE, aligned with the N-domain 79

Figure 4.10 Stick representation of RXPA380 within the active-site of tACE 82

Figure 4.11 Stick representation of rolipril within the active-site of PDE4 aligned with PDE7A1 84

Figure 4.12 Log scale comparison of the relative binding affinities of tACE active-site mutants for the N-selective RXP407 with that of wild-type N-domain 86

Figure A1 Original primers used for T282S and V380T mutations 94

List of Tables

Table 1.1. Summary of active-site residues implicated in domain selectivity 24

Table 2.1 Summary of the mutants generated 40

Table 3.1 Summary of protein construct purification from CHO-K1 cells 52

Table 3.2 Kinetic constants for the cleavage of the C-domain-selective Abz-LFK(Dnp)-OH FRET peptide by ACE constructs 55

Table 3.3 Kinetic constants for the cleavage of the N-domain-selective Abz-SDK(Dnp)P-OH FRET peptide by ACE constructs 60

Table 4.1 Summary of kinetic constants for the cleavage of the Abz-FRK(Dnp)P-OH FRET peptide by ACE constructs 68

Table 4.2 Kinetic parameters for the inhibition of ACE activity by RXPA380 and RXP407 69

Table 4.3 Kinetic parameters for the inhibition of ACE activity by keto-ACE, kAW and kAF 71

Table 4.4 Kinetic parameters for the inhibition of ACE by lisinopril and lis-W 73

Chapter 1: Review of the Literature

1.1 The renin-angiotensin and kallikrein-kinin systems

The renin-angiotensin system (RAS) (figure 1.1) plays a critical role in the regulation of blood pressure, as well as fluid and electrolyte homeostasis (reviewed in Inagami, 1994; Fyhrquist and Saijonmaa, 2008). Hypotension, defined as low blood pressure, is a result of decreased sodium levels or effective plasma volumes, which stimulates renal release of renin (Goldblatt et al., 1934; Houssay. and Fasciolo, 1937; Page and Helmer, 1940). Renin releases the N-terminal peptide angiotensin I (Ang I) from the glycoprotein angiotensinogen, a prohormone secreted by the liver (figure 1.1) (Inagami, 1994). Ang I is in turn converted to the potent vasopressor angiotensin II (Ang II) by angiotensin-converting enzyme (ACE) (Skeggs et al., 1954; Skeggs et al., 1956). Ang II mediates a variety of functions through two receptors, angiotensin II type I (AT_1) and type II (AT_2) receptors (de Gasparo et al., 1995). AT_1 is responsible for actions such as vasoconstriction, aldosterone release, salt and water reabsorption, sympathetic activation and cell growth proliferation (Timmermans et al., 1992; Timmermans et al., 1993). The AT_2 receptor effects however, seem to offset those mediated by AT_1 and include vasodilation, inhibition of growth and proliferation, differentiation and apoptosis (Horiuchi, 1996; Csikós et al., 1998). This receptor is highly abundant in the developing foetus, however levels lessen rapidly after birth (Lazard et al., 1994; Shanmugam and Sandberg, 1996).

The complexity of the RAS is further demonstrated by several other biologically active angiotensin peptides (figure 1.1). Aminopeptidase A produces the metabolite angiotensin III (Ang III) from Ang II, which mediates similar functions to its precursor via the same receptors, discussed above (Wright and Harding, 1997; Ardaillou and Chansel, 1997). The angiotensin type IV (AT_4) receptor specifically binds the angiotensin III cleavage product, angiotensin IV (Swanson et al., 1992; Albiston et al., 2001), and has been associated with a number of actions such as neuronal development, renal and cerebral blood flow and memory gain and retention (Wright and Harding, 1997). Angiotensin(1-7), produced mainly by the action of the ACE homologue ACE2 on Ang II (Donoghue et al., 2000; Turner et al., 2002), displays interesting vasodilatory effects, particularly within an activated RAS (Nakamoto et

al., 1995; Iyer et al., 2000; Nakamura et al., 2003), and has been shown to mediate these through the G-protein-coupled receptor Mas (Santos et al., 2003).

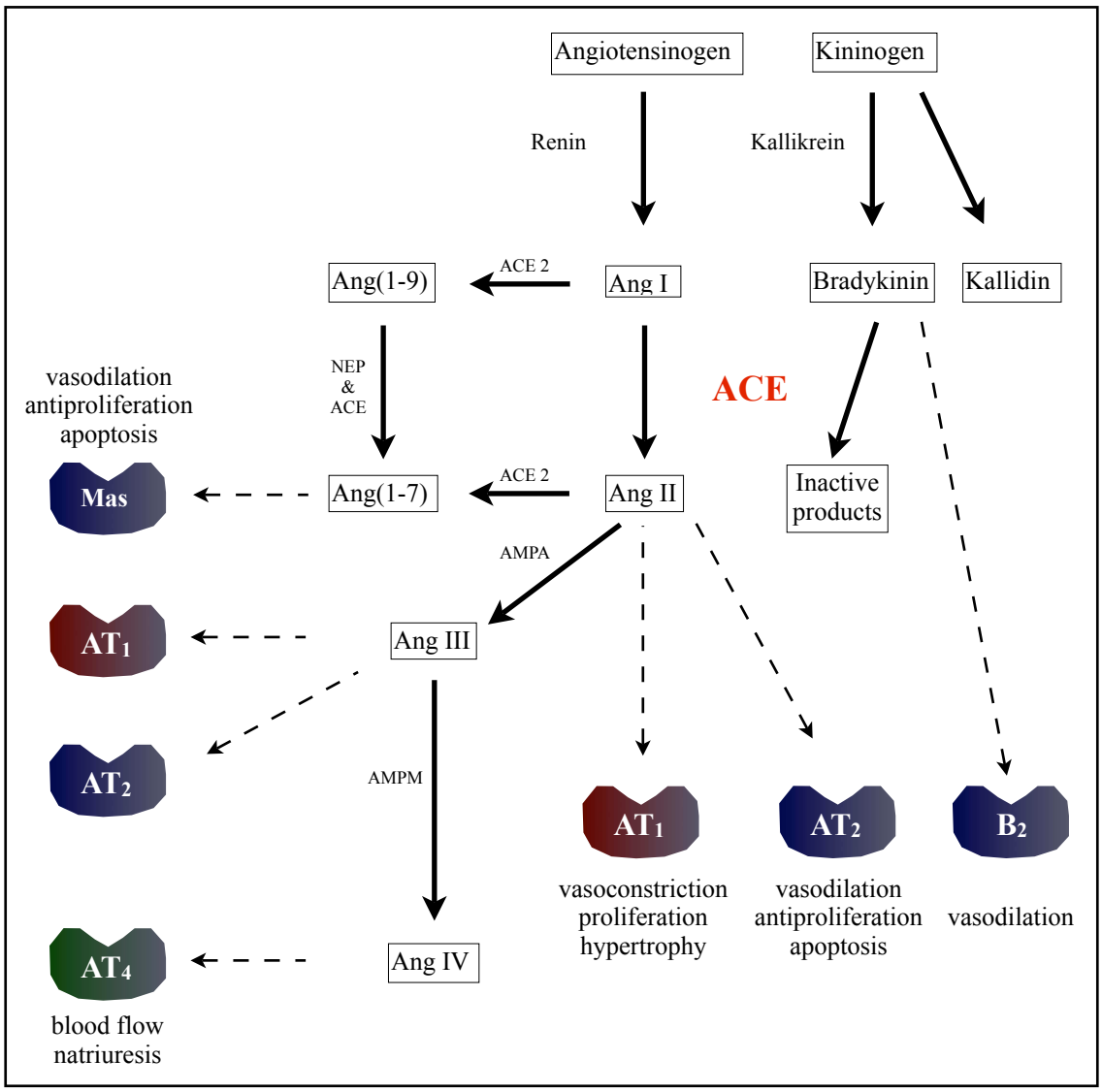

Figure 1.1. **The renin-angiotensin and kallikrein-kinin systems** (adapted from Acharya et al., 2003; Fyhrquist and Saijonmaa, 2008). Neutral endopeptidase (NEP); aminopeptidase A (AMPA); aminopeptidase M (AMPM); BK receptor (B_2). Solid lines indicate conversion of a peptide to a product, while broken arrows indicate action of a hormone on a receptor.

The kallikrein-kinin system (KKS) (figure 1.1) is chiefly a tissue-based system, which in some animals has been shown to play a role in a variety of functions including blood pressure regulation, sodium balance and inflammatory processes (Katori and Majima, 1996; Damas, 1996; Yang et al., 1997). In humans, plasma kallikrein produces the vasodilator bradykinin (BK) from the glycoprotein precursor, high molecular weight kininogen (reviewed in Bhoola et al., 1992). Tissue kallikrein is able to cleave this kininogen, as well as a second low

molecular weight kininogen, to form the product kallidin. These kinins mediate their actions mainly through the more dominant kinin type II (B_2) receptor, while products of kinin-carboxypeptidase activity (des-Arg^9-bradykinin and des-Arg^{10}-kallidin) have more potent effects on a second kinin type I (B_1) receptor induced during tissue damage (Regoli et al., 1989).

There is a unique interplay between these two systems, in which actions of the plasma KKS offset effects of the RAS (figure 1.1) (Schmaier, 2002). For example, plasma kallikreins have been shown to activate pro-renin (Sealey et al., 1979), and are able to produce Ang II directly from the angiotensinogen prohormone (Yamaguchi et al., 1991; Sasaguri et al., 1995). Furthermore, in addition to its role in Ang II production in the RAS as discussed above, ACE is responsible for the sequential degradation of the vasodilator BK at the Pro^7-Phe^8 and Phe^5-Ser^6 scissile bonds (Baudin, 2002), into inactive products (Erdos and Yang, 1967; Yang et al., 1970; Yang et al., 1971). Moreover, besides the effects of increasing and decreasing BK and Ang II levels, respectively, ACE inhibitors are also able to re-sensitise desensitised B_2 receptors to BK, via initiation of a process involving interaction between ACE and the receptor (Marcic and Erdös, 2000).

The critical role of the RAS has been clearly demonstrated by a variety of transgenic mouse models. Angiotensinogen (Kim et al., 1995), renin (Yanai et al., 2000), ACE (Krege et al., 1995; Esther et al., 1996) and AT_1 receptor (Ito et al., 1995; Chen et al., 1997; Tsuchida et al., 1998; Oliverio et al., 1998) knock-out mice all present with a significantly lowered blood pressure compared to wild-type animals. This blood pressure abnormality has been attributed to the absence of Ang II and not to BK accumulation, as evidenced by another mouse model lacking both the ACE and B_2 receptor genes, and displaying a similar hypotensive phenotype to that observed in the ACE knock-out model (Xiao et al., 2003). These studies clearly indicate that no other biological system is able to compensate for this Ang II deficiency, and highlights the fact that the RAS, particularly ACE, AT_1 receptors and renin, is an ideal target for the treatment of hypertension.

1.2 ACE - a zinc metallopeptidase

ACE (EC 3.4.15.1) is a dipeptidyl carboxypeptidase and a member of the gluzincin family (MA clan) of metalloproteases (Corvol and Williams, 1998). It is expressed as two isoforms, namely somatic ACE (sACE) and germinal or testis ACE (tACE) (Ehlers et al., 1989; Soubrier et al., 1988). Both are transcribed from a unique 21 kilobase ACE gene situated on chromosome 17q23, made up of 26 exons and under the control of two separate promoters (figure 1.2) (Howard et al., 1990; Hubert et al., 1991). The sACE promoter is 5' to the first exon, and the mRNA contains 25 of the exons, with the thirteenth exon spliced out. The germinal promoter is contained within intron 12, upstream to exon 13, and the tACE transcript contains exons 13 through to 26.

ACE is attached to the cell membrane via a transmembrane region, and contains both a small, C-terminal intracellular region, and a large N-terminal highly glycosylated extracellular region (figure 1.2) (Soubrier et al., 1988). The ectodomain of the 1277-residue sACE comprises two homologous domains, called the N- and C-domains. These two domains are believed to be a result of a gene duplication event, displaying an overall sequence identity of approximately 60 % (figure 1.3).

Each of these domains contains an active-site with the zinc binding motif HEMGH, and sequence identity increases to 89 % within this region. The somatic form is widely expressed in a variety of tissues including vascular endothelium, renal proximal tubule epithelium, intestinal epithelium and macrophages (Takada et al., 1984; Chai et al., 1987; Sibony et al., 1993). The testis ACE isoform plays a role in fertility (Hagaman et al., 1998), is expressed exclusively in male germinal cells (Langford et al., 1993) and consists of only one extracellular domain, which except for the unique 36-residue N-terminal region, is identical to that of the C-domain of sACE (figure 1.2). A soluble form of the sACE enzyme is present in plasma, and is a result of cleavage of the protein from the cell membrane, by an as yet unknown secretase (Ehlers et al., 1996; Woodman et al., 2000).

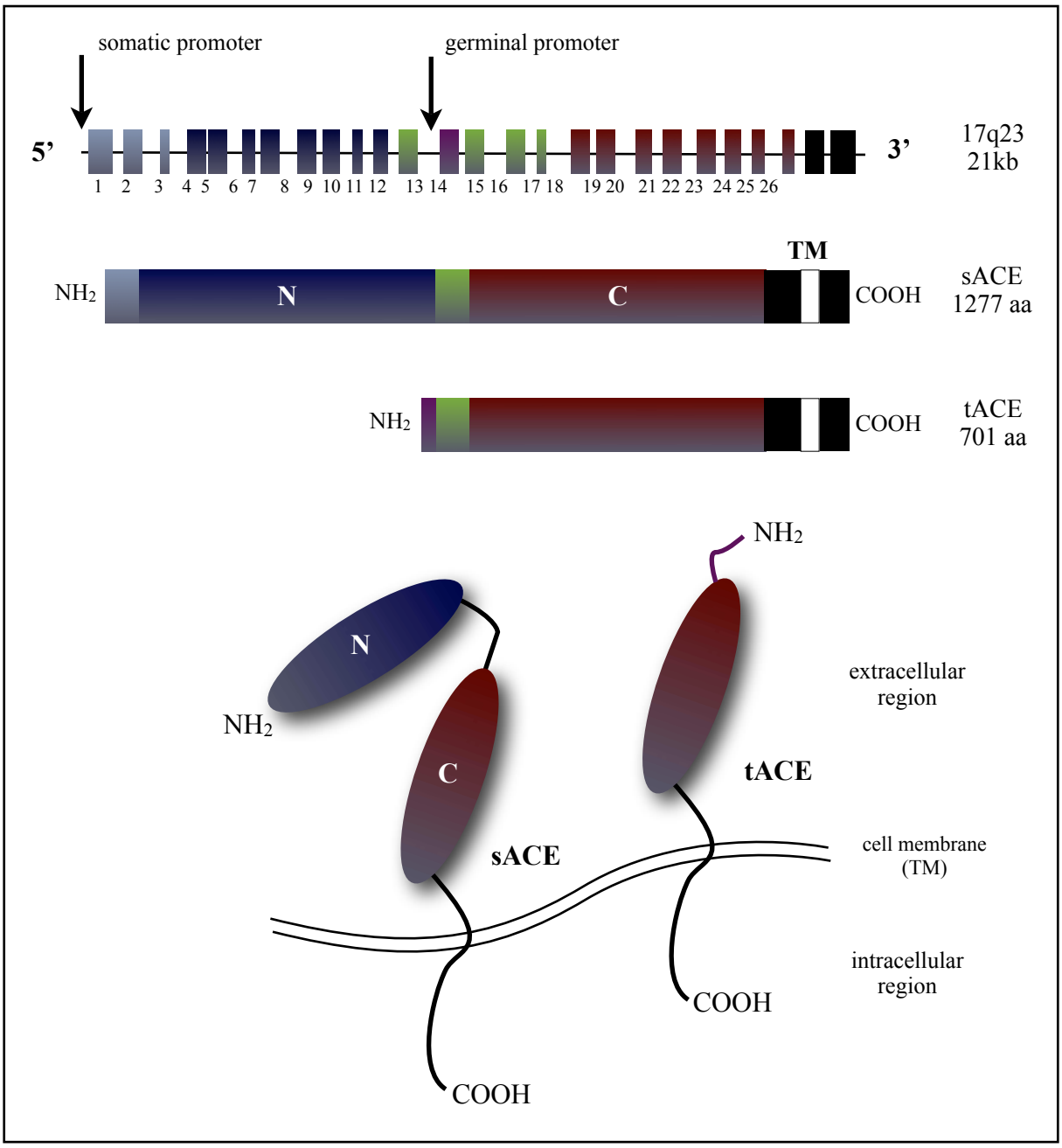

Figure 1.2. **Diagrammatic representation of the ACE gene and gene products.** The ACE gene, situated on chromosome 17q23, contains two separate promoters (somatic and germinal) giving rise to two different isoforms, sACE, containing an N-domain (blue) and C-domain (maroon) and tACE (identical to the C-domain, maroon). Transmembrane region (TM).

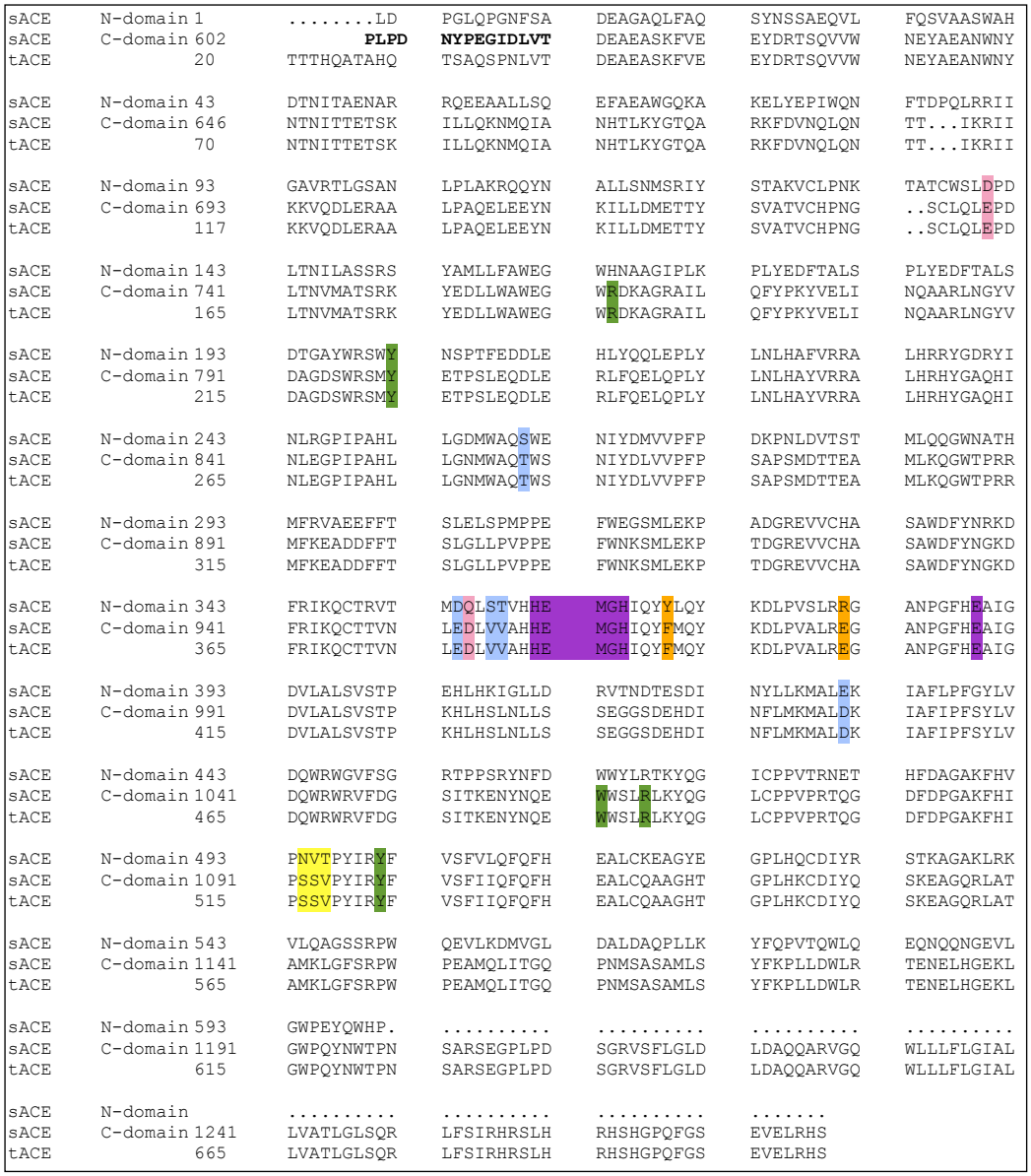

Figure 1.3. **Protein sequence alignment of sACE N- and C-domains, and tACE** (adapted from Acharya et al., 2003; Natesh et al., 2003; Corradi et al., 2006). Numbering and alignment according to that reported by Soubrier et al., (1988) and Ehlers et al., (1989). The zinc-binding ligands and HEMGH motif are highlighted in purple and the chloride binding residues in green. Active-site residues differing between domains are highlighted as follows: S_2 orange, S_1 yellow, S_1' pink, and S_2' in blue. Bold residues indicate the sACE linker region between the N- and C-domains.

Although the two catalytic domains of ACE display more than 60 % amino acid sequence identity (figure 1.3), they display some interesting differences. For example, the chloride requirement for the C-domain is much higher than that of the N-domain (Wei et al., 1991; Wei et al., 1992), while the latter has been shown to be more thermally stable (Voronov et al., 2002; O'Neill et al., 2008). Furthermore, a number of substrates have demonstrated C- or N-

domain selectivity, and several inhibitors have been reported to be able to discriminate between the two domains with high degrees of selectivity (discussed below).

1.2.1 The structures of tACE and the N-domain

Due to the lack of structural data for ACE, inhibitors were originally designed based on the structure of carboxypeptidase A (CPA), an enzyme displaying similar catalytic activity to ACE (Cushman et al., 1977). Interestingly however, resolution of the tACE-lisinopril complex in 2003 revealed that this enzyme shares little structural similarity to CPA, and in fact demonstrates a much higher resemblance to the core structures of neurolysin and *Pyrococcus furiosus* CPA, two enzymes with little sequence similarity to ACE (Natesh et al., 2003).

Testis ACE (protein data bank (PDB) code 1o86; figure 1.4a) is ellipsoid in shape, exhibiting dimensions of 72x57x48 angstroms (Å) (Natesh et al., 2003). It is made up of two sub-domains separated by an active-site cavity that extends approximately 30 Å into the protein, and contains a number of ordered water molecules. Three α helices, consisting of a number of charged amino acids, form an N-terminal lid region over the entrance to the active-site, limiting access to only smaller polypeptides. The overall structural architecture is mostly helical with 27 helices throughout the protein. The structure contains minimal beta structures. Six glycosylation sites occur on the surface of the enzyme, with a seventh site found within the transmembrane region.

The highly ordered catalytic zinc ion (figure 1.4), critical to catalysis, is bound to the active-site by four ligands: two histidines, H383 and H387 (tACE numbering; C-domain numbering 959 and 963) from the HEXXH zinc-binding motif on helix 13, E411 (C-domain 987) situated on helix 14, and an acetate ion provided by the crystallisation medium (Natesh et al., 2003).

The activity of tACE and the C-domain of sACE is highly dependent on the concentration of chloride ions. The tACE crystal structure revealed that two chloride ions are bound to tACE, chloride I and II, 20.7 and 10.4 Å from the zinc ion respectively (figure 1.4) (Natesh et al., 2003), both buried away from the active-site, 20.3 Å apart. Recent work by Rushworth *et al.* (Rushworth et al., 2008) has provided compelling evidence for the involvement of a number

of residues in the chloride sensitivity displayed by ACE. Mutation of the chloride I site chloride ion co-ordinating ligands, R186, R489 and W279, as well as the chloride II site chloride ligand R522, resulted in a marked decrease in the chloride dependence of tACE (Rushworth et al., 2008). Although the location of the chloride ions does not indicate direct interaction with the substrate, the main ligand co-ordinating chloride II, R522, is situated on the same helix as Y520 and Y523 (C-domain Tyr's 1096 and 1099), two residues involved in inhibitor (and probably substrate) interaction. It has been suggested that binding of a chloride ion to this site could facilitate movement of the Y523 into the active-site, and therefore binding at this site is believed to play a role in catalysis (Tzakos et al., 2003; Rushworth et al., 2008).

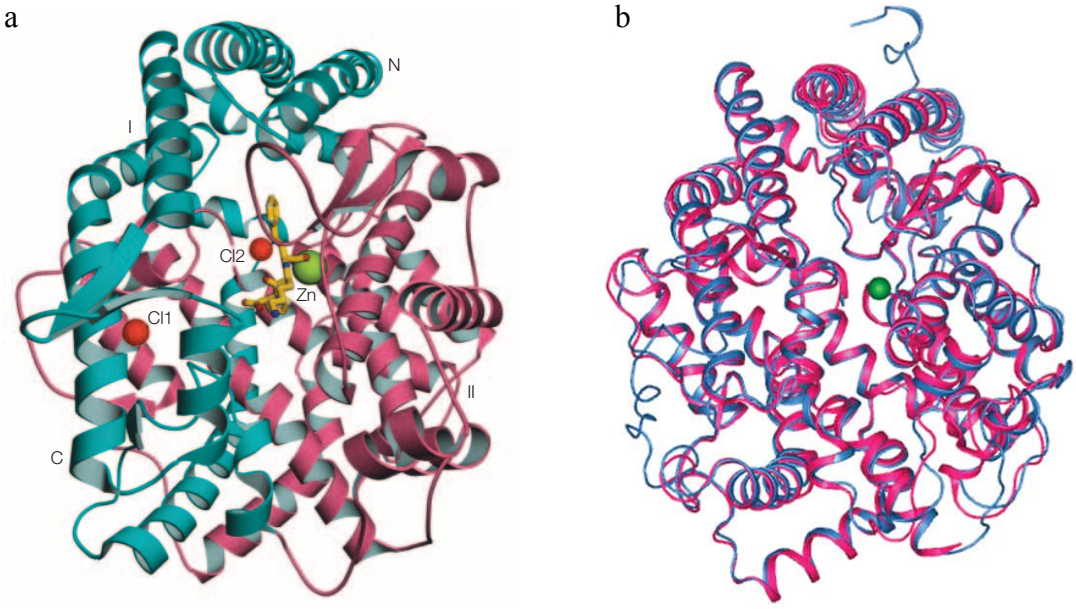

Figure 1.4. **Three-dimensional structures of the ACE domains.** a) The tACE-lisinopril complex (taken from Natesh et al., 2003). Each sub-domain is represented in cyan and pink, with the zinc and chloride ions highlighted in green and red, respectively. Lisinopril (yellow) is bound to the active-site of tACE. b) Alignment of the tACE (pink) and sACE N-domain (blue) 3-dimensional structures (taken from Corradi et al., 2006), with the zinc ion highlighted in green.

The crystal structure of the N-domain in complex with lisinopril was reported in 2006 (PDB code 2c6n; figure 1.4b) (Corradi et al., 2006). Although the overall structure of the N-domain is similar to that of the C-domain, a number of differences were observed. Ten glycosylation sites occur on the N-domain, of which only three are conserved between domains.

Interestingly, only one chloride ion was bound to this domain corresponding to the chloride II site of tACE, consistent with the lowered dependence on chloride concentration observed in N-domain catalysis. The site lacking a chloride ion, chloride I, contains a His residue replacing the corresponding Arg in tACE.

Lisinopril binds similarly to both active-sites (tACE and N-domain), in a highly ordered, extended conformation, with superimposition of the two complexes revealing conservation of inhibitor conformation as well as a number of conserved binding residue conformations (figure 1.5) (Natesh et al., 2003; Corradi et al., 2006). The binding of substrates and inhibitors to the catalytic site of ACE is commonly illustrated using the nomenclature model described by Schechter and Berger (Schechter and Berger, 1967). Residues on the N-terminal side of the scissile bond (or zinc-binding group) are allocated P_1-P_2-P_3-...-P_n, continuing outwards, while C-terminal residues are assigned P_1'-P_2'-P_3'-...-P_n'. The active-site to which the peptide or inhibitor binds is seen as a series of sub-site pockets into which the substrate or inhibitor residues or side-chains extend, and these pockets are designated with the corresponding S_n-...-S_2-S_1-S_1'-S_2'-...-S_n nomenclature.

We can therefore describe the ACE active-site to consist of four sub-sites, S_2, S_1, S_1' and S_2'. The P_1 phenylalanine of lisinopril extends into the S_1 pocket, interacting favourably with the tACE residue V518 (C-domain 1094), replaced by T496 in the N-domain. However, it has been suggested that the modest C-domain specificity observed for this inhibitor is due to the interaction of the P_1' lysine and the corresponding active-site pocket. The structure of the N-domain revealed a slightly different backbone conformation for this side-chain compared to that within the tACE complex. Furthermore, an electrostatic interaction between the lysyl amine and tACE E162 (C-domain 738) is lost in the N-domain, where the distance from the equivalent residue, D140, is 6.5 Å.

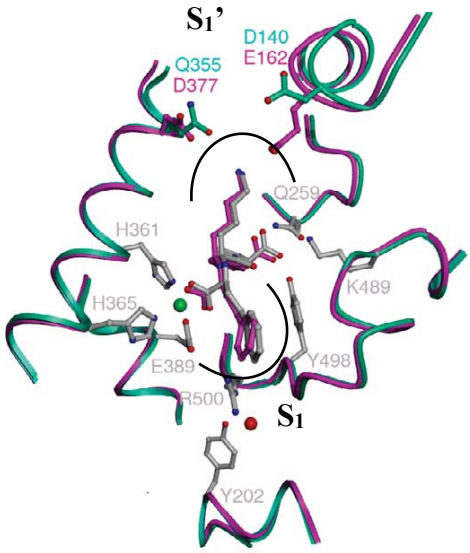

Figure 1.5. **Lisinopril bound to the active-site of ACE** (adapted from Corradi et al., 2006). Stick representation of lisinopril (grey / pink for N-domain and tACE, respectively) and binding residues within the active-site of the N-domain (cyan) and tACE (pink). Highlighted residues conserved between domains appear grey (tACE numbering). The zinc and chloride II site ions are highlighted in green and red, respectively.

1.2.2 Mechanism of substrate hydrolysis

The catalytic mechanism of substrate hydrolysis has not yet been established for ACE. However, it has been suggested that the mechanism is similar to that proposed for another member of the gluzincin family (MA clan), thermolysin (Matthews, 1988; Pelmenschikov et al., 2002).

Catalysis of thermolysin takes place via a general base-type mechanism (figure 1.6) (Matthews, 1988). It is believed that the incoming substrate displaces an active-site water molecule, bound to the zinc ion, towards a proximal glutamate residue, E143. This displacement sets up the water molecule for nucleophilic attack on the carbonyl carbon of the peptide, to produce a tetrahedral penta-co-ordinated carbonyl carbon intermediate. Subsequent breakdown of this intermediate occurs to yield the products.

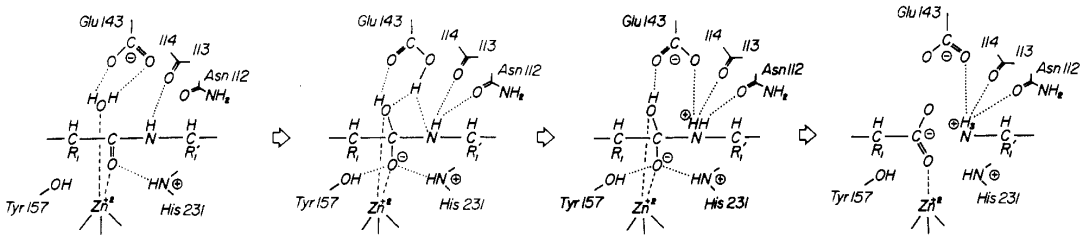

Figure 1.6. **The proposed mechanism of thermolysin substrate hydrolysis** (taken from Matthews, 1988).

A number of active-site residues crucial to ACE catalysis have been identified through site-directed mutagenesis and the resolution of the crystal structure. As mentioned above (section 1.2.1), the zinc-coordinating ligands comprise two His residues (383 and 387 in tACE) and E384 (tACE) (Wei et al., 1991; Williams et al., 1994). E384 (C-domain Glu 960) most likely corresponds to the E143 residue in thermolysin, while H513 (C-domain 1089) has been suggested to play a role in stabilising the transition state (Fernandez et al., 2001). Other tACE residues that have been implicated to play a role in stabilising the transition state are K511 and Y520 (C-domain 1087 and 1096, respectively) (Natesh et al., 2003).

1.2.3 ACE substrates

ACE is best known for its C-terminal dicarboxypeptidase activity, converting Ang I to Ang II and degrading BK (figure 1.7) (Skeggs et al., 1956; Erdos and Yang, 1967). However, the promiscuity of this enzyme has implicated it in a number of other physiological processes. Furthermore, this enzyme has been found to possess an endopeptidase-like activity on substrates containing amidated C-termini (Skidgel and Erdös, 1985). As mentioned in the preceding sections, the two domains display a number of differences, such as substrate selectivity (discussed below), chloride dependence (Wei et al., 1991; Wei et al., 1992) and thermostability (Voronov et al., 2002; O'Neill et al., 2008).

While the affinity of Ang I is roughly equal for both the C- and N-domains of ACE, hydrolysis of this substrate is performed more efficiently by the C-domain's active-site (Wei et al., 1991). BK is cleaved approximately 10 times more efficiently than Ang I, and cleavage is non-specific between the C- and N-domains (Jaspard et al., 1993). The C-domain is more dependent on chloride concentration than the N-domain (Wei et al., 1991), and this

phenomenon is further dependent on the type of substrate concerned. For example, Ang I cleavage is extremely chloride dependent, particularly for the C-domain, whereas the absolute chloride requirement for BK hydrolysis by either domain is significantly lower (Jaspard et al., 1993).

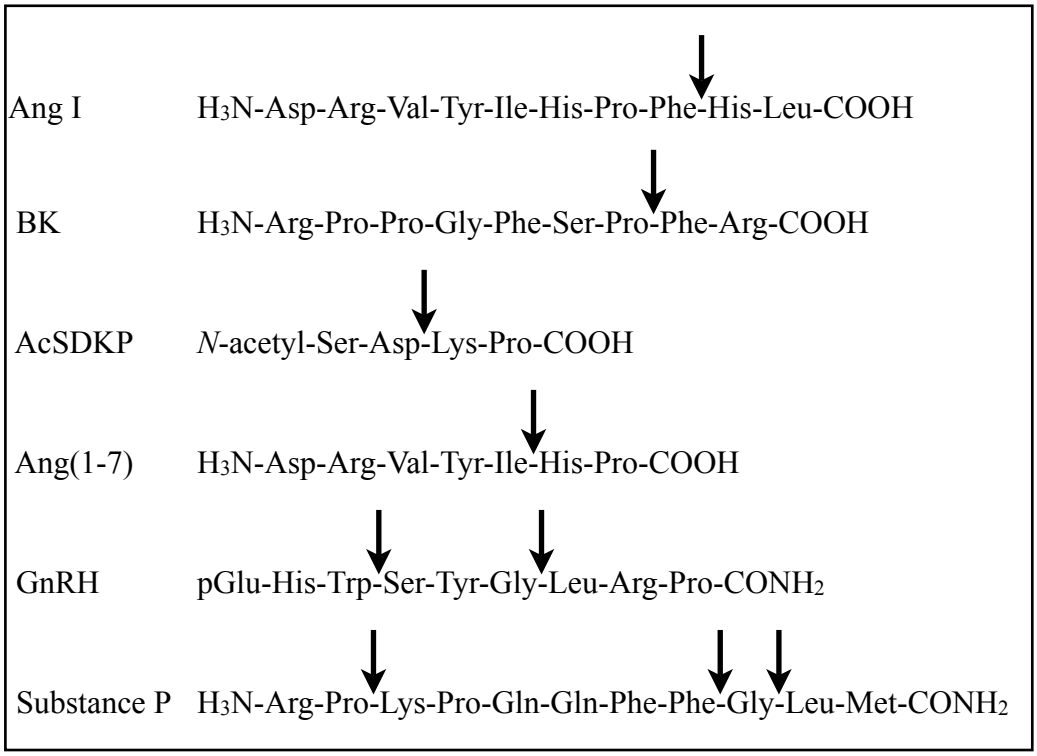

Figure 1.7. **Some physiological substrates of ACE.** The position of peptide bond cleavage is indicated with an arrow. Pyroglutamic acid (pGlu); amidated C-termini ($CONH_2$).

To date, a variety of peptide substrates have been described for this enzyme, some of which display interesting domain selectivity (figure 1.7). *N*-acetyl-Ser-Asp-Lys-Pro (AcSDKP), a negative regulator of hematopoiesis, has been shown to be preferentially cleaved by the N-domain of ACE, *in vitro* (Rousseau et al., 1995). *In vivo* inhibition of this domain of ACE using RXP407 demonstrated an approximately 6-fold increase in AcSDKP levels in mice (Junot et al., 2001). Other peptide substrates cleaved primarily by the N-domain include Ang(1-7) (Ehlers and Riordan, 1991; Deddish et al., 1994) and gonadotropin-releasing hormone (GnRH) (formally known as luteinizing-hormone releasing hormone) (Jaspard et al., 1993). The neuropeptide Substance P is preferentially cleaved by the C-domain of ACE, and this cleavage is dependent on the concentration of chloride (Jaspard et al., 1993). The physiological relevance of this hydrolysis is not yet clear, however both Substance P and ACE

have been shown to co-localise to certain areas of the brain (Defendini et al., 1983; Matsas et al., 1984; Strittmatter et al., 1984; Oblin et al., 1988; Barnes et al., 1988).

A number of synthetic peptide substrates have been designed for the enzymatic characterisation of ACE. The Ang I analogue hippuryl-His-Leu (HHL), is hydrolysed more efficiently by the C-domain of ACE to release HL and hippurate, and displays a similar chloride dependence to that of Ang I (Friedland and Silverstein, 1976). *Z*-Phe-His-Leu (*Z*-FHL), a second Ang I analogue, contains a Phe in the P_1 position which significantly decreases the selectivity of this peptide resulting in equivalent cleavage by both domains (Danilov et al., 1994; Michaud et al., 1997). Another peptide design resulted in furylacryloyl-Phe-Gly-Gly (FAPGG), cleavage of which by ACE yields the FAP tripeptide and GG dipeptide (Holmquist et al., 1979; Beneteau et al., 1986). Interestingly, hydrolysis of this substrate is chloride-dependent (Baudin, 2002).

Another class of peptide substrates commonly used are the fluorescence resonance energy transfer (FRET) peptides (Yaron et al., 1979). These internally quenched peptides contain a fluorescent donor group attached to the amino-terminal end, such as *o*-aminobenzoic acid (Abz), and a C-terminal quenching group (acceptor), such as 2,4-dinitrophenyl (Dnp) (Araujo et al., 1999). Hydrolysis within the FRET peptide separates the donor-acceptor pair, resulting in an increase in fluorescence from basal levels. A series of these peptides have been specifically designed for the analysis of ACE activity, and include the non-specific substrates Abz-FRK(Dnp)P-OH and Abz-YRK(Dnp)P-OH, the C-domain-specific Abz-LFK(Dnp)-OH and the N-domain-specific Abz-SDK(Dnp)P-OH (Araujo et al., 2000; Bersanetti et al., 2004).

1.2.4 ACE inhibitors

Due to the lack of any structural data for ACE, Cushman and Ondetti reasoned that the X-ray crystal structure of the distant homologue CPA should share a number of similarities with ACE (Skeggs et al., 1956; Cushman and Cheung, 1971; Das and Soffer, 1975). For example, both relied on a metal ion for their catalysis and displayed C-terminal exopeptidase-like activity, although ACE cleaved a dipeptide, while CPA only cleaved a single residue. Using the CPA structure (Steitz et al., 1967), they were able to develop a hypothetical prototype of the ACE active-site within which they could model potential inhibitors.

Another key step in this process was the observation that certain peptides potentiating the action of BK, derived from the venom of *Bothrops jararca*, a South American pit viper, were able to specifically block ACE activity (Ferreira et al., 1970). Further analysis revealed that the most potent peptides specifically inhibiting ACE comprised the C-terminal sequence Phe-Ala-Pro (Ondetti et al., 1971). The clinical use of these peptides was not however feasible as they lacked oral activity, and it was with the third key insight that led to a series of orally active ACE inhibitors.

A new and potent CPA inhibitor, benzylsuccinic acid, described as a by-product analogue (Byers and Wolfenden, 1973), presented a new design concept incorporating a strong active-site zinc co-ordinating group, as well as side-chain interactions analogous to those of the peptide product within the catalytic site. Cushman and Ondetti then synthesised the carboxy-Ala-Pro analogue, methylsuccinyl-Pro, which proved to be a specific ACE inhibitor but with low potency (Cushman et al., 1977). This potency was subsequently increased 1000-fold by substituting the carboxyl group with a superior zinc-binding sulphydryl group (Ondetti et al., 1977), producing captopril (figure 1.8), the first orally active ACE inhibitor approved for clinical use in the treatment of hypertension and heart failure.

Captopril did however display a number of side-effects such as loss of taste, dry cough and skin rash (McNeil et al., 1979), and this motivated further development of non-sulphydryl ACE inhibitors. Patchett *et al.* observed that captopril did not take advantage of interactions within the S_1 pocket, and lacked the hydrogen bond donor usually provided by the amide nitrogen in the scissile bond of a substrate (Patchett et al., 1980). They screened a library of *N*-carboxyalkyl dipeptides with the general formula R-$CHCO_2H$-X_1-X_2 and found that a benzylmethylene substituent in the P_1 position (R group), along with the dipeptides Ala-Pro or Lys-Pro (enalaprilat and lisinopril, respectively), yielded compounds that specifically inhibited ACE at nanomolar concentrations (figure 1.8) (Patchett et al., 1980).

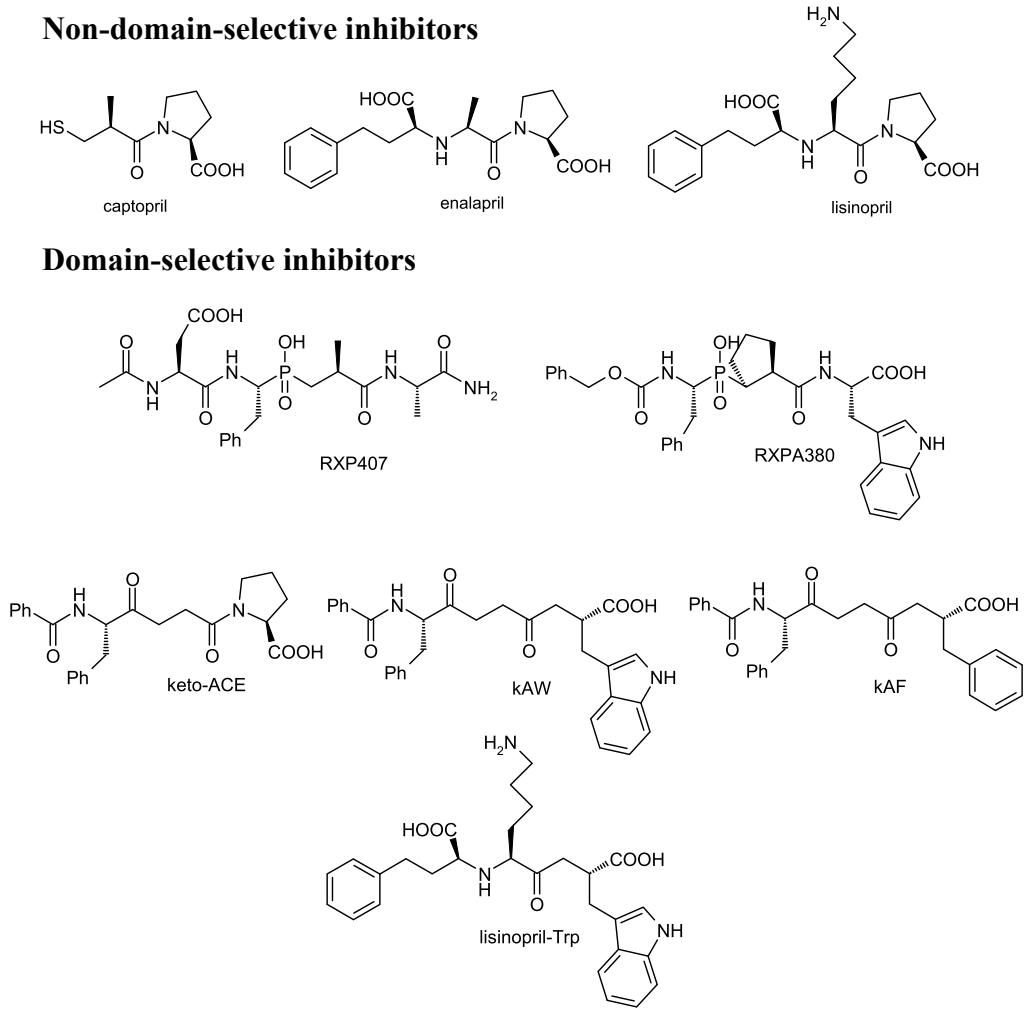

Figure 1.8. **Some well-known ACE inhibitors.**

Since the development of captopril, enalaprilat and lisinopril, a broad range of ACE inhibitors have been described, some of which are in clinical use today (Zaman et al., 2002). More recently, a number of inhibitors able to discriminate specifically between the two domains of ACE have been described. The phosphinic peptide inhibitors RXP407 and RXPA380 (figure 1.8) are able to selectively inhibit the N- and C-domains of ACE by three orders of magnitude, respectively (Dive et al., 1999; Georgiadis et al., 2003). Furthermore, the keto-ACE derivatives (figure 1.8) (5S)-5-[(N-benzoyl)-amino]-4-oxo-6-phenyl-hexanoyl-L-tryptophan (kAW) and (5S)-5-[(N-benzoyl)-amino]-4-oxo-6-phenyl-hexanoyl-L-phenylalanine (kAF) containing a Trp and a Phe in the P_2' position, respectively, both demonstrated C-domain selectivity (Redelinghuys et al., 2006). Moreover, lisinopril-Trp (lis-W) (figure 1.8), a lisinopril analogue containing a Trp in the P_2' position, was able to selectively inhibit the C-domain (Nchinda et al., 2006a).

1.3 Comparison of ACE with other two domain homologues

The occurrence of two homologous active-sites in one polypeptide chain is a rare phenomenon, thought to come about by gene duplication leading to the evolutionary development of new activities by modification and co-operativity (Bergdoll et al., 1998; Díaz-Mejía et al., 2007).

Two well-studied enzymes that also contain two catalytic sites on one polypeptide chain are sucrase-isomaltase (Hunziker et al., 1986) and lactase-phlorizin hydrolase (LPH) (Mantei et al., 1988), both involved in sugar metabolism on the brush-border membrane of the small intestine. The sucrase and isomaltase domains of sucrase-isomaltase are 40 % identical, with a further 41 % sequence similarity in non-identical amino acids. Each domain contains a conserved active-site aspartic acid residue, and like ACE, sequence similarity between domains increases substantially within the active-site. The precursor of this complex (prosucrase-isomaltase) is synthesised as a single polypeptide chain, and is cleaved extracellularly by pancreatic trypsin into two subunits, which remain strongly associated by non-covalent, ionic interactions. Jacob *et al.* (Jacob et al., 2002), have shown that the folding of the C-terminal sucrase domain is independent of the N-terminal isomaltase domain of the complex, and that the sucrase domain acts as an intramolecular chaperone for folding of the isomaltase subunit.

The precursor form of LPH comprises four 38 - 55 % homologous domains (I – IV, of which only regions III and IV, each containing a conserved catalytic glutamine, are present in the mature enzyme (Mantei et al., 1988). The lactase domain is responsible for the degradation of lactose, while the phlorizin hydrolase domain participates in the metabolism of β-glycoceramides, however the domain assignment of each of these activities to a particular region has been debated (Zecca et al., 1998). In 2000, Arribas *et al.* (Arribas et al., 2000) settled this issue using selective, mechanism-based inhibitors, assigning lactase activity to region IV, while phlorizin activity was allocated to region III. Although these homologous domains are similar, like ACE, they have demonstrated a number of differences such as temperature dependence (Schlegel-Haueter et al., 1972; Kraml et al., 1972; Colombo et al.,

1973; Skovbjerg et al., 1981). Interestingly, Beau *et al.* (Beau et al., 2007) have recently shown that rotaviruses, highly pathogenic agents with multiple mechanisms through which they induce diarrhoea, can affect the activity of LPH, and reported that a secreted rotaviral protein, NSP4, specifically inhibits the lactase activity of LPH.

Human carboxypeptidase D (CPD) has been reported to have a broad tissue distribution, with increased levels within the *trans* Golgi network and immature secretory vesicles (Song and Fricker, 1995; Song and Fricker, 1996; Tan et al., 1997). It contains three extracellular domains on a single polypeptide chain (Song and Fricker, 1995; Tan et al., 1997). The third domain (domain III) is catalytically inactive, and believed to be involved in binding proteins (Eng et al., 1998; Novikova et al., 1999). The first two catalytic domains cleave C-terminal residues presumably from the products of endopeptidases co-localised with CPD, such as furin (Seidah et al., 1992; Schäfer et al., 1993; Seidah et al., 1994; Zheng et al., 1994; Song and Fricker, 1996; Seidah et al., 1996). Although similar, these two domains have displayed some interesting, complementary differences (Novikova et al., 1999).

Of particular physiological interest, the pH optima and substrate selectivity of each is different (Novikova et al., 1999). The first domain (domain I) has an approximately neutral pH optimum of 6.3-7.5, consistent with being active in regions such as the Golgi and extracellular environment, while the second site (domain II) performs most efficiently in a slightly acidic medium (5.0-6.5), and is therefore probably the dominant domain in the *trans* Golgi network and immature and mature secretory vesicles (Johnson and Scarpa, 1976; Russell, 1984; Novikova et al., 1999). While both domains show a preference for an Ala residue in the penultimate position, the first and second domains respectively cleave C-terminal Lys or Arg amino acids more efficiently (Novikova et al., 1999).

A basis for the selectivity within these S_1 and S_1' pockets can be provided by crystallographic data reported for the second domain (Gomis-Rüth et al., 1999), as well as sequence and structural alignment of this domain to the first (figure 1.9) (Kuroki et al., 1995; Aloy et al., 2001). Residues surrounding the S_1 pocket are highly conserved between the two domains (Gomis-Rüth et al., 1999; Aloy et al., 2001). W748 dramatically reduces the size of this pocket thereby facilitating the preference for Ala residues in this position (figure 1.10). The

conserved D691 (D271 in domain I) provides the highly negative environment favouring the presence of positive residues in the C-terminal position of the substrate (figure 1.10). The higher selectivity for Lys and Arg by the first and second domains, respectively, is probably due to the larger space available within the S_1' pocket of the second domain. This larger space is a result of the respective substitution of Glu and Ile (335 and 351, respectively) in the first domain by the smaller residues P752 and V768 in the second domain (figure 1.10).

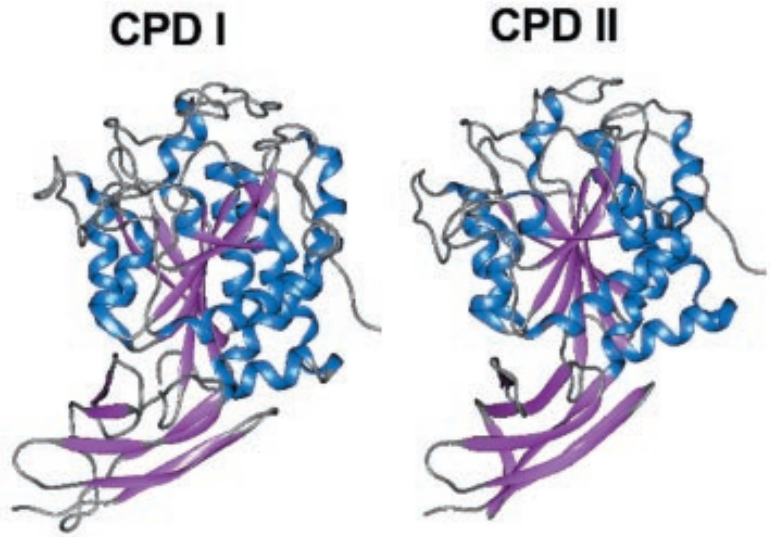

Figure 1.9. **Structural alignment of the crystal structure of CPD domain II (PDB code 1h8l) to the model of CPD domain I** (taken from Aloy et al., 2001).

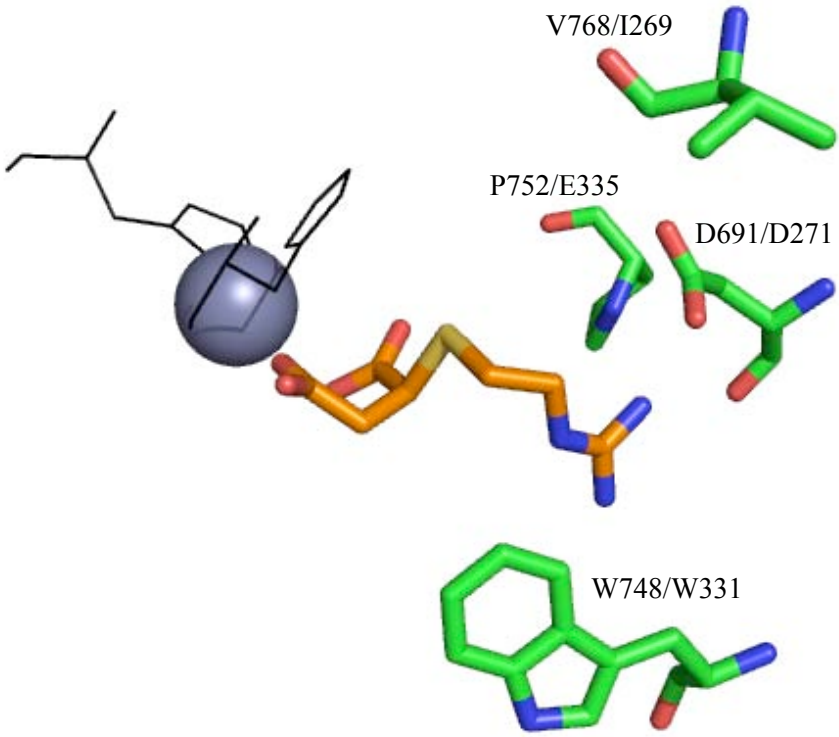

Figure 1.10. **Stick representation of the CPD inhibitor GEMSA (orange carbons) complexed to the active-site of domain II of CPD** (PDB code 1h8l) (Aloy et al., 2001). Residues of interest are indicated in green carbons, labelled as domain II / domain I. The active-site zinc ion is represented as a grey sphere and two zinc-chelating residues are shown as black lines (H573 and H680). This image were created in MacPyMOL version 0.99 (DeLano Scientific, Palo Alto, CA, USA).

A wide variety of neuroendocrine peptide products released by enzymes such as endopeptidases and carboxypeptidases, require further post-translational modification for full biological activity (Mains et al., 1990; Dickerson and Noel, 1991; Steiner, 1991; Jung and Scheller, 1991; Eipper et al., 1992). Sequential activity of the bifunctional peptidylglycine α-amidating monooxygenase (PAM), is responsible for α-amidation of a number of these bioactive peptides. The peptidyl-α-hydroxyglycine intermediate is produced from glycine-extended peptides, by the action of the first PAM domain, peptidylglycine α-hydroxylating monooxygenase (PHM), which requires the co-factors copper, molecular oxygen and ascorbate (Eipper et al., 1992). The second component of PAM, peptidyl-α-hydroyglycine α-amidating lyase (PAL), converts this intermediate into a peptide containing an α-amide, and a glyoxylate (Katopodis et al., 1990; Suzuki et al., 1990; Katopodis et al., 1991). Interestingly, PAM has a number of gene products, all transcribed from a single gene spanning approximately 160 kb of deoxyribonucleic acid (DNA) (Kato et al., 1990; Ouafik et al.,

1992). This large size is mostly due to four unusually long introns occurring within the PHM section of the gene.

In all of the homologous enzymes discussed above, a few active-site substitutions results in notably dissimilar functions, which are often interestingly complementary. In contrast with these examples, ACE exhibits a broad substrate selectivity, with each domain able to hydrolyse a wide range of substrates. However, as mentioned above, these domains have demonstrated a number of differences.

1.4 Domain selectivity of ACE

1.4.1 Rationale for domain-selective ACE inhibitor therapies

It is clear, as motivated above, that the RAS provides a number of excellent targets for anti-hypertensive therapy. Many agents are routinely used to interrupt this system at multiple stages. These include ACE (Waeber et al., 1982) and renin (Wood et al., 2003) inhibitors, and AT_1 (Ruilope et al., 2005) and aldosterone (Ménard, 2004) receptor blockers. Other therapeutic drugs commonly used for the treatment of this condition are beta blockers, calcium channel blockers, alpha blockers and diuretics (Cushman, 2003). All of these treatments, however, have high dosing, with a number of side-effects.

There is a wide range of clinical ACE inhibitor therapies currently used for the treatment of a number of cardiovascular related conditions, such as hypertension and heart failure (Bicket, 2002; Sleight, 2002). All of these agents demonstrate modest, if any, selectivity between the two domains of this enzyme (Menard and Patchett, 2001), and although they are generally well tolerated, they have been associated with a number of adverse side-effects, such as a persistent dry cough (5 - 20 % of cases) and the potentially fatal angioedema (0.1 - 0.5 % of cases) (Bicket, 2002; Adam et al., 2002; Dickstein et al., 2002; Morimoto et al., 2004). Both of these side-effects have been attributed to the resulting excess levels of BK caused by the non-selective inhibition of both domains with these therapies (Semple, 1995; Lalloo et al., 1996). It is important to mention that two non-domain-selective ACE inhibitors currently in

use for the treatment of cardiovascular conditions, Perindopril and Imidapril, have been shown to display significantly lowered side-effects, such as cough (Saruta et al., 1999; Huang et al., 2001; Tumanan-Mendoza et al., 2007). Therefore, the exact mechanism behind ACE inhibitor related side-effects is still not clear. However, a recent study comparing the effects of these inhibitors to two other commonly used ACE inhibitor therapies, Cilazapril and Enalapril, found that these lowered side-effects also resulted in a lowered control of hypertension over the latter treatments which demonstrated more efficient management of hypertension (Tumanan-Mendoza et al., 2007).

A number of studies investigating the role of each domain of ACE in Ang I and BK metabolism have been performed. The results of most of this work appear to indicate that while both domains contribute equally to BK degradation and soluble Ang I conversion, the C-domain seems to be primarily responsible for the systemic production of Ang II (Junot et al., 2001; Fuchs et al., 2004; van Esch et al., 2005; Fuchs et al., 2008). Support for this theory is provided by two studies involving the N- and C-domain-selective inhibitors RXP407 and RXPA380, respectively. While N-domain-selective inhibition by RXP407 decreased AcSDKP levels in mice by approximately 6-fold, it was unable to block the pressor action of Ang I injections, whereas lisinopril prevented the blood pressure increase observed in the absence of inhibitor (Junot et al., 2001). Further investigation by van Esch *et al.* involved analysis of Ang I metabolism in soluble versus membrane-bound ACE (van Esch et al., 2005). By examining the effect of RXPA380 and RXP407 on Ang I-induced contractions of porcine femoral arteries, they discovered that C-domain-selective inhibition was sufficient to block these contractions, while selective N-domain inhibition had no effect. The inhibition of both domains was however required to prevent Ang II production from Ang I added to diluted human plasma. Moreover, complete blockage of BK degradation was only achieved with the simultaneous inhibition of both domains of ACE (Georgiadis et al., 2003; van Esch et al., 2005).

A number of transgenic mouse models have been instrumental in gaining better insight into the physiological roles of ACE. Animals completely lacking both the somatic and germinal isoforms of this enzyme have presented with a number of phenotypes. Among these are hypotension, decreased male fertility, and structural and functional renal defects (Krege et al.,

1995; Esther et al., 1996; Tian et al., 1997; Cole et al., 2000). Later, more elegant studies involving mice containing a fully intact C-domain and inactivated N-domain (Fuchs et al., 2004), demonstrated that the presence of the C-domain restored blood pressure and normal renal development. Analysis of renin, Ang I and Ang II peptides confirmed equivalent levels to those of wild-type animals.

More recently, a similar mouse model was developed in which the sACE gene contains a catalytically active N-domain, but the C-domain and tACE isoforms were inactivated (Fuchs et al., 2008). These animals presented with normal blood pressure and Ang II peptide levels. However, further investigation revealed that this blood pressure restoration was due to a significant increase in renin and Ang I levels. The pressor response to Ang I infusion was half that of wild-type mice.

Taken together, these phosphinic inhibitor and transgenic mouse studies provide strong evidence that the C-domain alone is sufficient to maintain blood pressure and angiotensin metabolism, while the N-domain is much less efficient at Ang I cleavage. Furthermore, single domain inhibition does not block the degradation of BK. Therefore it is reasonable to propose that orally active C-domain-selective ACE inhibitors have the potential to effectively lower hypertension by blocking Ang II production, while displaying significantly lowered side-effects associated with current ACE inhibitor therapy, as the N-domain would be free to maintain BK levels (Georgiadis et al., 2003; Acharya et al., 2003).

1.4.2 The molecular basis for domain selectivity of ACE

With access to the crystal structures of both the C- and N-domains in complex with a variety of ACE inhibitors, a number of research groups have been able to dock different C- and N-domain-selective inhibitors within the active-sites of each domain. Together, this work has implicated a number of residues within these sub-site pockets of ACE which could play a role in conferring the domain selectivity of ACE (table 1.1, and see figures 3.4, 3.5, 4.6 and 4.9). There has, however, been no work reporting mutagenesis of these residues and their effects on binding and catalysis.

Table 1.1. **Summary of active-site residues implicated in domain selectivity.**

Pocket	tACE (C-domain) residue	N-domain residue	Crystal structure	References
S_2	Phe 391 (967)	Tyr 369	tACE-RXPA380 (PDB code 2oc2)	Acharya et al., 2003; Redelinghuys et al., 2005; Tzakos and Gerothanassis, 2005; Redelinghuys et al., 2006; Jullien et al., 2006; Corradi et al., 2006; Corradi et al., 2007.
	Glu 403 (979)	Arg 381	-	Acharya et al., 2003; Redelinghuys et al., 2005; Tzakos and Gerothanassis, 2005; Redelinghuys et al., 2006; Jullien et al., 2006; Corradi et al., 2006; Corradi et al., 2007.
S_1	Ser 516 (1092)	Asn 494	-	Bersanetti et al., 2004; Tzakos and Gerothanassis, 2005; Jullien et al., 2006.
	Ser 517 (1093)	Val 495	-	Jullien et al., 2006.
	Val 518 (1094)	Thr 496	tACE-lisinopril (PDB code 1o86) N-domain-lisinopril (PDB code 2c6n)	Acharya et al., 2003; Natesh et al., 2003; Natesh et al., 2004; Bersanetti et al., 2004; Redelinghuys et al., 2005; Tzakos and Gerothanassis, 2005; Jullien et al., 2006.
S_1'	Glu 162 (738)	Asp 140	tACE-lisinopril (PDB code 1o86) N-domain-lisinopril (PDB code 2c6n)	Natesh et al., 2003; Natesh et al., 2004; Bersanetti et al., 2004; Redelinghuys et al., 2005; Tzakos and Gerothanassis, 2005; Corradi et al., 2006.
	Asp 377 (953)	Gln 355	tACE-lisinopril (PDB code 1o86) N-domain-lisinopril (PDB code 2c6n)	Natesh et al., 2003Natesh et al., 2004; Bersanetti et al., 2004; Redelinghuys et al., 2005; Tzakos and Gerothanassis, 2005; Corradi et al., 2006.
S_2'	Thr 282 (858)	Ser 260	-	Georgiadis et al., 2004; Bersanetti et al., 2004; Tzakos and Gerothanassis, 2005.
	Glu 376 (952)	Asp 354	-	Georgiadis et al., 2004; Bersanetti et al., 2004; Tzakos and Gerothanassis, 2005.
	Val 379 (955)	Ser 357	tACE-RXPA380 (PDB code 2oc2)	Georgiadis et al., 2004; Bersanetti et al., 2004; Tzakos and Gerothanassis, 2005; Corradi et al., 2007.
	Val 380 (956)	Thr 358	tACE-RXPA380 (PDB code 2oc2)	Georgiadis et al., 2004; Bersanetti et al., 2004; Tzakos and Gerothanassis, 2005; Corradi et al., 2007.
	Asp 453 (1029)	Glu 431	tACE-RXPA380 (PDB code 2oc2)	Georgiadis et al., 2004; Bersanetti et al., 2004; Tzakos and Gerothanassis, 2005; Corradi et al., 2007.

1.4.2.1 The S_2 pocket

A number of structure-activity studies have indicated that N-selectivity seems to be enhanced with the presence of an acidic group in the P_2 position, as in the case of RXP407 (Dive et al., 1999), while substitution of this moiety with a large uncharged or basic side-chain seems to favour the C-domain S_2 sub-site (Acharya et al., 2003). Both F391 and E403 (tACE numbering), replaced by Tyr and Arg in the N-domain (table 1.1), have been identified as residues that may play a role in domain selectivity of some inhibitors (Redelinghuys et al., 2005; Tzakos and Gerothanassis, 2005; Redelinghuys et al., 2006; Jullien et al., 2006; Corradi et al., 2007).

The crystal structure of tACE in complex with RXPA380 revealed that the P_2 Phe forms a favourable aromatic interaction with F391 (Corradi et al., 2007). Initial docking experiments of the C-selective inhibitor keto-ACE, as well as its analogue kAW, into the C-domain active-site indicated possible stacking interactions between the P_2 Phe and F391 (Redelinghuys et al., 2005; Tzakos and Gerothanassis, 2005; Redelinghuys et al., 2006). These interactions would not only be lost in the N-domain with the replacement of this residue with Y369, but steric hindrance, as is indicated by superimposition of the N-domain structure onto the tACE-RXPA380 complex, would probably result in a different orientation of the inhibitor within the active-site (Corradi et al., 2007). Therefore, this aromatic interaction is believed to be a major factor in facilitating C-domain selectivity of the inhibitors RXPA380, keto-ACE and kAW.

Furthermore, the positively charged P_2 aspartate of RXP407 has been suggested to significantly contribute towards its N-selectivity (Dive et al., 1999; Jullien et al., 2006). Docked models of this inhibitor within the N-domain suggest hydrogen bond interactions between this group and Y369 as well as R381, interactions that would not only be lost in the C-domain when replaced with Phe and Glu, respectively, but could possibly develop repulsive forces in the latter case (table 1.1) (Tzakos and Gerothanassis, 2005; Jullien et al., 2006; Corradi et al., 2006).

1.4.2.2 The S_1 pocket

The three substitutions that occur within the S_1 pocket of ACE are S516/N494, S517/V495 and V518/T496 of tACE / N-domain, respectively (Bersanetti et al., 2004; Tzakos and

Gerothanassis, 2005; Jullien et al., 2006). The bulky P_1 pseudo-Phe of keto-ACE is another moiety that has been implicated to contribute to the modest C-selectivity of this inhibitor (Acharya et al., 2003; Redelinghuys et al., 2005); however, Tzakos *et al.* suggested that the 40-fold preference of perindoprilat for the C-domain is probably partly due to favourable non-polar interactions occurring between V518 and the P_1 alkyl chain (Tzakos and Gerothanassis, 2005). Moreover, modelling of the C-domain-specific fluorogenic peptide, Abz-LFK(Dnp)-OH into the tACE active-site indicated hydrophobic interactions between the P_1 Leu and the V518 and S516 residues at distances of 2.3 and 5.0 Å, respectively (Bersanetti et al., 2004). Replacement of this Val residue by T496 in the N-domain would decrease the hydrophobicity of this pocket, and therefore V518 is believed to play a significant role in the selectivity of these inhibitors and substrates.

1.4.2.3 The S_1' pocket

The tACE-lisinopril complex revealed a deep S_1' sub-site able to accommodate large, polar P_1' moieties (Natesh et al., 2003; Natesh et al., 2004). The lysyl substituent of the modestly C-selective lisinopril has been shown to form hydrogen bond interactions with E162 and favourable water-mediated interactions with D377. These electrostatic interactions are significantly lowered in the N-domain due to increased distances caused by replacement with D140 and Q355, respectively (Corradi et al., 2006).

The marked C-domain selectivity of Abz-LFK(Dnp)-OH has been attributed to interaction of the P_1' Phe with these two S_1' residues, E162 and D377 (Bersanetti et al., 2004). Furthermore, Bersanetti *et al.* suggested that hydrophobic interaction of V380 , which they defined as an S_1' pocket residue, with this P_1 Phe moiety facilitates favourable binding to the C-domain.

1.4.2.4 The S_2' pocket

This pocket is a large sub-site in both the N- and C-domains of ACE, able to tolerate a variety of inhibitor moieties. The P_2' Trp of RXPA380 has been implicated to play a role in the C-selectivity of this inhibitor (Georgiadis et al., 2004). Interestingly, substitution of this position with a Trp or Phe side-chain in the ketomethylene derivatives kAW and kAF, respectively resulted in an increase in C-domain selectivity over that of keto-ACE (Redelinghuys et al.,

2006). A number of differences between domains have been identified within this sub-site, namely T282/S260, E376/D354, V379/S357, V380/T358 (V380 is defined as an S_1' pocket residue by some groups (Bersanetti et al., 2004; Tzakos and Gerothanassis, 2005)), and D453/ E431 in tACE / N-domain (table 1.1) (Georgiadis et al., 2004).

Most notable of these was the replacement of two hydrophobic Val residues with the N-domain polar residues Ser and Thr, respectively. The tACE-RXPA380 crystal structure revealed that the distance between the P_2' Trp and the C-domain valines is approximately 4.5 Å, and the hydrophobicity of this pocket would entropically exclude hydrophilic groups which would be more readily accommodated in the N-domain S_2' pocket (Georgiadis et al., 2004; Corradi et al., 2007). N-selectivity of RXP407 seems to be attributed mainly to the P_2' amidated C-terminus (Dive et al., 1999), which suggests binding of this inhibitor in an extended conformation, allowing interaction of this side-chain with the acidic residues at the opposite side of the pocket (Corradi et al., 2006).

Tzakos *et al.* suggested that the presence of the larger E431 and S260 side-chains in the N-domain (replaced by Asp and Thr in the C-domain, respectively), may result in a reduction in the size of the N-domain pocket compared to that of the C-domain (tACE) (Tzakos and Gerothanassis, 2005). Furthermore, the distance between the RXPA380 Trp and D453 was shown to be more than 5.5 Å, which precludes the formation of a hydrogen bond interaction (Georgiadis et al., 2004; Corradi et al., 2007). Moreover, the favourable interactions between T282 and D453 and the dinitrophenyl group attached to the P_2' Phe of Abz-LFK(Dnp)-OH are also believed to contribute to the C-selectivity of this fluorogenic peptide (Bersanetti et al., 2004). It has therefore been suggested that a substituent extending toward the D453 residue, and exploiting this pocket more efficiently, may facilitate increased C-domain selectivity (Corradi et al., 2007).

Hypothesis

Particular residues within the active-site of the ACE protein confer C-domain specificity.

Aim and objectives of this study

A number of inhibitors able to discriminate between domains with a high degree of selectivity have been described to date, including the phosphinic peptide inhibitors RXPA380 and RXP407 (Dive et al., 1999; Georgiadis et al., 2003), the keto-ACE derivatives kAW and kAF (Redelinghuys et al., 2006), and the lisinopril-Trp derivative, lis-W (Nchinda et al., 2006a). Although similar, the N- and C-domains of ACE have demonstrated a number of differences with respect to their structure, and their substrate and inhibitor specificities. The aim of this study was therefore to probe the contribution of particular residues within the different sub-sites towards the domain specificity of these inhibitors. The information gained from this work should pave the way to a better understanding of the active-site determinants of domain specificity.

The following objectives have been identified:

1. Construction of tACE mutants containing corresponding N-domain residues of interest.
2. Expression and purification of mutant constructs.
3. Kinetic characterisation of active constructs using domain-specific fluorogenic peptides, and domain-selective inhibitors.

Chapter 2: Cloning and Mutagenesis of tACE Constructs

2.1 Introduction

To investigate the importance of particular active-site side-chains in ACE C-domain specificity, a series of tACE mutants were generated with selected amino acids converted to their N-domain counterparts by site-directed mutagenesis. A number of residues were selected based on various observations of crystal structures and models of ACE in complex with different domain-specific ACE substrates and inhibitors, implicating particular residues in conferring this selectivity.

The objectives of the present work were therefore to:

1. To sub-clone the tACEΔ36NJ coding region, truncated between S625 and A626, and lacking the 36 N-terminal *O*-glycosylated region (making it identical to the C domain of sACE)(figure 2.1) (Yu et al., 1997), into the expression vector pcDNA3.1(+).
2. To engineer a stop codon downstream of tACEΔ36NJ, following the *Eco*RI site, to ensure proper termination of translation.
3. To sub-clone an appropriate fragment of the tACE coding region into the pGEM11Zf(+) shuttle vector to facilitate mutagenesis.
4. To generate a panel of mutants within the pGEM - fragment shuttle construct converting particular amino acids within the active-site to their corresponding N-domain residues.
5. To reintroduce these mutated fragments into the pcDNA-tACEΔ36NJ expression vector containing the stop codon, for transfection into mammalian cells.

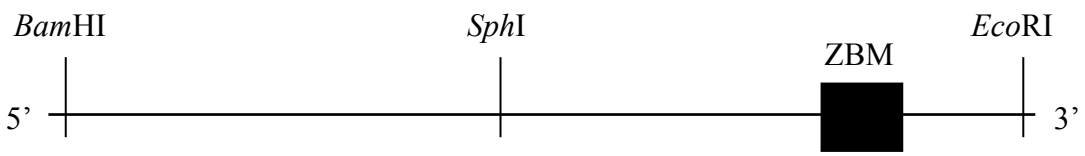

Figure 2.1. **Schematic representation of the tACEΔ36NJ coding.** The region encoding the zinc-binding motif is highlighted in black.

2.2 Experimental procedure

2.2.1 Chemicals

Restriction endonucleases *Eco*RI, *Bgl*II, *Hind*III, *Nhe*I, *Sph*I, *Bam*HI, *Xho*I and restriction endonuclease buffers were acquired from Roche. JM109 cells, λ DNA, *Hpa*I and restriction buffer, *Pfu* polymerase, polymerase buffer, polymerase chain reaction (PCR) nucleotide mix, $MgCl_2$, *Dpn*I, pGEM-11Zf(+) and the Wizard SV Gel System were all purchased from Promega. Fermentas supplied *Nsb*I (*Fsp*I), *Xma*JI, *Ssp*I and restriction buffers, while New England Biolabs supplied *Bsa*AI and *Bbv*CI with buffers. T4 ligase and ligation buffer were obtained from USB, and pcDNA3.1(+) from Invitrogen. The midi-prep plasmid purification kit was purchased from QIAGEN. Inqaba Biotech, South Africa performed nucleotide sequencing and synthesised all primers.

2.2.2 Cloning

pSFV4.2-tACEΔ36NJ (obtained from E. D. Sturrock) and pcDNA3.1(+) were each digested with *Bam*HI and *Eco*RI (described in Appendix I), and separated by agarose gel electrophoresis (Appendix I). The bands of interest were excised from the gel, and purified using the Promega Wizard® SV Gel and Clean-Up System as per manufacturer's instructions. The tACEΔ36NJ gene fragment and the digested pcDNA3.1(+) vector were ligated (section 2.2.2.1), and transformed into competent *Escherichia coli* (*E. coli*) JM109 cells (Appendix I). Ampicillin was used to facilitate selection of plasmid-containing colonies, and DNA was extracted (section 2.2.2.3). Restriction endonucleases *Bgl*II and *Nhe*I were utilised to screen for the desired construct, pcDNA-tACE36NJ (figure 2.2), and fragments were visualised on agarose gels (Appendix I). A stock solution of the plasmid construct was obtained using a QIAGEN midiprep kit in accordance with the manufacturer's instructions (methods adapted from Ausubel et al., 1992).

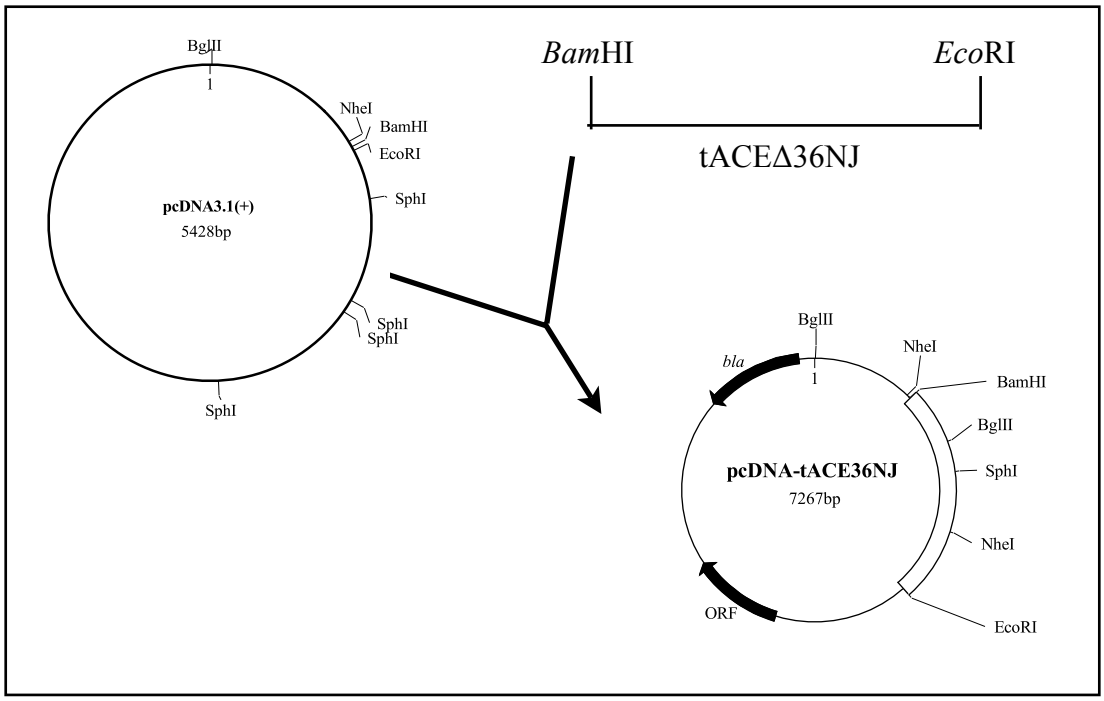

Figure 2.2. **Strategy used to sub-clone tACEΔ36NJ into the pcDNA3.1(+) expression vector**, using restriction endonucleases *Bam*HI and *Eco*RI.

2.2.2.1 Vector insert ligations

One μL of each digested, purified fragment was visualised on an agarose gel with DNA of known concentration to determine the insert and vector concentrations. Ligation reaction mixtures (2 μL 10 x ligation buffer, 1 unit T4 ligase, appropriate DNA concentrations at a molar ratio of 3:1 vector to insert DNA, made up to 20 μL total volume with sterile de-ionised H_2O (dH_2O)) were incubated at room temperature overnight, and 10 μL was transformed into competent *E. coli* JM109 cells. In the case of three part ligations, a DNA molar ratio of 3:1:1 vector to insert to insert was used (method adapted from Ausubel et al., 1992).

2.2.2.2 Transformation of E. coli competent cells

Ten μL of ligation reaction mixture or PCR reaction mixture, was added to 200 μL of competent *E. coli* JM109 cells and incubated on ice for 1 hour. DNA uptake was facilitated by heat shock at 42^{o}C for 40 sec, followed by 2 min incubation on ice. Nine hundred μL of LB medium was added to the cells, and the culture was shaken at 37^{o}C for 1 hour to allow expression of the ampicillin gene. Cells were centrifuged for 2 min, resuspended in 50 μL LB

broth, plated out on LB agar (15 $g.L^{-1}$) plates containing 100 $\mu g.mL^{-1}$ ampicillin and incubated at 37°C overnight (method adapted from Ausubel et al., 1992).

2.2.2.3 Mini-preparation plasmid DNA Isolation

This method was adapted from that in Sambrook and Russel (2001). Transformed colonies were grown overnight shaking in 5 mL LB medium containing 100 $\mu g.mL^{-1}$ ampicillin. One mL of the culture was harvested by centrifugation for 2 min, and the pellet was resuspended in 250 μL STET buffer (233 mM sucrose, 50 $mg.mL^{-1}$ triton X-100, 50 mM ethylenediaminetetraacetic acid (EDTA), 50 mM Tris-HCl, pH 8.0), containing 1 $mg.mL^{-1}$ lysozyme. Cells were boiled for 1 min and centrifuged for 8 min. The pellet was removed using a toothpick, and 250 μL of isopropanol was added to the supernatant, and centrifuged for 8 min. The supernatant was discarded, and the pellet dried in a vacuum dryer, followed by resuspension in 20 μL 1/10 Tris-EDTA buffer (1 mM Tris-HCl, 0.1 mM EDTA, pH 8.0). To facilitate resuspension, DNA was heated at 60°C, and centrifuged for 2 min. One-2 μL of mini-preparation DNA was used in restriction digests.

2.2.3 Sub-cloning of S_2' fragment into pGEM-11Zf(+)

A smaller fragment of tACE containing all of the residues of interest was sub-cloned into pGEM-11Zf(+) (method adapted from Ausubel et al., 1992). The restriction endonucleases utilised were *Eco*RI and *Sph*I, producing a 1839 bp fragment containing all of the sites to be mutated.

An *Sph*I site occurs more than once in the pcDNA3.1(+) vector, therefore pcDNA-tACEΔ36NJ was first digested with *Bam*HI and *Eco*RI and the vector and insert were separated using agarose gel electrophoresis and purified (described above). The insert was subsequently digested with *Sph*I, and pGEM-11Zf(+) with *Eco*RI and *Sph*I. Fragments were separated on agarose gels, excised and purified. The *Sph*I-*Eco*RI tACE fragment (which will be referred to as the S_2' fragment hereafter) and pGEM vector were ligated and transformed into *E. coli* (described above). Selection and screening was done as described above, using a double restriction endonuclease digest with *Nhe*I and *Hind*III, releasing a 515 bp band, to identify the pGEM-S_2' construct (figure 2.3).

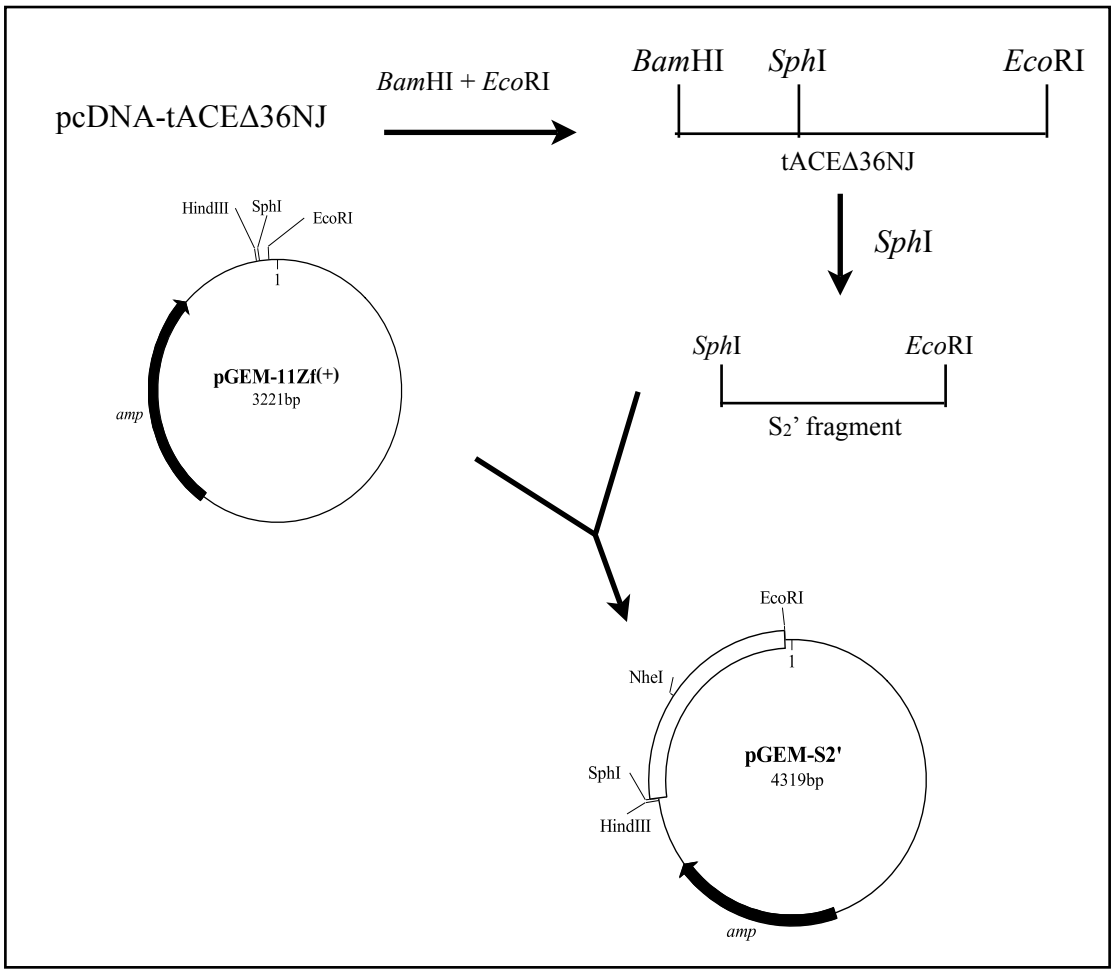

Figure 2.3. **Strategy used to sub-clone the tACE S_2' fragment into pGEM-Zf(+)**, using restriction endonucleases *Eco*RI and *Sph*I.

2.2.4 Site-directed mutagenesis

A *Dpn*I method, adapted from Papworth *et al.* (Papworth et al., 1996), was used to perform the site-directed mutagenesis. It involves the design of complementary primers, containing the desired mutation, which bind to a template plasmid containing the gene of interest. A thermostable DNA polymerase with 3' to 5' exonuclease activity performs primer extension producing daughter strands consisting of the mutation of interest. Design ensures that primers binding to daughter strands bind only to the 3' end, and extension is therefore prohibited, preventing exponential amplification of any spurious mutations. A number of temperature cycles of template separation, primer-template binding, and primer extension are performed, and template DNA is digested using *Dpn*I endonuclease, selecting for the unmethylated, mutated DNA. This DNA can then be transformed into *E. coli* for DNA replication (figure 2.4).

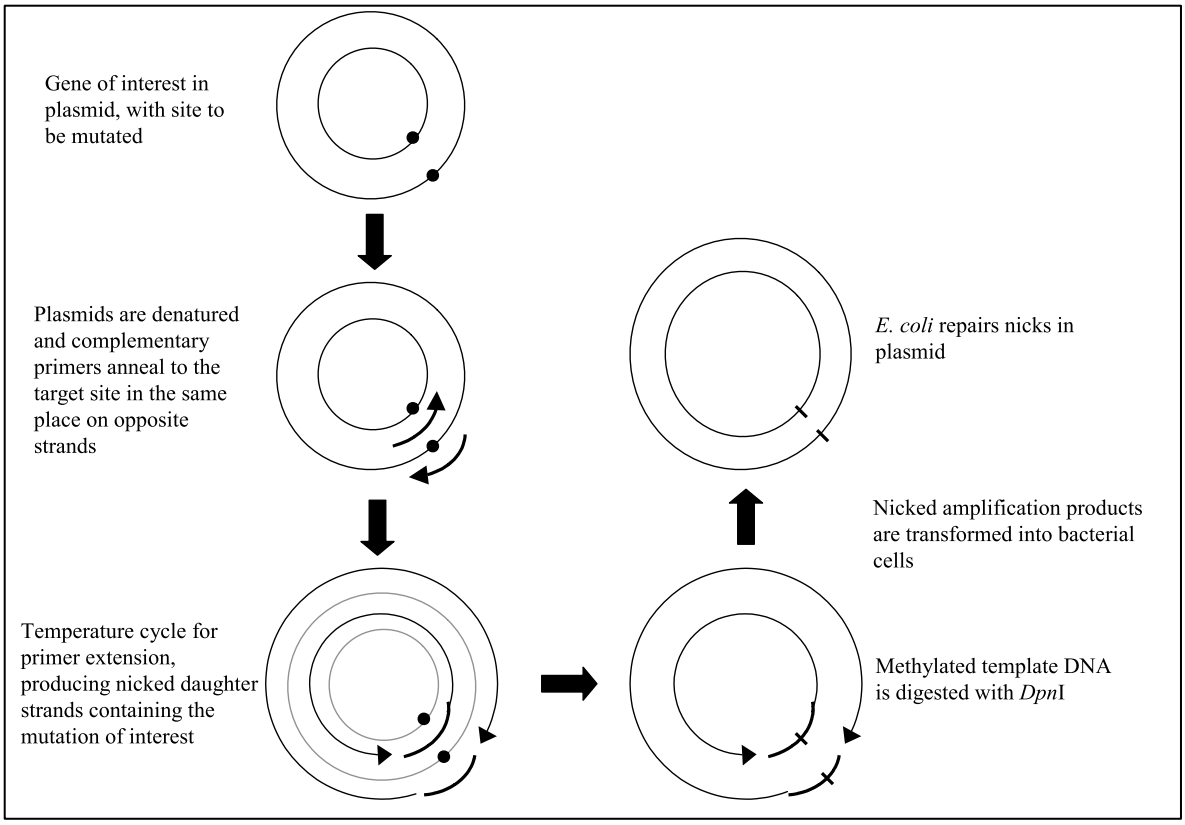

Figure 2.4. **Scheme representing the *Dpn*I site-directed mutagenesis approach** (taken from Papworth et al., 1996).

2.2.4.1 Stop codon insertion into pcDNA-tACEΔ36NJ

Due to the lack of a stop codon in the pcDNA-tACEΔ36NJ construct, this step was required to ensure proper termination of translation (new coding sequence see Appendix I). The PCR amplification reaction mixture was prepared as follows: 5 μL 10 X polymerase buffer; 2 μL 10 mM PCR nucleotide mix; 2 μL 10 μM forward primer (figure 2.5); 2 μL 10 μM reverse primer (figure 2.5); 5 μL 10 ng.μL^{-1} pcDNA-tACEΔ36NJ template; 4-8 μL 25 mM $MgCl_2$; 2 μL dimethyl sulphoxide (DMSO); 1.5 units *Pfu* polymerase; and sterile dH_2O making the total volume up to 50 μL. A control containing no template DNA was included, to ensure amplification was of the desired template. The denaturation step was carried out at 94^{o}C for 5 min, followed by 16 cycles of 94^{o}C for 30 sec, 55-56^{o}C for 30 sec and 72^{o}C for 12 min. The mixture was then incubated at 72^{o}C for 20 min, and stored at 4^{o}C. Amplification products were visualised on agarose gels. 2 μL of *Dpn*I (20 units) was added to the reaction mixtures and incubated at 37^{o}C for 1 hour. Transformations into competent *E. coli* JM109 cells were performed using 10 μL of the digested reaction mixture. DNA isolation (described above) was performed on colonies, which were screened with *Pst*I and *Xma*JI restriction

endonucleases (figure 2.5), and visualised on agarose gels. Positive clones were then confirmed by nucleotide sequencing.

Mutant	Primer		RE
Stop	For	5'-CGCCGAATTCC**TAG**GATATCCAGCAC-3'	*Pst*I
	Rev	5'-GTGCTGGATATC**CTA**GGAATTCGGCG-3'	*Xma*JI

Figure 2.5. **Primer design for insertion of a stop codon into pcDNA-tACEΔ36NJ.** Complementary mutagenic primers (For, forward; Rev, reverse) were designed containing the mutation of interest, as well as a silent mutation introducing a unique restriction endonuclease site (RE) to facilitate screening. Positive mutants were confirmed by nucleotide sequencing. The stop codon mutation appears in bold. Silent mutations result in the insertion of an *Xma*JI site (underlined) and loss of a *Pst*I restriction site to aid screening.

2.2.4.2 Conversion of S_2' tACE residues to corresponding N-domain residues

Reaction mixtures were set up as for the stop codon mutation above, replacing the pcDNA-tACEΔ36NJ template DNA with pGEM-S_2', and the forward and reverse primers with those described in figure 2.6. Appropriate temperature cycles were carried out, followed by *Dpn*I digestion on amplification products, transformation into competent *E. coli* JM109 cells, and DNA isolation of colonies (described above). Restriction endonucleases used for screening are detailed in figure 2.6, and restriction digests were visualised on agarose gels. Positive clones were confirmed by nucleotide sequencing. Three part ligations (section 2.2.2.1) were performed with the S_2' fragments containing the mutations of interest, along with the *Bam*HI-*Sph*I fragment, and the pcDNA-tACEΔ36NJ vector DNA cut with *Bam*HI and *Eco*RI (section 2.2.3), to generate the pcDNA-tACEΔ36NJ constructs containing the desired mutation.

2.2.4.3 S_2, S_1 and S_1' pocket mutants

A number of tACE constructs containing N-domain substitutions within the S_2 (F391Y, E403R), S_1 (S516N, S517V, V518T) and S_1' (E162D, D377Q, ED/DQ) pockets (see table 2.1) were generated by a colleague (H. G. O'Neill) in a similar manner as described above. Three multiple mutants were also created; TEVD (containing the mutations T282S, E376D, V380T and D453E), TEVVD (containing the V379S mutation in addition to the TEVD substitutions), and S_2'F (which contains the F391Y mutation in addition to those in the TEVVD construct) (see table 2.1). Except for E162D, all of the above mutations were generated using the

pGEM-S_2' shuttle vector described above. The E162D substitution was performed using the pGEM-11Zf(-) vector, containing the *Bam*HI-*Sph*I fragment of the tACEΔ36NJ gene. Multiple mutants were obtained by sequential mutagenesis using previously mutated pGEM-S_2' constructs as templates.

Mutant	Primer		RE
T282S	For	5'-GGGAACATGTGGGCGCAG**AGT**TGGTCCAATATTTATG-3'	
	Rev	5'-CATAAATATTGGACCA**ACT**CTGCGCCCACATGTTCCC-3'	*Ssp*I
E376D	For	5'-CACCGTTAACTTG**GAC**GACCTGGTGGTGG-3'	
	Rev	5'-CCACCACCAGGTC**GTC**CAAGTTAACGGTG-3'	*Hpa*I
V379S	For	5'-GAACTTGGAGGACCTC**AGC**GTGGCCCACCACG-3'	
	Rev	5'-CGTGGTGGGCCAC**GCT**GAGGTCCTCCAAGTTC-3'	*Bbv*CI
V380T	For	5'-GGAGGACCT*A*GT**AAC**TGCGCA*T*CACGAAATGG-3'	
	Rev	5'-CCATTTCGTGATGCGCA**GTT**AGTAGGTCCTCC-3'	*Nsb*I
VV/ST	For	5'-GAACTTGGAGGACCTCAGC**ACA**GCCCACCACGAAATGG-3'	
	Rev	5'-CCATTTCGTGGTGGGC**TGT**GCTGAGGTCCTCCAAGTTC-3'	*Bbv*CI
D453E	For	5'-GATGAAGATGGCCCTC**GAG**AAGATCGCCTTTATCC-3'	
	Rev	5'-GGATAAAGGCGATCTT**CTC**GAGGGCCATCTTCATC-3'	*Xho*I

Figure 2.6. **Primer design for site-directed mutagenesis of S_2' mutants.** Complementary mutagenic primers (For, forward; Rev, reverse) are designed containing the mutation of interest, as well as a silent mutation introducing a unique restriction endonuclease site (RE) to facilitate screening. Positive mutants were confirmed by nucleotide sequencing. Residues in bold indicate the codon to be mutated, restrictions sites are underlined. V380T also contained further silent mutations (grey, italics) to eliminate primer self-complementarity. VV/ST contains both the V379S and V380T mutation.

2.3 Results and discussion

2.3.1 Sub-cloning

tACEΔ36NJ was inserted into the expression vector pcDNA3.1(+), and positive constructs were identified using restriction endonucleases. A fragment encoding the S_2' residues of interest was sub-cloned from the pcDNA-tACEΔ36NJ construct into a pGEM11-Zf(+)

cloning vector for subsequent site-directed mutagenesis. The smaller S_2' fragment was utilised to facilitate nucleotide sequencing and reduce the occurrence of spurious mutations.

Positive pGEM-S_2' clones displayed the presence of two bands (3182 and 1137 bp) when cut with *Eco*RI and *Sph*I (figure 2.7, lane 2), compared to the empty pGEM11-Zf(+) vector that displays only one visible band of 3182 bp (figure 2.7, lane 1). Furthermore, co-digestion with *Nhe*I and *Hind*III revealed the presence of two bands 3804 and 515 bp in size (figure 2.7, lane 4), compared to the empty vector displaying one band of 3221 bp (figure 2.7, lane 3).

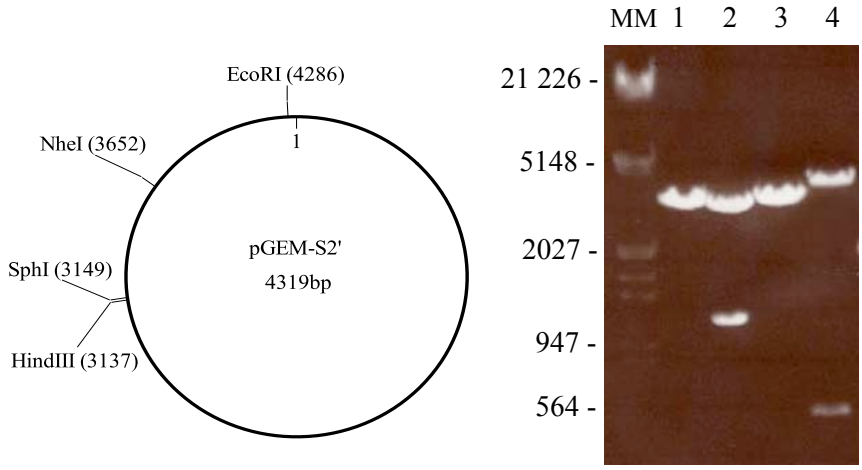

Figure 2.7. **Sub-cloning of S_2' fragment into pGEM-11Zf(+).** Colonies were screened with restriction endonucleases as follows: pGEM-11Zf(+) cut with *Eco*RI and *Sph*I (lane 1); pGEM-S_2' cut with *Eco*RI and *Sph*I (lane 2); pGEM-11Zf(+) cut with *Nhe*I and *Hind*III (lane 3); pGEM-S_2' cut with *Nhe*I and *Hind*III (lane 4). Lambda DNA digested with *Eco*RI and *Hind*III was used as a molecular marker (lane MM).

2.3.2 Site-directed mutagenesis

2.3.2.1 Stop codon insertion into pcDNA-tACEΔ36NJ

Because there was no stop codon in the pcDNA-tACEΔ36NJ construct, one was inserted downstream of the *Eco*RI restriction site to ensure proper termination of translation. The mutagenic primer (figure 2.5) removed and introduced the restriction endonuclease sites *Pst*I and *Xma*JI, respectively. Positive clones displayed the disappearance of the two 1356 and 1156 bp bands (figure 2.8, lane 2), and the appearance of a 2512 band (figure 2.8, lane 3) for *Pst*I digestion, while *Xma*JI digestion resulted in the appearance of two 1097 and 6170 bp bands (figure 2.8, lane 4), compared to the unmutated construct, which is linearised (figure 2.8, lane 5). Sequences were confirmed by nucleotide sequencing.

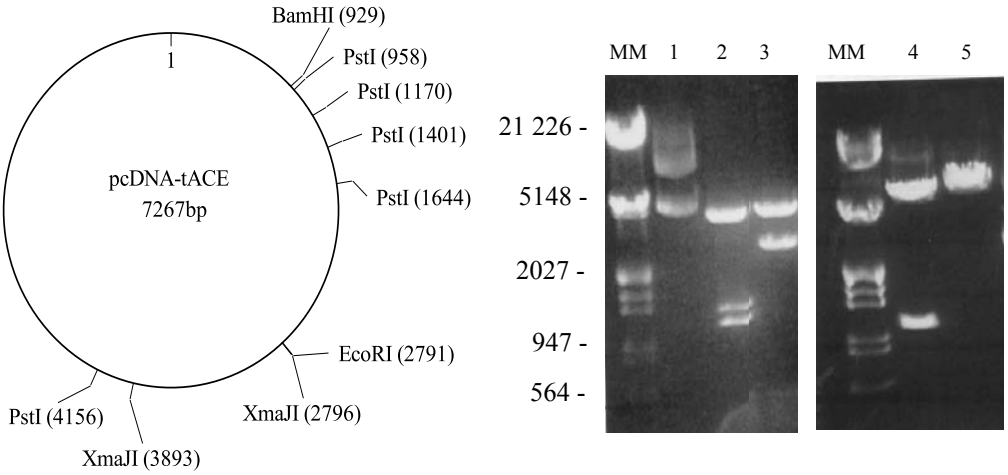

Figure 2.8. **Stop codon was inserted into the pcDNAtACEΔ36NJ construct downstream of the tACE gene.** Colonies were screened with restriction endonucleases as follows: uncut pcDNAtACE (lane 1); pcDNAtACE cut with *Pst*I (lane 2) and *Xma*JI (lane 5); and pcDNAtACE with the stop codon mutation cut with *Pst*I (lane 3) and *Xma*JI (lane 4). Lambda DNA digested with *Eco*RI and *Hind*III was used as a molecular marker (lane MM) for each gel.

2.3.2.2 Construction of active-site mutants

The selection of mutants generated (table 2.1) was based on a number of studies that have identified differences between domains, within the sub-site pockets of ACE (discussed in section 1.3) (Natesh et al., 2003; Georgiadis et al., 2004; Bersanetti et al., 2004; Redelinghuys et al., 2005; Tzakos and Gerothanassis, 2005; Redelinghuys et al., 2006; Jullien et al., 2006; Corradi et al., 2006; Corradi et al., 2007).

Site-directed mutagenesis was performed in the pGEM-S_2' shuttle construct. S_2' residues were converted to their corresponding N-domain residues. In the first attempt, PCR products were obtained for mutants V379S, VV379/380ST and D453E, transformed into *E. coli*, and screened with the appropriate restriction endonucleases.

Table 2.1. **Summary of the mutants generated.**

Pocket	Mutant Name	tACE (C-domain)	N-domain
S_2	F391Y	Phe 391 (967)	Tyr 369
	E403R	Glu 404 (979)	Arg 381
S_1	S516N	Ser 516 (1092)	Asn 494
	S517V	Ser 517 (1093)	Val 495
	V518T	Val 518 (1094)	Thr 496
S_1'	E162D	Glu 162 (738)	Asp 140
	D377Q	Asp 377 (953)	Gln 355
	ED/DQ	Glu 162, Asp 377	Asp 140, Gln 355
S_2'	T282S	Thr 282 (858)	Ser 260
	E376D	Glu 376 (952)	Asp 354
	V379S	Val 379 (955)	Ser 357
	V380T	Val 380 (956)	Thr 358
	VV/ST	Val 379, Val 380	Ser 357, Thr 358
	D453E	Asp 453	Glu 431
S_2' multiple	TEVVD	T282, E376, V379, V380, D453	S260, D354, S357, T358, E431
	TEVD	T282, E376, V380, D453	S260, D354, T358, E431
S_2' and S_2 multiple	S_2'F	T282, E376, V379, V380, D453, F391	S260, D354, S357, T358, E431, Y369

The pGEM-S_2' plasmid encodes a 1139 bp fragment of the coding sequence of tACE between the restriction endonuclease sites *Eco*RI and *Sph*I (described in 2.2.3). The uncut plasmid resolved as two bands representing supercoiled and nicked plasmid DNA (figure 2.9, lanes 1, 3 and 5). The pGEM-S_2' V379S, VV/ST and D453E plasmids encode the same sequence except containing Val 379 to Ser, Val 379 and Val 380 to Ser and Thr, and Asp 453 to Glu substitutions, respectively (table 2.1). The identity of positive clones were confirmed by restriction endonuclease analysis (figure 2.9). The pGEM-S_2' V379S, VV/ST and D453E plasmids were linearised by digestion with *Bbv*CI, *Bbv*CI and *Xho*I, respectively, yielding

single bands (4319 bp) in agreement with the expected size. Sequences were confirmed by nucleotide sequencing.

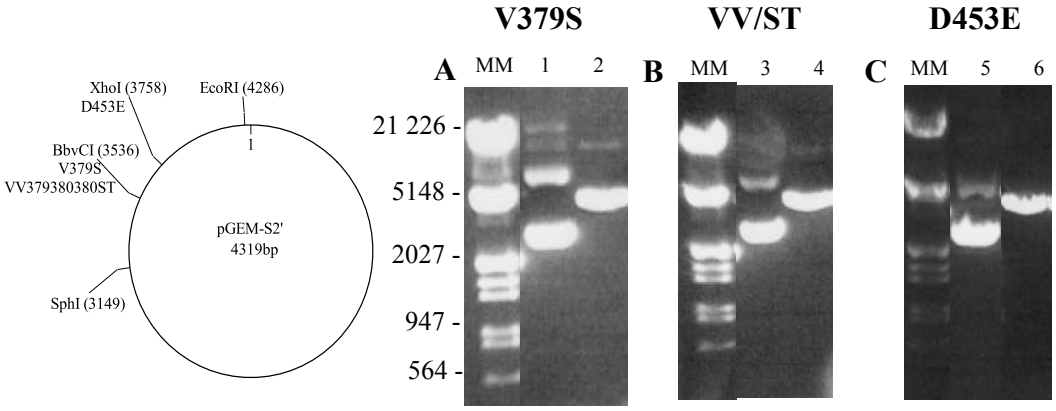

Figure 2.9. **The S_2' residues of interest were converted from C-domain to corresponding N-domain residues by site-directed mutagenesis, using a *Dpn*I PCR method.** Mutants were screened with appropriate restriction endonucleases as follows: **A**, pGEM-S_2' (lane 1) and pGEM-S_2' V379S (lane 2) digested with *Bbv*CI; **B**, pGEM-S_2' (lane 3) and pGEM-S_2' VV379/380ST (lane 4) digested with *Bbv*CI; and **C**, pGEM-S_2' (lane 5) and pGEM-S_2' D453E (lane 6) digested with *Xho*I. All clones were confirmed by nucleotide sequencing. Lambda DNA digested with *Eco*RI and *Hind*III was used as a molecular marker (lane MM) for each gel.

A Mg concentration titration (representative gel, figure 2.10) was performed to obtain products for the T282S, E376D and V380T mutants. *Pfu* polymerase requires free Mg to function, however Mg also binds to the nucleotides and DNA, decreasing the specificity of the primer for the template (Innis and Gelfand, 1990). Therefore an increased Mg concentration often improves the product yield for a primer with a number of mismatches. This increased concentration can, however, also cause the production of non-specific products; hence the process sometimes requires some optimisation (Henegariu et al., 1997). Further optimisation of these PCR reactions also involved the addition of DMSO. This is believed to improve the efficiency of the amplification in a number of ways including affecting primer melting temperature (T_m) and / or the polymerase activity profile and increasing the product yield (Innis and Gelfand, 1990).

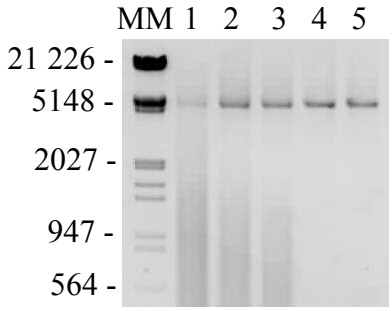

Figure 2.10. **Representative gel of a Mg titration in a PCR reaction.** Final Mg concentrations 0, 2, 4, 6 and 8 mM (lanes 1-5, respectively), molecular marker (lane MM).

A final concentration of 6 mM Mg yielded appropriate PCR products for each of the above constructs. The E376D mutagenic primer introduced a unique *Hpa*I restriction endonuclease site. The unmutated pGEM-S_2' plasmid ran as uncut plasmid DNA with two bands (supercoiled and nicked plasmid DNA; figure 2.11 A, lane 1), and a putative mutant plasmid was identified with the linearisation of the pGEM-S_2' E376D construct, revealing a single band of 4319 bp (figure 2.11 A, lanes 1 and 2). No putative mutant plasmids were identified from the T282S and V380T products.

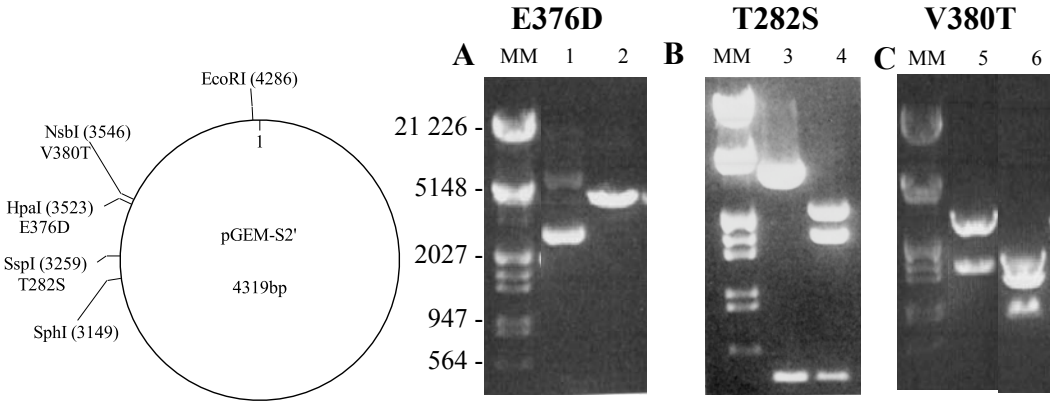

Figure 2.11. **The S_2' residues of interest were converted from C-domain to corresponding N-domain residues by site-directed mutagenesis, using a *Dpn*I PCR method.** Mutants were screened with appropriate restriction enzymes as follows: **A**, pGEM-S_2' (lane 1) and pGEM-S_2' E376D (lane 2) digested with *Hpa*I; **B**, pGEM-S_2' (lane 2) and pGEM-S_2' T282S (lane 3) digested with *Ssp*I; and **C**, pGEM-S_2' (lane 4) and pGEM-S_2' V380T (lane 5) digested with *Nsb*I. All mutations were confirmed by nucleotide sequencing. Lambda DNA digested with *Eco*RI and *Hind*III was used as a molecular marker (lane MM) for each gel.

The original T282S primer was 45 bp in length (Appendix I, figure A1). This length was used because a single silent mutation only produced a *Bmr*I restriction endonuclease site 22 bp

away from the mutated codon. When the primer was re-analysed, it was found that if two silent mutations were used, an *Ssp*I restriction site could be engineered 12 bp from the mutated codon, allowing the design of a primer 37 bp in length. This primer (figure 2.6) introduced a third *Ssp*I restriction endonuclease site, cutting a 3883-bp fragment into two 2214 and 1669 bp fragments. Template pGEM-S_2' DNA ran as two bands, 3883 and 436 bp, while a putative mutant plasmid was identified, displaying the presence of three bands 2214, 1669 and 436 bp in size (figure 2.11 B, lanes 3 and 4).

The original primer designed for V380T contained the V/T mutation 6 bp from the end of the oligonucleotides (Appendix I, figure A1). This primer was however unsuccessful in producing a mutant plasmid, possibly due to the primer not annealing to the desired site, and redesign of the primer involved the inclusion of an additional two silent mutations to eliminate self-complementarity (figure 2.6). The new V380T mutagenic primer introduced a third *Nsb*I restriction site, causing a 2842-bp band to be cut into two 1909 and 933 bp bands. Unmutated pGEM-S_2' plasmid revealed two bands (2842 and 1477 bp), and a potential mutant plasmid was identified by the presence of three bands of 1909, 1477 and 933 bp (figure 2.11 C, lanes 5 and 6).

As mentioned above, the S_2, S_1, S_1' and multiple mutants were generated by a colleague (H.G. O'Neill) using a similar approach to that used to construct the S_2' mutants. All constructs were confirmed by nucleotide sequencing.

The tACE S_2' fragments containing the corresponding N-domain mutations of interest were cut out of the pGEM-S_2' constructs using *Eco*RI and *Sph*I, and reintroduced into the pcDNA-tACEΔ36NJ vector construct by a three part ligation with the S_2' fragments containing the mutations of interest, the *Bam*HI-*Sph*I fragment, and the pcDNA-tACEΔ36NJ vector DNA cut with *Bam*HI and *Eco*RI (described in section 2.2.2.1). All plasmid constructs were confirmed using cloning and unique site restriction endonuclease sites introduced in the site-directed mutagenesis.

2.4 Summary

In summary, the tACEΔ36NJ gene was sub-cloned into the pcDNA3.1(+) expression vector, and a fragment containing the residues to be mutated (S_2' fragment) was sub-cloned into the shuttle vector pGEM11Zf(+) to facilitate site-directed mutagenesis. Residues of interest were converted to their corresponding N-domain counterparts using a *Dpn*I mutagenesis method, and positive clones were identified using restriction endonucleases, and confirmed by nucleotide sequencing. The mutated S_2' fragments were re-introduced back into the pcDNA-tACEΔ36NJ construct by a three part ligation, for subsequent expression in mammalian cells.

Chapter 3: Protein Expression, Purification and Substrate Hydrolysis of tACE Mutant Proteins

3.1 Introduction

A panel of tACE mutants was generated (described in chapter 2; see table 2.1) containing particular active-site residue N-domain substitutions. These were transfected into CHO cells not expressing endogenous ACE, and mutant protein was expressed and purified for subsequent enzyme kinetic analysis. Constructs were characterised using the domain-selective FRET peptides Abz-LFK(Dnp)-OH (C-domain-selective) and Abz-SDK(Dnp)P-OH (N-domain-selective).

The objectives of the present work were therefore to:

1. Transfect the plasmids encoding soluble tACE mutants into CHO cells and harvest media containing these protein constructs.
2. Confirm activity of mutant constructs using an HHL activity assay.
3. Isolate tACE mutant constructs using a Sepharose-28-lisinopril affinity column, and N-domain using immuno-affinity chromatography.
4. Determine the active concentration of each construct using an active-site titration.
5. Characterise the hydrolysis of domain-specific fluorogenic peptides by particular mutant constructs.

3.2 Experimental procedure

3.2.1 Chemicals

Fetal calf serum (FCS) and trypsin were supplied by Gibco, and Dulbecco's modified eagle's medium (DMEM) and Ham's F12 were obtained from Highveld Biologicals. N-2-hydroxyethylpiperazine-N'-2-ethanesulphonic Acid (HEPES), G418, HHL, HL, *Z*-FHL, *o*-phthaldialdehyde, protein G agarose and $ZnCl_2$ were purchased from Sigma. Chinese hamster ovary K1 (CHO-K1) cells were supplied by American Type Culture Collection (ATCC® CCL-61), the Profection® Mammalian Transfection System from Promega, and the BIO

RAD protein assay from BIO RAD. Ethanolamine was from Saarchem, NaCl from Merck, and lisinopril from Zeneca Pharmaceuticals.

3.2.2 Expression of constructs

pcDNAtACEΔ36NJ mutant constructs were transfected into CHO-K1 cells using the Profection® Mammalian Transfection System. Ten mL of CHO-K1 growth medium (50 % DMEM, 50 % Ham's F12, 20 mM HEPES, pH 7.5, supplemented with 10 % FCS (heat-inactivated for 30 min at 56^{o}C)) was inoculated with 500 μL of a CHO-K1 stock solution, and incubated at 37^{o}C, 5 % CO_2, until confluent. Cells were seeded into 10 cm^2 culture dishes and incubated overnight, as before. Three hours before transfection, the cells were washed with 1 x phosphate-buffered saline (PBS) and further incubated with fresh growth medium. A 500 μL solution containing 10 μg of DNA and 248 mM $CaCl_2$ was bubbled through 500 μL of HEPES buffered saline, incubated at room temperature for 30 min, and added drop-wise to the cells. Cells were incubated for 3-4 hours, glycerol-shocked at room temperature for 1.5-2 min using 15 % glycerol in PBS, and then washed with PBS. Cells were then incubated in CHO-K1 growth medium overnight at 37^{o}C, 5 % CO_2. The following day, medium was replaced with 0.8 mg.mL^{-1} G418-supplemented medium to select for positive colonies, and incubated until separate clones of approximately 1-2 mm were visible. Colonies were picked using sterile swabs dipped in trypsin-EDTA, and seeded into 12 well plates. Clonal lines were screened for ACE activity (section 3.2.3), and stocks were prepared from the clone exhibiting the highest ACE activity using HHL for tACE and tACE constructs, and *Z*-FHL for the N-domain.

3.2.3 HHL and *Z*-FHL assays

ACE cleaves the substrates HHL and *Z*-FHL to produce the product HL. The latter forms a fluorescent adduct with *o*-phthaldialdehyde, which can be measured spectrofluorometrically (λ excitation = 360 nm; λ emission = 485 nm) (Friedland and Silverstein, 1976). Medium or purified samples (2-20 μL) were incubated with 120 μL HHL substrate in HHL assay buffer (5.7 mM HHL in 50 mM HEPES, pH 7.5, 0.3 M NaCl; Appendix II), or 120 μL *Z*-FHL in *Z*-FHL buffer (1 mM *Z*-FHL in 0.1 M KPO_4 buffer, pH 8.3, 0.3 M NaCl, 10 μM $ZnSO_4$; Appendix II) at 37^{o}C for 15 min, and the reaction was stopped with 725 μL 0.028 M NaOH.

Fifty µL of 20 mg.mL^{-1} *o*-phthaldialdehyde was added, incubated at room temperature for 10 min, and the reaction stopped with 100 µL 3 M hydrochloric acid. Fluorescence was measured from 250 µL of the reaction mixture in a 96 well plate, using a Varian Eclipse Fluorescence Spectrophotometer. An HL standard curve (0-20 nmol HL) was generated to convert fluorescent units into milliunits (mU) ACE activity, where 1 unit is defined as 1 nmole of HL produced per min^{-1}.mL^{-1}, at 37^{o}C in HHL assay buffer.

3.2.4 Isolation and purification of tACE modified derivatives

CHO-K1 clonal lines were grown up in growth medium, and transferred to T175 cm^2 flasks. Once 90 - 100 % confluent, medium was replaced with growth medium (50 % DMEM, 50 % Ham's F12, 20 mM HEPES, supplemented with 2 % FCS (heat-inactivated for a further 15 min at 70^{o}C), and media were harvested every 2 - 3 days. Harvested media were stored at -20^{o}C until required for purification.

Testis ACE proteins were purified from spent growth media with affinity chromatography, using a Sepharose-28-lisinopril affinity column (Ehlers et al., 1991). Ten mL Columns were washed with wash buffer (20 mM HEPES, pH 7.5, 0.5 M NaCl) to eliminate non-specific binding and the tACE and mutant derivatives were eluted with 50 mM borate buffer (pH 9.5), of which 1.5 mL fractions were collected and analysed for ACE activity. Those containing substantial ACE activity were pooled and dialysed overnight in 2 x 2 L of dialysis solution (5 mM HEPES, pH 7.5) 0.1 mM PMSF) at 4^{o}C. Protein concentrations were determined using a BIORAD Bradford assay as per manufacturer's instruction, and activity was measured using the HHL assay. Purified proteins were visualised on a 10 % polyacrylamide sodium dodecylsulphate gel electrophoresis (SDS-PAGE) gel (Laemmli, 1970) to ensure purity and correct size. Purified protein aliquots of 0.5 - 1 mL were stored at 4 and -20^{o}C.

3.2.5 Isolation and purification of N-domain derivatives of sACE

A CHO-K1 cell line expressing a soluble N-domain derivative D629, containing the N-terminal residues 1-629 of sACE (a kind gift from S. M. Danilov; Balyasnikova et al., 2003), sub-cloned (by P. Redelinghuys) into the expression vector pcDNA3.1(+) using the restriction endonucleases *Xba*I and *Eco*RI, was obtained from S. L. W. Schwager, and harvested medium was prepared and stored as described above.

Protein G is an immunoglobulin-binding protein able to bind the Fc segment of mammalian IgG (Sjöbring et al., 1990). It is therefore commonly used to remove excess levels of this protein from culture medium. To improve selectivity of the N-domain immuno-affinity chromatography column, spent medium was passed through a pre-protein G agarose column to reduce the excess levels of IgG, and N-domain was consequently bound to an N-domain-specific antibody, 5C5 (kindly provided by S. M. Danilov), coupled to a protein G agarose column (Corradi et al., 2006). The columns were washed with wash buffer as described above, and elution of the N-domain was mediated with 50 mM ethanolamine (pH 11.5). Protein was collected, dialysed, analysed and stored as described above.

3.2.6 Fluorogenic peptide assay

Domain-selective internally quenched FRET peptides, containing an Abz fluorescent donor and a Dnp acceptor group, were used to characterise the activity of ACE. Cleavage of these peptides between the donor-acceptor pair releases fluorescence that can be measured continuously in a fluorometer (Yaron et al., 1979; Araujo et al., 1999).

The fluorogenic peptides (kind gifts from A. K. Carmona), supplied in powder form, were dissolved in a small volume of DMSO to approximately 10 mM. Concentrations (C) were calculated based on the Beer-Lambert equation A = E.C.l, where the extinction coefficient (E) was 17300 $M^{-1}cm^{-1}$, absorbance (A) of the stock solutions was measured at 365 nm, and the pathlength (l) of the cell was 1 cm. Stock solutions of 1 mM were made up in DMSO, and working solutions were made up from these stocks in the FRET assay buffer constituting 50 mM HEPES buffer (pH 6.8), 200 mM NaCl, and 10 µM $ZnCl_2$.

Cleavage of these peptides was characterised in a continuous assay at ambient temperature (20 - 25^oC), under initial rate conditions of less than 10 % hydrolysis, over time (s). Briefly, in triplicate, 0.2 nM enzyme was added to substrate concentration ranges of 0 - 12 µM, to final volumes of 300 µL in the FRET assay buffer (adjusted from Carmona et al., 2006), and fluorescence was measured at λ_{ex} = 320 nm and λ_{em} = 420 nm. A standard curve converting fluorescence to nmol product was generated from total hydrolysis of fluorogenic peptides (Appendix II). Kinetic parameters were calculated using the Direct Linear plot method (Eisenthal and Cornish-Bowden, 1974), and all replicates displayed an error within 5 %.

3.2.7 Active enzyme concentration determination

In order to determine more accurate concentrations of active enzyme present, active-site titrations were performed with the inhibitor lisinopril, known to bind in a ratio of 1:1, inhibitor molecule to enzyme active-site. Limitations of this method include the high concentrations of enzyme and inhibitor that should ideally be used to ensure that the $E + I \rightleftharpoons EI$ reaction is driven mainly to the right (Bieth, 1995). Stock solutions of lisinopril were made by dissolving the inhibitor in dH_2O and preparing a dilution series in the FRET assay buffer. Active-site titrations were performed by incubating 10 µL enzyme (in the assay buffer) with an equal volume of each of the lisinopril dilutions for 1.5 hours at ambient temperature. Residual enzyme activity was measured, by pipetting out 20 µL of the incubation mixture into a 96-well plate, adding Abz-FRK(Dnp)P-OH (4 µM final substrate concentration), to a total volume of 300 µL, in triplicate, and measuring the continuous fluorescence at λ_{ex} = 320 nm and λ_{em} = 420 nm, at ambient temperature.

The active-site concentration was calculated as described by Knight, 1995 (Knight, 1995). Briefly, the stoichiometry of inhibition (SI) value was calculated from a plot of percent activity versus the molar ratio of lisinopril to ACE (I:E; protein concentrations of ACE were determined from Bradford's assays). The x-intercept of the initial portion indicates the SI, where the ratio of the number of moles of inhibitor is equal to that of the enzyme in the case of ACE and lisinopril (SI = 1). Based on this expectation, we can determine the active protein concentration by multiplying the total protein concentration determined by the Bradford's assay, by the SI value calculated from the plot.

3.3 Results and discussion

3.3.1 Protein expression and purification

CHO cell lines expressing adequate levels of tACE, N-domain and tACE active-site mutants were established by transfection, and the line exhibiting the highest HHL activity was selected for protein expression. Pooled media containing expressed protein were applied to a Sepharose-28-lisinopril affinity column for purification of tACE constructs, and N-domain

was purified using an immuno-affinity column. Each protein construct was analysed on an SDS-PAGE gel to confirm size and purity. Bands for all the mutants were observed to have a molecular weight of approximately 78 kDa, which was in good agreement with the calculated weight of 78 kDa for fully glycosylated tACEΔ36NJ (representative SDS-PAGE in figure 3.1). This molecular weight was calculated using the tACEΔ36NJ sequence and adding six glycans of 1700 Da each.

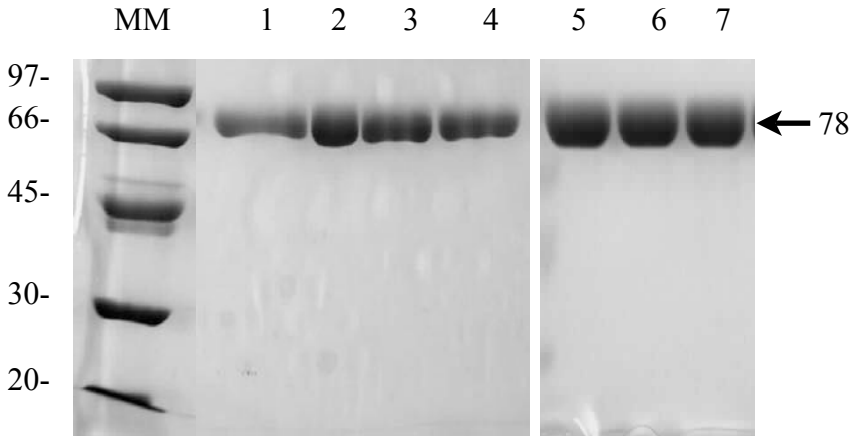

Figure 3.1. **Representative SDS-PAGE (10 %) indicating purity of a selection of tACE mutants.** Lanes 1, tACE; 2, VV/ST; 3, D453E; 4, T282S; 5,V379S; 6, V380T; 7, E376D. Lanes were loaded with approximately 10 μg of protein. Arrow indicates the size of the tACE constructs (78 kDa). Molecular marker (lane MM) sizes in kDa.

Bradford assays were performed to determine protein concentration and calculate yields of purified protein (table 3.1; Bradford, 1976) with total protein obtained ranging from 0.2 to 6 mg, and HHL assays were performed to confirm ACE activity in all constructs. Interestingly, high yields were obtained for most of the mutants, particularly for E376D and D453E. These are believed to be extremely high expressing cell lines, as similar yields were obtained in subsequent transfections and purifications. This phenomenon could be due to either multiple insertion of the gene into the genome or perhaps the active-site substitution plays some role in improving the stablility of the final protein product.

Table 3.1. **Summary of protein purification yields from CHO-K1 cells.**

Protein derivative	Protein Yield ($mg.L^{-1}$ medium)	Protein derivative	Protein Yield ($mg.L^{-1}$ medium)
tACE	2.1	T282S	4.4
N-domain	7.4	E376D	25.7
F391Y	2.3	V379S	3.4
E403R	1.1	V380T	1.2
S516N	3.8	VV/ST	7.2
S517V	1.8	D453E	12.3
V518T	1.1	S_2'	7.3
E162D	2.6	TEVD	11.3
D377Q	1.7	S_2'F	3.2
ED/DQ	3.1		

3.3.2 Active enzyme concentration determination

Although affinity chromatography is assumed to result in a fully active stock solution of the enzyme, degradation of protein may occur when stored for long periods of time, resulting in lowered concentrations of active enzyme (Knight, 1995). Furthermore, inaccurate measurements can be obtained from absorbance readings due to dissolved contaminants or tightly bound water molecules. Active concentrations of each construct were therefore determined using active-site titrations with the tight-binding inhibitor lisinopril, before performing any subsequent fluorogenic assays (representative active site titration, figure 3.2).

Generally, the active-site concentrations obtained using this method were approximately 10-25 % of those displayed by the Bradford's method (results not shown). These assays were however performed on samples that had been stored for more than a month at 4^{o}C, in 5 mM HEPES and no NaCl. It was also found that under these conditions, certain mutants, particularly V518T, demonstrated rapid degradation within a week (figure 3.3). Furthermore, there are a number of limitations to the Bradford's method, such as its sensitivity to protein

composition and non-protein contaminants (Bradford, 1976). This highlights the importance of accurately determining the active concentration of a construct before subsequent kinetic analysis, to ensure that the effect of amino acid substitutions can be correctly attributed to their effects on binding and catalysis, as opposed to their influence on protein stability (Knight, 1995).

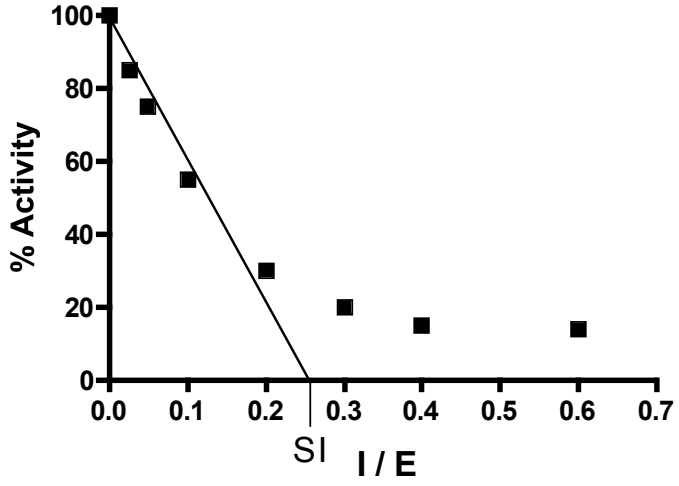

Figure 3.2. **Plot of percentage activity versus the molar ratio of inhibitor to enzyme.** The SI value is indicated.

Optimisation of storage conditions for the V518T mutant was carried out by storing stocks at different HEPES and NaCl concentrations. Three stock samples of V518T were stored in 5 mM HEPES (no NaCl), 25 mM HEPES 100 mM NaCl and 50 mM HEPES 200 mM NaCl, (all pH 7.5) at 4^{o}C, for one month. Complete and slight degradation of the 5 mM and 50 mM HEPES sample was observed, respectively, while the 25 mM HEPES sample displayed none (figure 3.3A). Furthermore, storage of S516N in 5 mM HEPES at -20^{o}C resulted in less degradation of protein than those stored at 4^{o}C (figure 3.3B). It can be therefore be suggested that ACE constructs containing active site mutations, should ideally be stored at -20^{o}C in 5 mM HEPES, or in 25 mM HEPES.

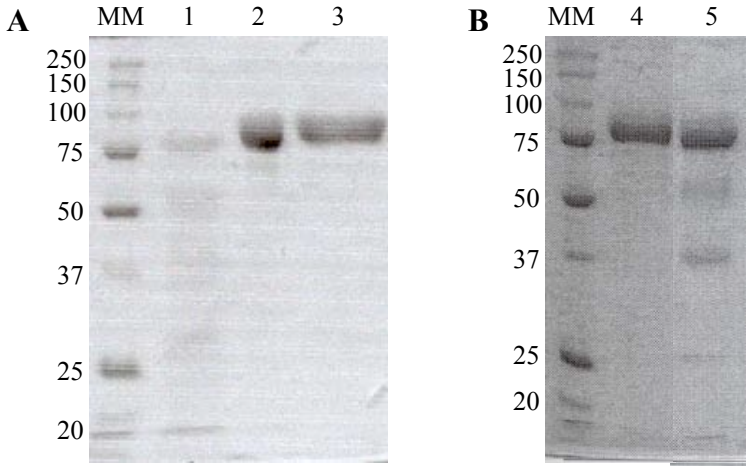

Figure 3.3. **SDS-PAGE (10 %, denaturing) displaying A) V518T and B) S516N mutants stored under different conditions for one month.** Lane 1, 5 mM HEPES, no NaCl (4°C); 2, 50 mM HEPES, 200 mM NaCl (4°C); 3, 25 mM HEPES, 100 mM NaCl (4°C); 4, 5 mM HEPES (-20°C); 5, 5 mM HEPES (4°C). Lanes were loaded with approximately 10 µg of protein. Lane MM, molecular marker, sizes in kDa.

3.3.3 Hydrolysis of FRET peptides

Kinetic constants were calculated for the hydrolysis of FRET peptides Abz-LFK(Dnp)-OH and Abz-SDK(Dnp)P-OH, by tACE, N-domain and the tACE mutants (tables 3.2 and 3.3).

3.3.3.1 Hydrolysis of Abz-LFK(Dnp)-OH

Abz-LFK(Dnp)-OH, which is cleaved by ACE at the Leu-Phe bond, is highly selective for the C-domain (Bersanetti et al., 2004). This selectivity has mainly been attributed to the high catalytic rate with which this substrate is cleaved by the C-domain compared to the N-domain. This effect was observed here too (table 3.2), where the k_{cat} value for tACE (53.3 s^{-1}) was 120-fold greater than that of the N-domain (0.44 s^{-1}), while the K_M values were similar (tACE, 14.5 µM; N-domain, 9.5 µM).

Table 3.2. **Kinetic constants for the cleavage of the C-domain-specific Abz-LFK(Dnp)-OH FRET peptide by ACE constructs.** Cleavage of Abz-LFK(Dnp)-OH by a series of tACE mutants and the wild-type tACE and N-domain constructs was analysed. Initial velocities for each substrate concentration were determined in triplicate, and kinetic constants were calculated using the direct linear plot method (Eisenthal and Cornish-Bowden, 1974).

Mutant	Abz-LFK(Dnp)-OH	
	K_M(μM)	k_{cat} (s^{-1})
tACE	14.5	53.3
Ndom	9.5	0.44
S516N	12.5	30.2
V518T	16.7	27.6
E162D	13.9	50.0
D377Q	7.5	18.0
ED/DQ	8.8	25.6
V379S	3.5	23.4
V380T	5.3	18.2
VV/ST	2.4	18.2

To elucidate the molecular basis for this selectivity, the hydrolysis of Abz-LFK(Dnp)-OH by a selection of tACE active-site mutants was tested (table 3.2). These mutants were chosen based on pockets implicated to play a role in the C-selectivity of Abz-LFK(Dnp)-OH through scanning of peptide libraries with differing P_3 to P_1' substituents (particularly S_1') (Bersanetti et al., 2004), as well as analysis of specific interactions of a docked model of Abz-LFK(Dnp)-OH complexed to tACE (particular residues within the S_1 and S_2' pocket) (Bersanetti et al., 2004). As expected, there was not much variation with the K_M values, with the lowest K_M values being obtained for mutations within the S_2' pocket, V379S, V380T and VV/ST (3.5, 5.3 and 2.4, respectively; table 3.2; figure 3.4).

Slight decreases in k_{cat}, approximately 3-fold, were observed for D377Q, V380T and VV/ST (k_{cat} = 18.0, 18.2, 18.2 s^{-1}, respectively). The substitution of a Gln residue for the Asp in D377Q not only results in the loss of a negative charge, but could potentially position the

polar Gln side-chain closer to the P_1' Phe side-chain of Abz-LFK(Dnp)-OH than the shorter Asp (5.8 Å for Q, compared to 7.5 Å for D; figure 3.4). The mutations V380T and VV/ST decrease the hydrophobicity of the S_2' pocket. A model of Abz-LFK(Dnp)-OH docked into the active-site of tACE (figure 3.4) (Bersanetti et al., 2004) revealed distances of approximately 7.8 and 3.8 Å between the P_2' Phe and residues V379 and V380, respectively. Therefore, the VV/ST substitution's effect is likely due to the V380T mutation, as is further evidenced by a similar k_{cat} obtained for this single mutation, compared to the double mutant (table 3.2). All of these substitutions are more than 10 Å away from any of the residues believed to play a role in stabilising the transition state and are therefore unlikely to play a direct role in hindering the formation of the tetrahedral intermediate. It can be suggested however, that these conversions may cause a change in the orientation of the substrate molecule, which may result in unfavourable interactions with these stabilising residues, thereby reducing the efficiency with which the substrate is cleaved.

None of these mutations caused a decrease in k_{cat} equivalent to that of the N-domain, suggesting that other residues within the active-site contribute to the high selectivity of this substrate for the C-domain (discussed below). Furthermore, additional factors such as access of the substrate into the active-site and interactions of the substrate with residues elsewhere in the protein, such as the lid region or entrance to the active-site, may also contribute to some extent. This idea is supported by a tACE construct developed in our group, containing an N-domain-like lid region, where tACE residues 1-163 were replaced by the corresponding N-domain residues 1-141 (Woodman et al., 2006). This construct revealed interesting shifts in substrate specificity displaying catalytic efficiencies more comparable to that of the N-domain, for the C-selective substrates HHL and Abz-LFK(Dnp)-OH. This implies that the lid region of the N-domain may play a role in access or release of the substrate or products, affecting the efficiency with which particular substrates are cleaved.

Another example of factors outside the active-site affecting substrate specificity was demonstrated by Behera and Mazumdar (Behera and Mazumdar, 2008). They showed that Cytochrome P450cam, an oxygenase from *Pseudomonas putida* involved in camphor metabolism, contains residues at the entrance to the putative substrate access channel that seem to play a major role in the binding and recognition of camphor, therefore facilitating

access of this substrate into the active-site. This suggests that other proteins such as ACE, may have residues at the entrance to or in the substrate channel that may contribute to substrate specificity, especially considering the lid regions of these two domains display a low sequence identity (approximately 25 %), with some interesting differences in charge and hydrophobicity (Woodman et al., 2006).

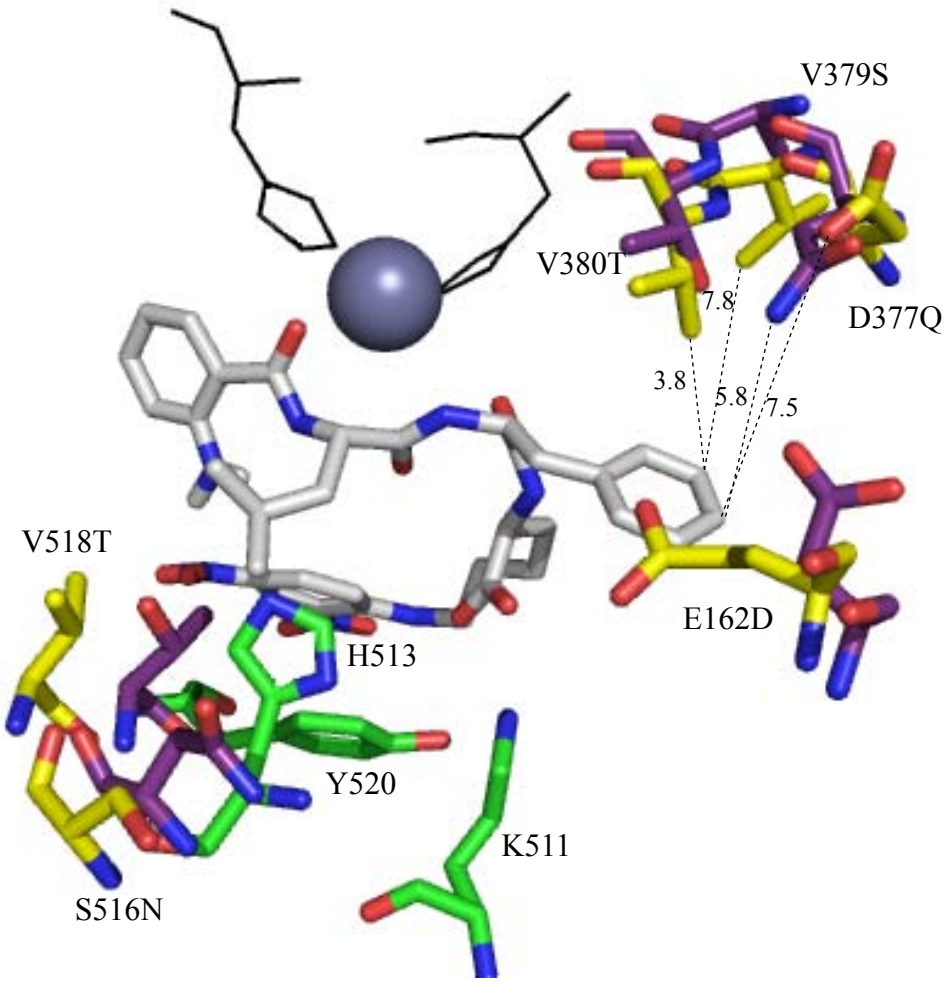

Figure 3.4. **Stick representation of Abz-LFK(Dnp)-OH (grey carbon atoms) docked into the tACE active-site** (PDB code 1o86) (kindly provided by A.T. Nchinda; Bersanetti et al., 2004), aligned to the N-domain structure (PDB code 2c6n). Residues differing between tACE and the N-domain are shown in yellow and purple, respectively, tACE residues stabilising the transition state are coloured green. The active-site zinc ion is represented as a grey sphere and two of the zinc-chelating residues are shown as black lines (H383 and H387). All distances are given in Å. Images were created using MacPyMOL 0.99 (DeLano Scientific, Palo Alto, CA, U.S.A).

Further analysis of residues within 6 Å of Abz-LFK(Dnp)-OH in the docked tACE structure (Bersanetti et al., 2004) aligned to the N-domain (PDB code 2c6n), revealed some interesting differences between the two active-sites (figure 3.5). In addition to the residues that were mutated above (table 3.2), N277 (Asp 255 in the N-domain) and S461 (Gly 439 in the N-domain) differed between domains. Moreover, a residue conserved between domains, D465/ D443 (tACE / N-domain numbering), was within 6 Å of the substrate side-chain for the N-domain, while the distance in tACE was greater than 6 Å (figure 3.5).

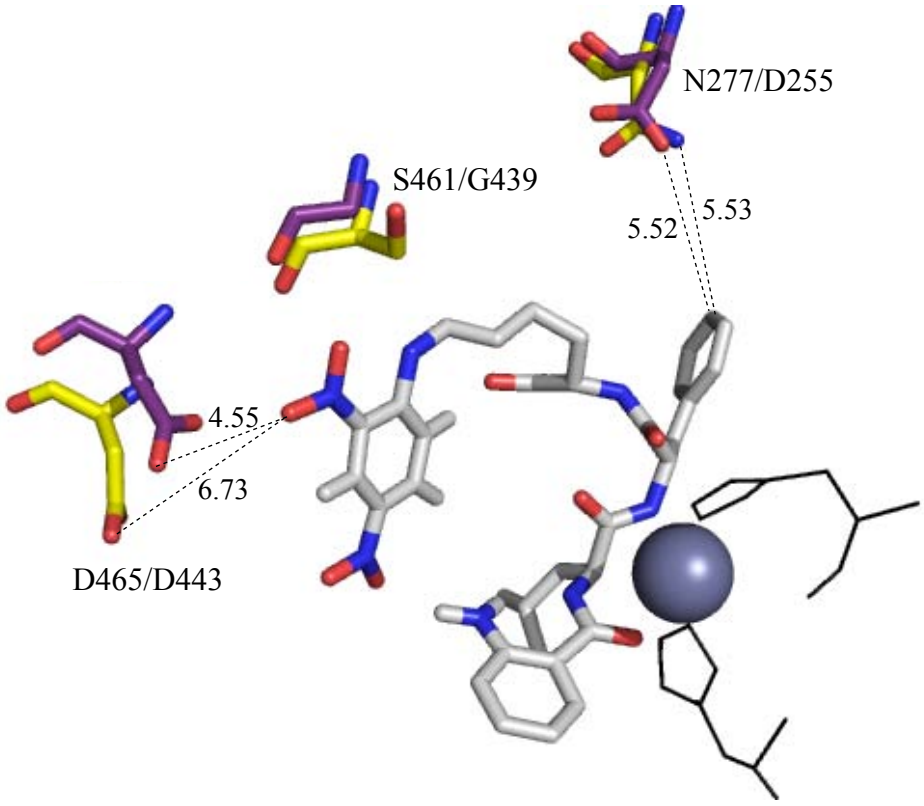

Figure 3.5. **Additional residues that may play a role in the C-domain-specificity of Abz-LFK(Dnp)-OH** (docked model kindly provided by A.T. Nchinda; Bersanetti et al., 2004), aligned to the N-domain structure (PDB code 2c6n). Residues differing between tACE and the N-domain are shown in yellow and purple, respectively. The active-site zinc ion is represented as a grey sphere and two of the zinc-chelating residues are shown as black lines (His 383 and His 387). All distances are given in Å.

N277 is a polar hydrophilic amino acid, which probably does not interact favourably with the substrate P_1' Phe (figure 3.5). The N-domain substitution of an Asp in this position would introduce an acidic, negatively charged amino acid, making the interaction between these residues even less favourable. Replacement of the tACE S461 residue with the N-domain Gly

would decrease the size and hydrophilicity of this residue interacting with the hydrophilic Dnp group (figure 3.5). D443 (N-domain) and D445 (tACE) are approximately 4.6 and 6.7 Å from the oxygens of the Dnp moiety, respectively (figure 3.5). This difference could result in a notably altered orientation of the substrate, which could ultimately lead to a much lowered catalytic efficiency. Support for these ideas would however, require further mutational and kinetic studies, involving converting the tACE or N-domain residues to the corresponding domain counterparts, or for the cases of conserved residues, converting them to amino acids of similar size, but different properties.

3.3.3.2 Hydrolysis of Abz-SDK(Dnp)P-OH

The K_M values obtained for the cleavage of Abz-SDK(Dnp)P-OH by tACE and the N-domain were 7.3 and 7.7, respectively (table 3.3). These results, although slightly lower, are consistent with those reported by Araujo *et al.* (Araujo et al., 2000). A 4.5-fold selectivity was observed for the catalytic activity of the N-domain over that of tACE (tACE , k_{cat} = 0.31 s^{-1}; N-domain, k_{cat} = 1.4 s^{-1}; table 3.3). Araujo et al. (Araujo et al., 2000) found that N-selectivity is increased for fluorogenic peptides with a Ser and Asp in the P_2 and P_1 positions, respectively, while residues differing in the P_1' and P_2' positions had minimal effect on N-specificity. This led us to test the hydrolysis of Abz-SDK(Dnp)P-OH with the S_2 and S_1 pocket mutants described above (table 3.3). Again, the K_M values were similar for all the proteins tested (table 3.3), however no increase in k_{cat} from that of tACE was observed (table 3.3). Therefore the modest 4.5-fold selectivity of Abz-SDK(Dnp)P-OH for the N-domain may be due to other factors such as access of the peptide to the active-site and/or interactions of the peptide elsewhere in the active-site or in the remainder of the protein (discussed above).

Table 3.3. **Kinetic constants for the cleavage of the N-domain-specific Abz-SDK(Dnp)P-OH FRET peptide by ACE constructs.** Cleavage of Abz-SDK(Dnp)P-OH by a series of tACE mutants and the wild-type tACE and N-domain constructs was analysed. Initial velocities for each substrate concentration were determined in triplicate, and kinetic constants were calculated using the direct linear plot method (Eisenthal and Cornish-Bowden, 1974).

Mutant	Abz-SDK(Dnp)P-OH	
	K_M(μM)	k_{cat} (s^{-1})
tACE	7.3	0.31
Ndom	7.7	1.4
E403R	4.1	0.18
F391Y	10.9	0.22
S516N	15.2	0.17
S517V	11.5	0.14
V518T	9.7	0.57

The 4-fold N-selectivity of Abz-SDK(Dnp)P-OH determined in this study was dramatically lower than the 250-fold selectivity reported by Araujo *et al.* (Araujo et al., 2000). A number of factors can explain this discrepancy. Firstly, there were some differences in the method employed for the reaction, such as the temperature at which the reactions were performed (37°C by Araujo *et al.* compared to 25°C in this work), and the use of cuvettes with final volumes of 2 mL (Araujo *et al.*) versus white 96 well plates using final volumes of 300 μL. However, repeating these assays using similar techniques to those employed by Araujo *et al.* (Araujo et al., 2000) yielded similar results to those obtained in table 3.3 (results not shown). Secondly, the mutant proteins used in each study were different; Araujo *et al.* used full-length proteins with an inactivated domain, while we used soluble single domains (described in 2.1 and 3.2.5). Furthermore, work demonstrating the N-specificity of the naturally occurring ACE substrate, AcSDKP, was also performed on full-length ACE mutants containing one of the two catalytic sites inactivated (Rousseau et al., 1995). This suggests that the marked selectivity observed by Araujo *et al.* (Araujo et al., 2000) and Rousseau *et al.* (Rousseau et al., 1995) for Abz-SDK(Dnp)P-OH and AcSDKP, respectively, may be partly due to interactions between the two domains of ACE as evidenced by a high degree of co-operativity previously observed between the domains (Ehlers and Riordan, 1991; Binevski et al., 2003; Woodman et

al., 2005; Skirgello et al., 2005; Andújar-Sánchez et al., 2007;), rather than specific residues within the active-site that seem to contribute only slightly (table 3.3).

Araujo *et al.* (Araujo et al., 2000) reported that Abz-SDK(Dnp)P-OH, containing Abz and Dnp moieties, was hydrolysed more efficiently than the naturally occurring N-domain-specific substrate, AcSDKP (Rousseau et al., 1995; Araujo et al., 2000). This result was not confirmed in this work, since the catalytic efficacy of ACE for Abz-SDK(Dnp)P-OH was markedly lower than that reported by Araujo *et al.* (Araujo et al., 2000). Structure-function studies were also performed by Michaud et al. (Michaud et al., 1999), substituting the N-terminal acetyl-Ser with a BzGly. This substrate demonstrated a 5-fold lower N-selectivity (k_{cat} / K_M) compared to that of AcSDKP, however, this change was mainly attributed to an increased K_M and only slightly increased k_{cat}. Further work is being performed by another member of our group (R. G. Douglas) to investigate these phenomena.

3.4 Summary

In summary, all of the active-site mutant proteins were successfully expressed and isolated. Particular tACE active-site mutants were analysed with the FRET peptides Abz-LFK(Dnp)-OH (C-domain-selective) and Abz-SDK(Dnp)P-OH (N-domain-selective). Comparable K_M values were obtained amongst the different peptides for those tACE constructs tested, while some variation was observed with the k_{cat} results. However, for the two domain-selective substrates, no shift in k_{cat} was equivalent to that of the N-domain from tACE. Therefore the selectivity of these substrates is probably a result of a combination of factors, such as active-site residues as well as interactions elsewhere in the protein.

Chapter 4: Kinetic Characterisation of tACE Proteins

4.1 Introduction

Although the C- and N-domains of ACE display almost 60 % sequence identity, they have demonstrated a number of interesting differences, particularly in their substrate and inhibitor specificities. Over the past decade, a number of highly domain-selective ACE inhibitors have been described. These include two phosphinic peptide inhibitors, RXP407 and RXPA380 (Dive et al., 1999; Georgiadis et al., 2003), two keto-ACE derivatives, kAW and kAF (Redelinghuys et al., 2006), and the lisinopril analogue lis-W (Nchinda et al., 2006a) (figure 1.8).

Dive *et al.* have described two phosphinic inhibitors, RXP407 and RXPA380, each demonstrating a selectivity of three orders of magnitude for the N- and C-domains, respectively (Dive et al., 1999; Georgiadis et al., 2003). The selectivity of RXP407 has been attributed to three structural features of this compound: the presence of a carboxyamide group on the P_2' Ala, an aspartic acid moiety in the P_2 position, and the presence of an acetyl group on this N-terminal Asp (Dive et al., 1999). Structure-function studies of RXPA380 analogues revealed that the P_2' Trp played an important role in the marked C-selectivity of this inhibitor (Georgiadis et al., 2004). More recently, crystallographic data has provided evidence that the hydrophobic interaction of the P_2 Phe with the S_2 F391 residue could also play a critical role in the domain specificity of RXPA380 (Corradi et al., 2007). These two phosphinic peptide inhibitors were therefore used to probe the importance of the S_2 and S_2' sub-sites in ACE domain selectivity.

Keto-ACE is an analogue of the tripeptide ACE substrate, Bz-Phe-Gly-Pro (Weare et al., 1981), which binds the catalytic zinc ion of ACE via its ketone group. It displays inhibition in the nanomolar range, with a modest 30- to 40-fold C-domain selectivity believed to reside in its bulky P_1 moiety and the benzyl substituent in the P_2 position (Acharya et al., 2003; Deddish et al., 1998). Using keto-ACE as a platform, our group has synthesised a number of novel derivatives containing modified P_1' and P_2' substituents (Nchinda et al., 2006b). Two of these compounds, kAW and kAF, containing P_2' Trp and Phe substituents, respectively, have

demonstrated some interesting C-selectivity (Redelinghuys et al., 2006). These three inhibitors are all similar in structure differing only at their P_2' substituent, and therefore providing some interesting tools to investigate particular interactions between the P_2' substituent and S_2' residues such as V379 (tACE numbering). Furthermore, although it has a ketone zinc binding group, versus the phosphinic group of RXPA380, kAW has similar P_2, P_1 and P_2' substituents to those of RXPA380. Therefore, comparison of results between these two inhibitors could provide important insights into the effects of the different zinc co-ordinating moieties versus the sub-site pocket side-chains.

Lisinopril is a potent ACE inhibitor widely used for the treatment of hypertension and CVD. This compound was also used by our group as a platform to develop more domain-selective inhibitors of ACE. Substitution of the P_2' group with a Trp moiety results in two enantiomers, *S*- and *R*-lis-W (figure 4.1). Previous work reported the *S*-isomer displaying more potent inhibition of tACE compared to that of the *R*-isomer (Nchinda et al., 2006a). Moreover, attempts to crystallise *R*-lis-W complexed with tACE resulted in ACE co-crystals containing the *S*-enantiomer within the active-site (Watermeyer, 2008). This suggests that the C-domain active-site selected for the *S*-isomer, which could have been present in trace amounts in the purified *R*-lis-W solution. Watermeyer suggested that occlusion of the *R*-enantiomer is probably caused by steric hindrance between the alcohol group of Y523 and the β carbon of the P_1 Phe (Watermeyer, 2008). This selection is consistent with previous reports of ACE inhibitors containing an *S*-configuration in this position displaying markedly higher affinities over their *R*-counterparts (Brenner et al., 1990; Stefan et al., 1998). Furthermore, this configuration is consistent with the L-amino acid chirality observed in biological peptides.

The aim of this work was to gain a better understanding of the molecular basis to ACE domain selectivity. This panel of inhibitors provides an excellent tool to characterise important interactions by analysing the effect of binding to tACE active-site mutants containing relevant N-domain substitutions. The results of these studies provide useful insight into specific residues driving the domain selectivity of ACE.

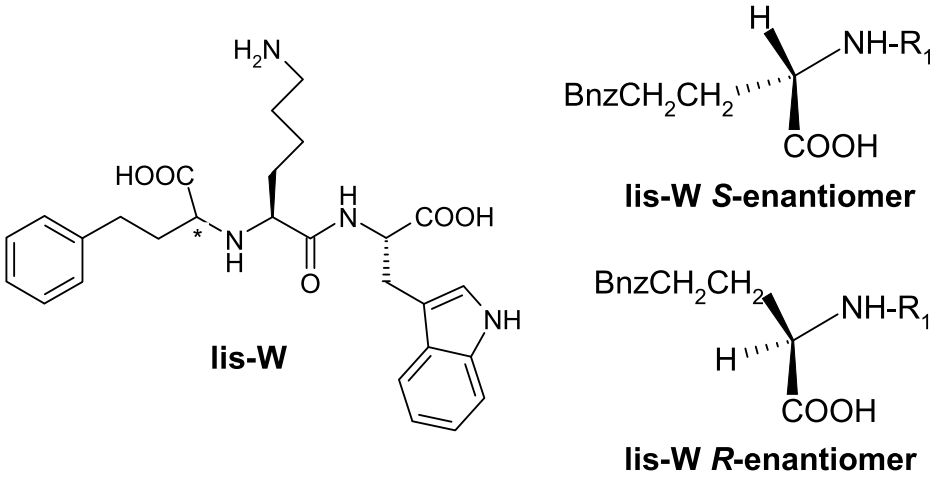

Figure 4.1. **The *S*- and *R*-enantiomers of lis-W.** The star indicates the chiral centre concerned, and R_1 represents the remainder of lis-W (the P_1' and P_2' substituents).

The objectives of the present work were therefore to:

1. Characterise the hydrolysis of the non-domain-specific fluorogenic peptide Abz-FRK(Dnp)P-OH by mutant constructs.
2. Perform kinetic characterisation of the panel of domain-selective inhibitors, using tACE mutant proteins containing active-site substitutions potentially forming interactions conferring selectivity.

4.2 Experimental procedures

4.2.1 Chemicals

Acetonitrile (ACN) was purchased from Burdick and Jackson, and trifluoroacetic acid (TFA) was supplied by Merck.

4.2.2 Preparation of Abz-FRK(Dnp)P-OH

Fluorogenic peptides were prepared as described in section 3.2.6.

4.2.3 Preparation of inhibitors

The phosphinic peptide inhibitors RXP407 and RXPA380 were kindly provided by V. Dive (Dive et al., 1999; Georgiadis et al., 2003). Keto-ACE and its derivatives kAW and kAF were

synthesised by A. T. Nchinda (Nchinda et al., 2006b). Lis-W was synthesised by A. Mahajan (Nchinda et al., 2006a) and the *S*- and *R*-isomers were separated by S. L. W. Schwager using high-performance liquid chromatography (HPLC) (section 4.2.4).

Phosphinic peptide inhibitors, lisinopril and lis-W were dissolved in dH_2O, while keto-ACE and its derivatives were dissolved in a small volume of DMSO. An appropriate dilution series was prepared for each inhibitor in FRET assay buffer (section 3.2.6).

4.2.4 Purification of lis-W isomers

The separation of the lis-W enantiomers was achieved by HPLC, using a semi-preparative reversed-phase column (TRACER EXCEL TR-016174 120ODSB, 5 µm, 25 cm x 1 cm; from Teknokroma), with a gradient elution 26-30 % ACN in 0.1 % TFA over 30 min, at a flow rate of 2.5 $mL.min^{-1}$. Peaks were detected at the UV wavelengths 215 and 280 nm. The *R*-isomer eluted at t_R = 27 min, while the *S* counterpart eluted at t_R = 33 min. The structure and purity of the *S*-isomer of lis-W was confirmed by nuclear magnetic resonance, as this was the only isomer found to co-crystalise with tACE (Watermeyer, 2008), and has been shown to be C-domain-selective (Nchinda et al., 2006a).

4.2.4 Fluorogenic assay

The fluorogenic assay was performed using the non-domain-selective peptide Abz-FRK(Dnp)P-OH, as described in section 3.2.6.

4.2.5 Inhibition assay

Approximately 0.2 nM of enzyme was incubated with an appropriate concentration range of inhibitor, at ambient temperature (20 - 25^oC) for 60 min. For inhibitors dissolved in DMSO, the final concentration of this solvent was below 1 %. Twenty µL of this enzyme-inhibitor mixture, was added, in triplicate, to a reaction mixture of 4 or 8 µM Abz-FRK(Dnp)P-OH in FRET assay buffer, to a final volume of 300 µL. Residual enzyme activity was monitored by fluorescence, as described in section 3.2.6.

Inhibition constants were calculated using the Dixon method (Dixon, 1953). Briefly, linear regression curves were plotted on a graph of the reciprocal of initial velocities (v, defined

as < 10 % of substrate hydrolysis) versus inhibitor concentrations, using GraphPad Prism 4.01. The point of intersection, $m_1\alpha + c_1 = m_2\alpha + c_2$, corresponds to the negative K_i value, where m = gradient, α = x co-ordinate and c = y-intercept (figure 4.2).

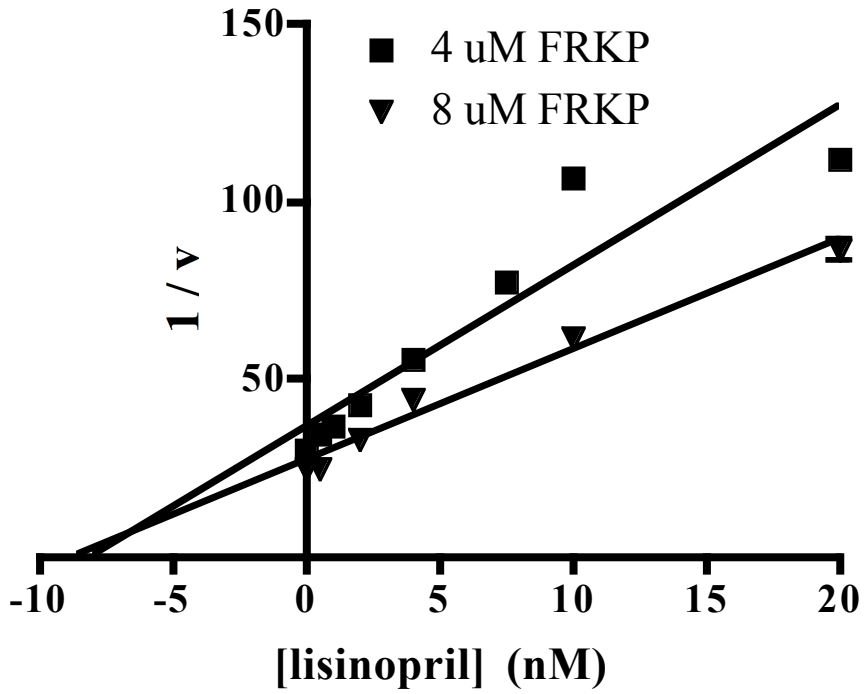

Figure 4.2. **Representative Dixon plot.** N-domain inhibition by lisinopril at two substrate concentrations: 4 (squares) and 8 (triangles) μM Abz-FRK(Dnp)P-OH.

4.3 Results and discussion

Mutant proteins having key residues replaced with their N-domain counterparts (see table 2.1), were characterised using a series of domain-selective inhibitors, with the fluorogenic substrate Abz-FRK(Dnp)P-OH.

4.3.1 Hydrolysis of Abz-FRK(Dnp)P-OH

Abz-FRK(Dnp)P-OH has been shown to display little selectivity between the ACE domains (Araujo et al., 2000) and was therefore used for characterising the interaction of mutants with the domain-selective inhibitors. The C- (tACE) and N-domain constructs demonstrated K_M values of 3.9 and 3.7 μM, respectively, for the hydrolysis of Abz-FRK(Dnp)P-OH, consistent with those reported by Araujo *et al.* (Araujo et al., 2000). All of the mutants displayed similar

K_M values but there was greater variation amongst the k_{cat} values, ranging from 0.6 to 37 s^{-1} for the E376D mutant and TEVVD, respectively (table 4.1).

Table 4.1. **Summary of kinetic constants for the cleavage of the Abz-FRK(Dnp)P-OH FRET peptide by ACE constructs.** Cleavage of Abz-FRK(Dnp)P-OH by a series of tACE mutants as well as the wild-type tACE and N-domain proteins was analysed. Initial velocities for each substrate concentration were determined in triplicate, and kinetic constants were calculated using the direct linear plot method (Eisenthal and Cornish-Bowden, 1974).

Mutant	Abz-FRK(Dnp)P-OH	
	K_M(µM)	k_{cat} (s^{-1})
tACE	3.9	25.6
Ndom	3.7	11.4
E403R	3.7	30.2
F391Y	10.3	4.5
S516N	10.6	3.9
V518T	12.0	6.9
E162D	4.5	22.5
D377Q	4.0	9.2
ED/DQ	6.5	16.5
T282S	5.0	1.2
E376D	9.9	0.6
V379S	5.9	29.6
V380T	10.6	27.0
VV/ST	6.8	33.0
D453E	5.5	5.5
TEVD	26.8	27.7
TEVVD	18.4	36.8
S_2'F	6.7	28.8

4.3.2 Domain selectivity of the phosphinic inhibitors

RXPA380 displayed C-domain-specific inhibition of the hydrolysis of Abz-FRK(Dnp)P-OH, with an approximately 880-fold higher affinity for the C-domain than for the N-domain (table 4.2, figure 4.3). In contrast, RXP407 demonstrated potent inhibition of the N-domain, with a more than 500-fold selectivity over that of the C-domain (table 4.2). Both of these trends are consistent with previously published data (Dive et al., 1999; Georgiadis et al., 2003). The inhibition of the active-site mutants will be discussed in detail under the various sub-sites later in this chapter.

Table 4.2. **Kinetic parameters for the inhibition of ACE activity by RXPA380 and RXP407.** Inhibition constants for wild-type tACE and N-domain, as well as tACE active-site mutants containing corresponding N-domain residue substitutions, using the fluorogenic peptide Abz-FRK(Dnp)P-OH, were determined using the Dixon method (Dixon, 1953).

Construct	Pocket	RXPA380 K_i (nM)	RXP407 K_i (nM)
tACE (C-domain)	-	69	2800
N-domain	-	60900	5.2
F391Y	S_2	2326	1500
E403R	S_2	97.5	1800
V518T	S_1	276	11000
T282S	S_2’	251	n.d.
E376D	S_2’	363	n.d.
V379S	S_2’	36.4	330
V380T	S_2’	462	800
VV/ST	S_2’	177	1100
D453E	S_2’	288	n.d.
TEVD	S_2’	2236	6600
TEVVD	S_2’	1160	760
S_2’F	S_2’ and S_2	5300	16.1

n.d. not determined.

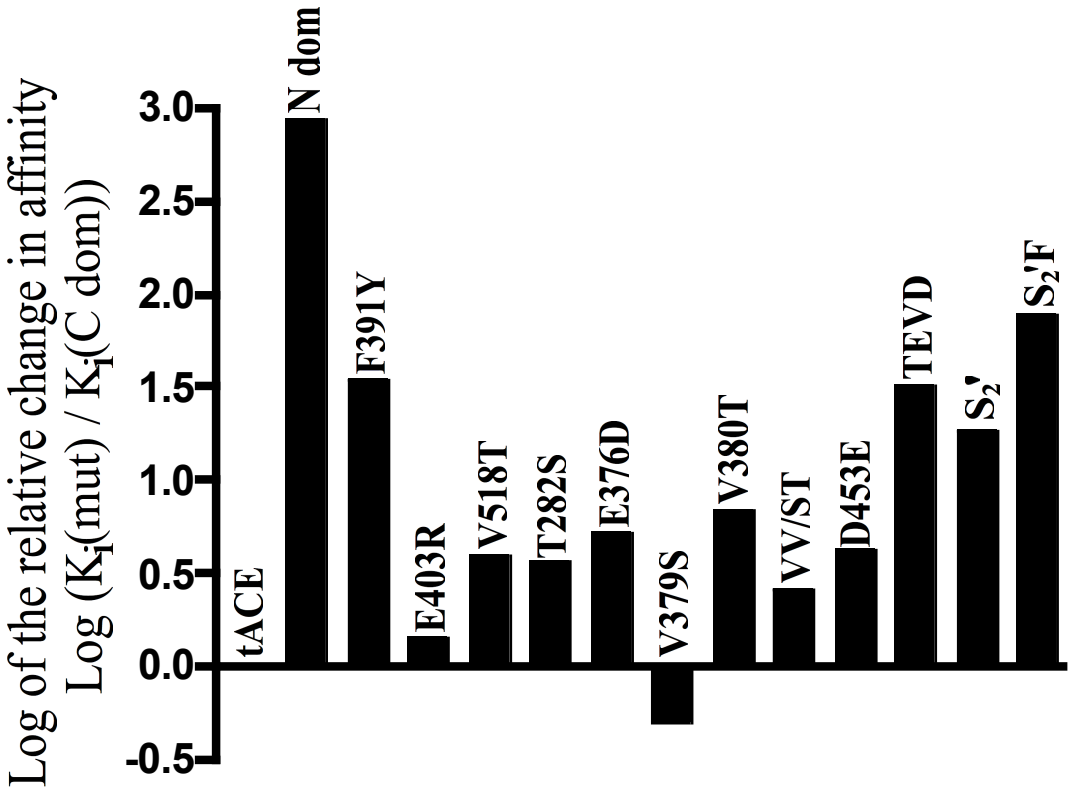

Figure 4.3. **Log scale comparison of the relative binding affinities of tACE active-site mutants for RXPA380 with that of wild-type tACE (C-domain).** Values above zero represent a decrease in affinity relative to that of tACE, towards a more N-domain-like K_i.

4.3.3 Domain selectivity of keto-ACE and its derivatives

Under the conditions described, keto-ACE displayed a 30-fold higher affinity for the C-domain (K_i = 0.05 μM) than for the N-domain (K_i = 1.5 μM, table 4.3). Two novel C-domain-selective keto-ACE derivatives have been developed in our group, kAW and kAF, containing a Trp and Phe residue in the P_2' position, respectively. Due to solubility problems with kAF, a K_i value for the N-domain was not obtainable, however no inhibition was observed up to 500 μM (table 4.3). These inhibitors both demonstrated high domain selectivity under the conditions tested (table 4.3), with kAW and kAF having approximately 1200- and >600-fold higher affinity for the C-domain, respectively (figure 4.4). However, it should be noted that the potency of these inhibitors for the C-domain is approximately 10-fold lower than that obtained for RXPA380 and keto-ACE. The inhibition of the active-site mutants will be discussed in detail under the various sub-sites later in this chapter.

Table 4.3. **Kinetic parameters for the inhibition of ACE activity by keto-ACE, kAW and kAF.** Inhibition constants for wild-type tACE and N-domain, as well as tACE active-site mutants containing corresponding N-domain residue substitutions, using the fluorogenic peptide Abz-FRK(Dnp)P-OH, were determined using the Dixon method (Dixon, 1953).

Construct	Pocket	keto-ACE K_i (μM)	kAW K_i (μM)	kAF K_i (μM)
tACE (C-domain)	-	0.05	0.68	0.83
N-domain	-	1.5	854	>500
F391Y	S_2	0.43	4.8	3.9
E403R	S_2	n.d.	0.24	n.d.
S516N	S_1	0.012	0.50	n.d.
V518T	S_1	1.3	9.7	18.1
T282S	S_2’	n.d.	0.92	n.d.
E376D	S_2’	n.d.	2.3	2.4
V379S	S_2’	n.d.	0.064	0.81
V380T	S_2’	n.d.	2.7	1.9
VV/ST	S_2’	n.d.	0.87	n.d.
D453E	S_2’	n.d.	0.62	n.d.

n.d. not determined.

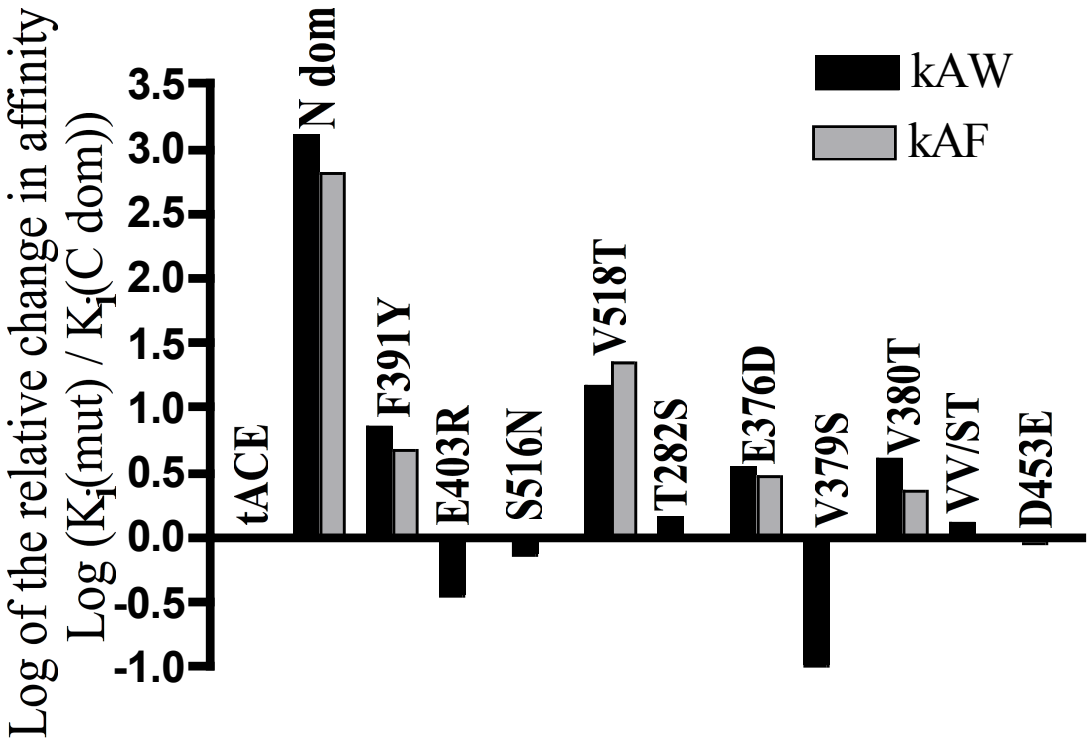

Figure 4.4. **Log scale comparison of the relative binding affinities of tACE active-site mutants for kAW (black bars) and kAF (grey bars), with that of wild-type tACE (C-domain) (adapted from Watermeyer et al., 2008).** Values above zero represent a decrease in affinity relative to that of tACE, towards a more N-domain-like K_i. K_i's were not determined for T282S, VV/ST, D453E, S516N and E403R with kAF as these mutations did not cause a noticeable shift for keto-ACE or kAW (table 4.2).

4.3.4 Domain selectivity of lisinopril and lis-W

Lisinopril is a potent ACE inhibitor, demonstrating modest domain selectivity (tACE K_i = 1.2 nM, N-domain K_i = 4.8 nM; table 4.4). Inhibition by the *S*-enantiomer of lis-W displayed K_i's of 6.6 nM and 1700 nM for tACE and N-domain, respectively (table 4.4, figure 4.5). The inhibition of the active-site mutants will be discussed in detail under the various sub-sites later in this chapter.

Resolution of the tACE–lis-W (*S*-enantiomer) crystal structure revealed lis-W is bound in a very similar conformation to lisinopril within the active-site of tACE, but with a slight deviation in the position of the P_1' lysyl amine (Watermeyer, 2008) (see figure 4.9). Interestingly, the P_2' Trp moiety is in a different orientation than that observed in the RXPA380 and kAW structures. This difference has been attributed to strong entropically favourable hydrophobic interactions between the P_1' Lys and the tACE V380 residue.

Moreover, this new orientation allows the formation of a hydrogen bond interaction between the indole N and D415, a residue that is conserved between domains. In the kAW structure, this N is shown to form hydrogen bond interactions with water molecules within this pocket (Watermeyer et al., 2008; Watermeyer, 2008).

Table 4.4. **Kinetic parameters for the inhibition of ACE by lisinopril and lis-W.** Inhibition constants for wild-type tACE and N-domain, as well as tACE active-site mutants containing corresponding N-domain residue substitutions, using the fluorogenic peptide Abz-FRK(Dnp)P-OH, were determined using the Dixon method (Dixon, 1953).

Construct	Pocket	lisinopril K_i (nM)	lis-W K_i (nM)
tACE (C-domain)	-	1.2	6.6
N-domain	-	4.8	1700
F391Y	S_2	n.d.	9.7
V518T	S_1	1.6	8.7
E162D	S_1’	0.83	8.5
D377Q	S_1’	1.3	17.5
ED/DQ	S_1’	0.89	26.5
T282S	S_2’	n.d.	10.3
E376D	S_2’	n.d.	24.8
V379S	S_2’	n.d.	2.1
V380T	S_2’	0.3	1.1
VV/ST	S_2’	0.7	9.5
D453E	S_2’	n.d.	15.6
TEVD	S_2’	n.d.	75.4
TEVVD	S_2’	n.d.	104.6

n.d. not determined.

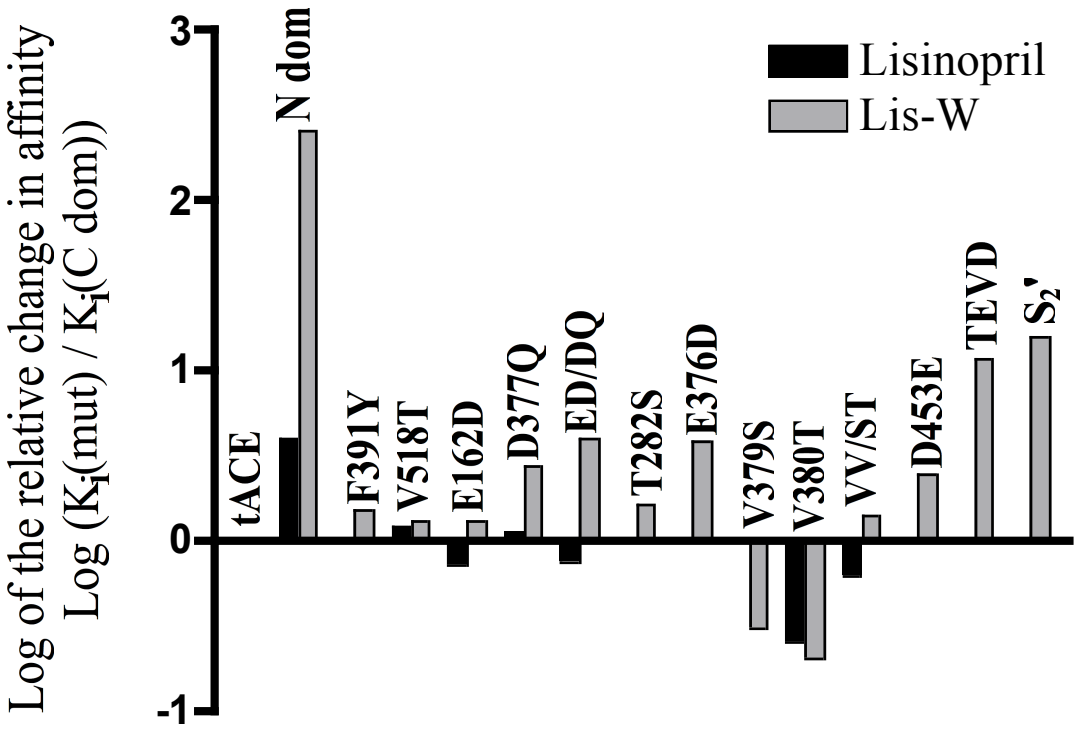

Figure 4.5. **Comparison of the relative binding affinities of tACE active-site mutants for lisinopril (black bars) and lis-W (grey bars) with that of wild-type tACE (C-domain).** Values above zero represent a decrease in affinity relative to that of tACE, towards a more N-domain-like K_i. K_i's were not determined for F391Y, T282S, E376D, V379S, D453E, TEVD and TEVVD with lisinopril, as these residues were not expected to play a role in lisinopril binding.

4.3.5 Roles of tACE active-site residues in the selectivity of C-domain-selective inhibitors

In order to gain a better understanding of the roles of the various active-site residues in inhibitor binding, we tested these selective inhibitors against the mutants generated.

4.3.5.1 Roles of S_2 residues

The highest shift in K_i observed for the single mutations when tested with RXPA380 was a 34-fold increase from that of tACE (K_i = 69 nM) for F391Y (K_i = 2326 nM; table 4.2, figure 4.3). This mutant protein also demonstrated a considerable decrease in affinity for keto-ACE and its derivatives, relative to that of tACE (table 4.3, figure 4.3). The E403R mutant displayed no change in affinity for the inhibitors tested, kAW or RXPA380, compared to that of wild-type tACE (tables 4.2 and 4.3, figures 4.3 and 4.4).

The tACE-RXPA380 crystal structure (PDB code 2oc2) revealed a hydrophobic interaction between the inhibitor P_2 Phe and F391 of tACE in the S_2 pocket (Corradi et al., 2007). This interaction seems to be responsible for positioning the inhibitor optimally within the active-site, and would be lost in the N-domain where this residue is replaced by Y369 (figure 4.6A). Moreover, the hydroxyl group of this Tyr may result in steric hindrance with the inhibitor Phe, which could result in RXPA380 adopting a different orientation within the N-domain active-site (figure 4.7). Therefore, based on the X-ray crystal structure and mutational and kinetic analysis, it is likely that F391 makes a critical contribution to the C-domain specificity of RXPA380.

The structures of tACE in complex with kAW (PDB code 3bkl) and kAF (3bkk) revealed hydrophobic contacts between the inhibitor P_2 group and F391 (figure 4.6B and C, respectively) (Watermeyer et al., 2008). The hydroxyl group introduced into this pocket by the N-domain Y369 would result in steric hindrance with the binding of keto-ACE (or its derivatives) containing a benzoyl moiety in this position, reducing the affinity with which these inhibitors would bind.

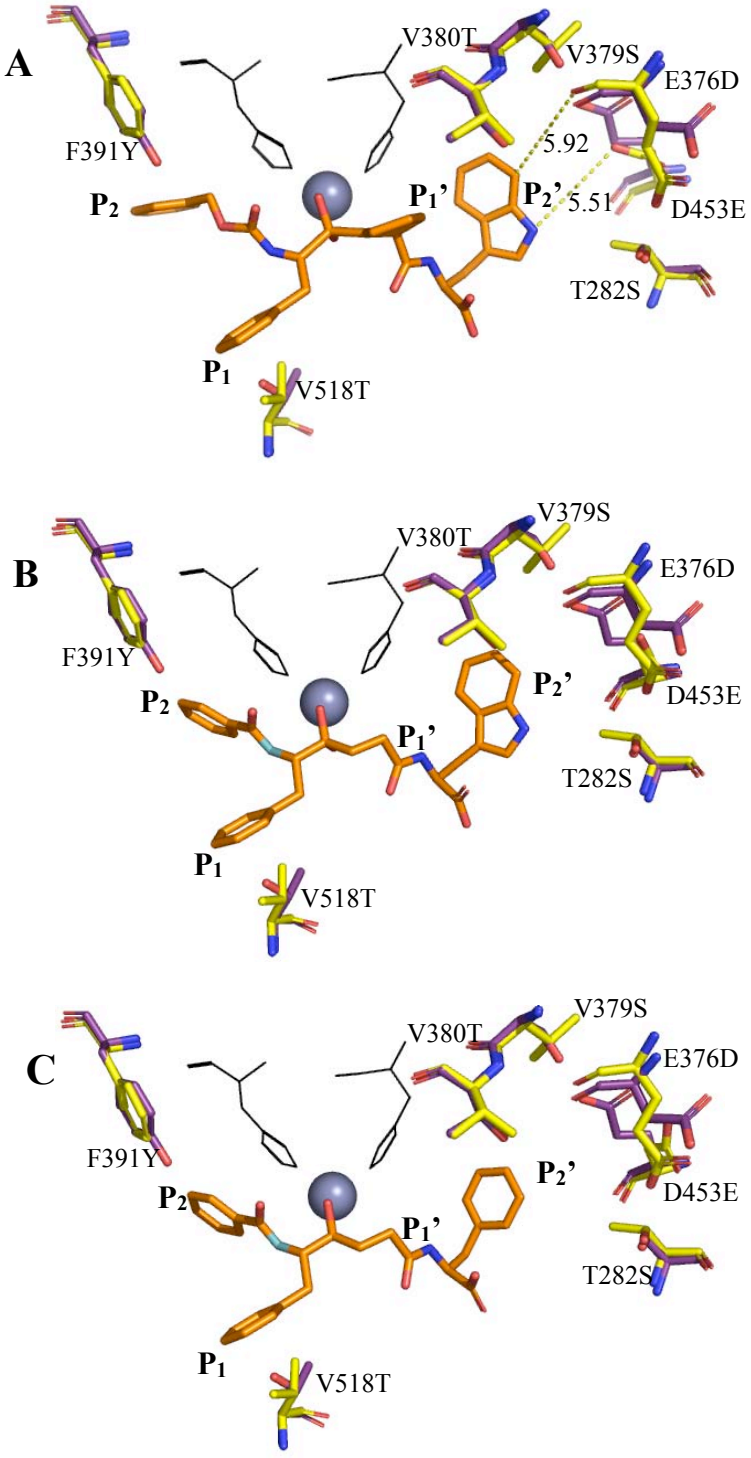

Figure 4.6. **Stick representation of inhibitors A) RXPA380 (PDB code 2oc2) (Corradi et al., 2007), B) kAW (3bkl) (Watermeyer et al., 2008) and C) kAF (3bkk) (Watermeyer et al., 2008) within the tACE active-site, aligned with the N-domain (2c6n).** Particular residues differing between tACE and the N-domain are shown in yellow and purple sticks, respectively. The active-site zinc ion is represented by a grey sphere, and two of the two zinc-chelating residues (H383 and H387) are shown in black lines. All distances are given in Å. Images were created using MacPyMOL 0.99 (DeLano Scientific, Palo Alto, CA, U.S.A).

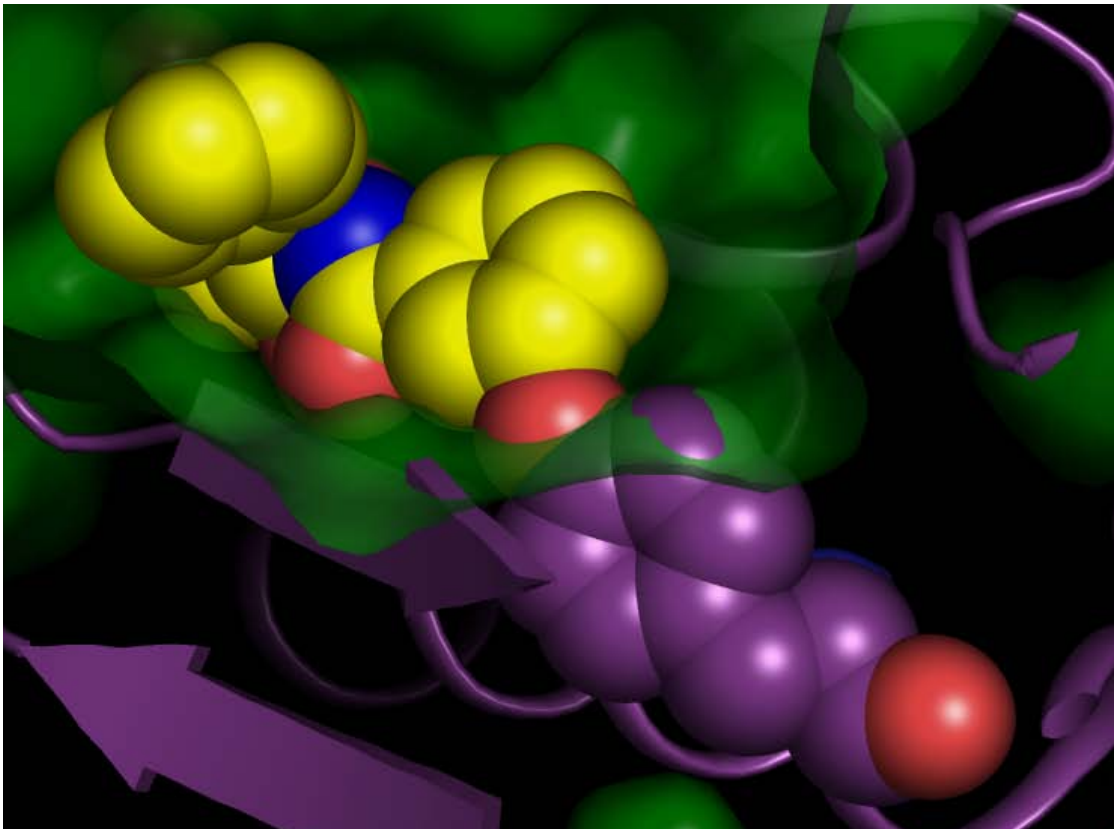

Figure 4.7. **Sphere representation of RXPA380 (yellow carbons) and N-domain Y369 (purple carbons).** Red and blue spheres represent oxygen and nitrogen, respectively. Surface representation of the N-domain represented in green. This model was obtained by aligning the N-domain-lisinopril structure (PDB code 2c6n) with the tACE-RXPA380 co-crystal structure. It is clear from this diagram that there may be steric clash within this pocket (S_2), which would probably result in the inhibitor adopting a different orientation within the N-domain.

4.3.5.2 Roles of S_1 residues

For keto-ACE, the V518T mutation (K_i = 1.3 μM) caused a marked decrease (26-fold) in affinity, resulting in a K_i equivalent to that of the N-domain (K_i = 1.5 μM; table 4.3). Notable decreases in affinity were also observed for kAW and kAF (table 4.3, figure 4.4), while a slight decrease (4-fold) and no change in affinity were displayed for RXPA380 (table 4.2, figure 4.3) and lis-W (table 4.4, figure 4.5), respectively. The S516N mutant displayed no change in affinity for kAW and the phosphinic inhibitor RXPA380, while a slight increase in affinity was observed with keto-ACE (tables 4.2 and 4.3, figures 4.4 and 4.5).

Substitution of Val with a Thr in the V518T mutant protein is unlikely to cause any steric hindrance within this pocket; however, the N-domain T496 would decrease the

hydrophobicity of this pocket, which could result in less favourable binding of keto-ACE and its derivatives (figures 4.6B, 4.6C and 4.8) (Watermeyer et al., 2008).

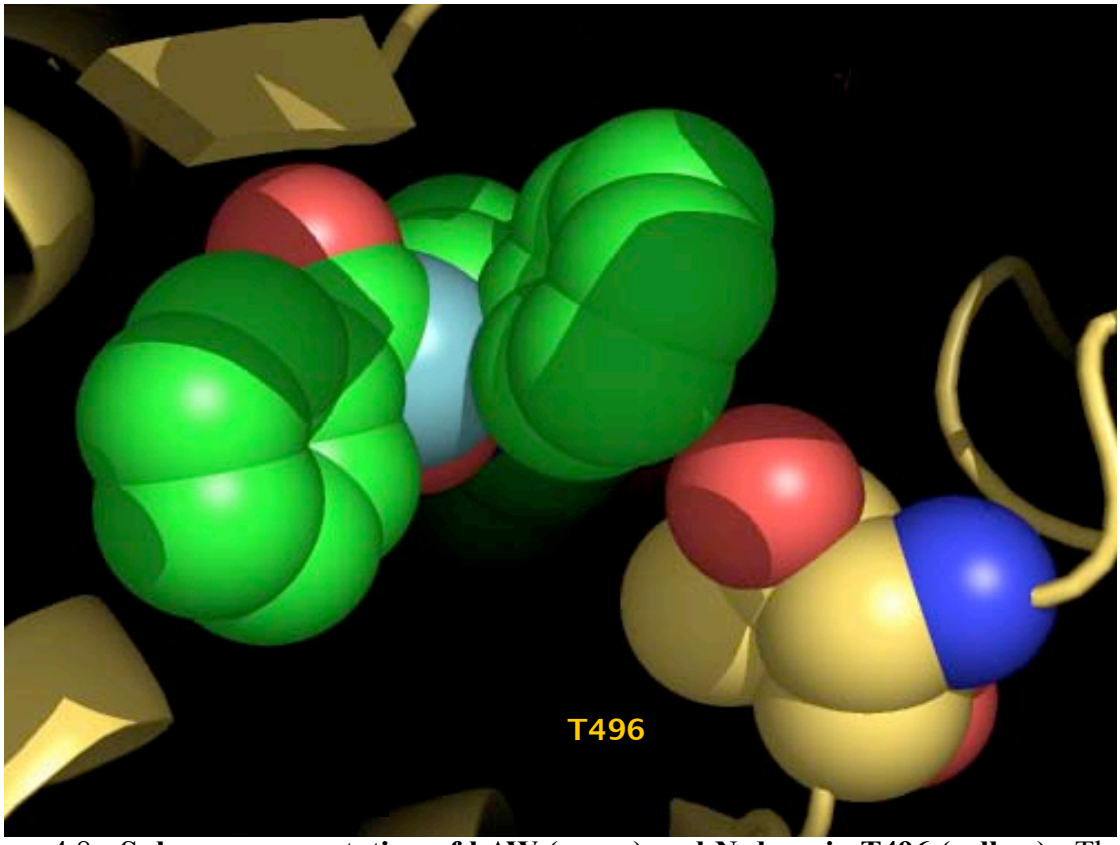

Figure 4.8. **Sphere representation of kAW (green) and N-domain T496 (yellow).** The N-domain-lisinopril structure (PDB code 2c6n) was aligned to the tACE-kAW co-crystal structure (3bkl). It is clear from this diagram that there may be unfavourable interactions within this pocket (S_1) due to the increased hydrophilicity caused by the Val to Thr substitution (V518T). This could result in the inhibitor binding with a markedly lower affinity, as evidenced by the change in K_i's (table 4.3).

4.3.5.3 Roles of S_1' residues in lisinopril and lis-W binding

Interestingly, the S_1' mutations E162D, D377Q and the double mutant ED/DQ (see table 2.1) had no effect on the minor C-selectivity of lisinopril (table 4.4, figure 4.5). The E162D construct also showed no difference for the highly C-selective lis-W, however the D377Q and ED/DQ mutations caused slight increases in K_i's (2.7- and 4-fold, respectively; table 4.4, figure 4.5).

Although the resolution of the N-domain-lisinopril structure is limited, it does imply a slightly different backbone confirmation for the P_1' lysyl side-chain compared to that within the tACE

complex (Natesh et al., 2003; Corradi et al., 2006). It has been suggested that the mild C-domain selectivity demonstrated by this inhibitor could be attributed to the electrostatic interaction between the lysyl amine and D162, which is assumed to be lost in the N-domain where the distance between these two groups is 6.5 Å (Corradi et al., 2006). However, no shift in affinity was observed with the E162D mutant (table 4.4, figure 4.9). This observation could be explained in two ways. Firstly, scaffolding residues surrounding E162 in tACE (and Asp in the E162D mutant) may hold this residue in a conformation or position that facilitates ideal electrostatic interaction with the inhibitor, while residues supporting D140 in the N-domain do not enable such interactions. Secondly, this N-domain Asp residue (in E162D) is still located on the tACE backbone which does display small differences in conformation in this region when aligned to the N-domain backbone. Therefore the proximity of this Asp in tACE E162D to the lysyl amine in this protein may still be close enough for the occurrence of favourable electrostatic interactions. Hence, E162 may contribute towards lisinopril's C-selectivity, however crystallographic data of E162D would provide conclusive evidence in this regard. A similar result was obtained for lis-W, however the selectivity of this inhibitor is probably more reliant on the P_2' Trp (discussed below).

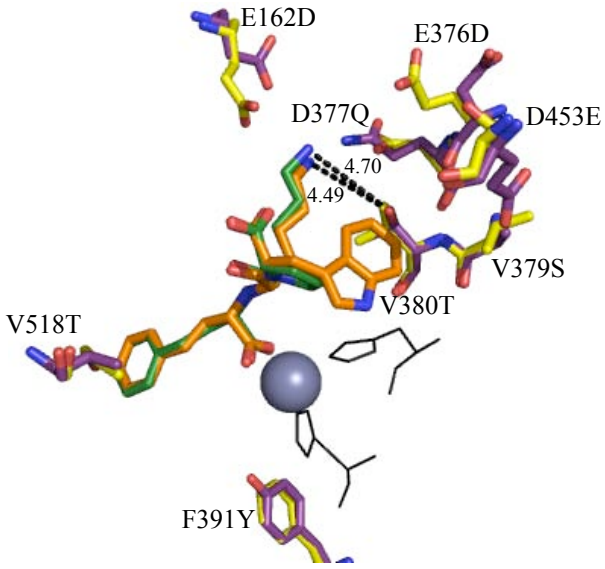

Figure 4.9. **Stick representation of lisinopril (green, PDB code 1o86) and lis-W (orange) (Watermeyer, 2008) within the active-site of tACE, aligned with the N-domain (2c6n).** Residues differing between tACE and the N-domain are shown in yellow and purple sticks, respectively. The active-site zinc ion is represented by a grey sphere, and two of the three zinc-chelating residues (H383 and H387) are shown in black lines. Distances between the inhibitor S_1' amide and V380T are given in Å.

D377 in tACE has been shown to establish favourable water-mediated interactions with lisinopril's P_1' lysine (figure 4.9) (Natesh et al., 2003; Corradi et al., 2006). The presence of these water molecules in the N-domain-lisinopril structure was not apparent owing to the lower resolution of the structure obtained (Corradi et al., 2006), therefore it is not clear whether this residue plays a role in the slight C-selectivity of lisinopril, but because of the lack of any shift in K_i for this mutant (D377Q; table 4.4) it is likely that it plays a negligible role. The minor shift observed for this mutant with lis-W from that of tACE (table 4.4), may be due to the effect of the P_2' Trp. The presence of this hydrophobic moiety may occlude water molecules needed for this interaction, thereby decreasing the binding affinity to this mutant (figure 4.9).

4.3.5.4 Roles of S_2' residues in binding of inhibitors containing a P_2' Trp or Phe

For most of the single S_2' mutants (and double mutant VV/ST), only slight decreases in affinity were observed, if any. The highest shifts in affinity for RXPA380 and the keto-ACE derivative inhibitors within this pocket were displayed by V380T and E376D (tables 4.2 and 4.3, figures 4.3 and 4.4). Lis-W also displayed a decrease in K_i for the E376D mutant, however a slight increase in affinity was observed for V380T with this inhibitor, a result similar to that obtained for its parent molecule, lisinopril (table 4.4, figure 4.5). The V379S mutation caused an unexpected decrease in K_i from that of the C-domain for all of the C-selective inhibitors containing a P_2' Trp: RXPA380 (table 4.2, figure 4.3), kAW (table 4.3, figure 4.4) and lis-W (table 4.4, figure 4.5). Moreover, an N-domain mutant S357V (kindly provided by R. G. Douglas), which is a soluble N-domain construct containing the corresponding tACE V379 residue in position 357, displayed a K_i of 320 μM for RXPA380 (result not shown), demonstrating a decrease in affinity for this inhibitor compared to that of the N-domain. These data confirm the unexpected observation seen with the tACE V379S mutant, that a Ser in this position favours the binding of a Trp moiety.

The decrease in affinity demonstrated by V380T with RXPA380 is probably due to the decreased hydrophobicity resulting from the Val to Thr conversion (Figure 4.6). Similar changes in affinity were observed for kAW and kAF. The relatively minor shifts displayed by mutations within this pocket are probably due to the excess space available between the inhibitor and the S_2' residues. For example, in the tACE-RXPA380 structure (Corradi et al.,

2007), E376 and D453 are 5.9 and 5.5 Å from the RXPA380 Trp, respectively (figure 4.6A). It can therefore be suggested that the design of compounds with more extensive non-polar or negatively charged P_2' substituents could potentially lead to considerably increased domain-specific inhibition due to favourable hydrophobic or electrostatic interactions with the tACE S_2' pocket. Furthermore, it is important to note that the architecture of the S_1' and S_2' pockets together essentially form a continuous chamber within the active-site. This therefore allows for even more latitude for positioning of P_1' and P_2' moieties.

For lisinopril and lis-W, V380T caused 4- and 6-fold increases in affinity, respectively (table 4.4). A closer look at the alignment of the crystal structures of these two inhibitors in complex with tACE, with the crystal structure of the N-domain (Natesh et al., 2003; Corradi et al., 2006; Watermeyer, 2008) revealed that the N-domain Thr was 4.7 and 4.5 Å from the inhibitors' P_1' lysyl amine groups, for lisinopril and lis-W respectively (figure 4.9). Being within 5 Å, these side-chains would therefore be able to form favourable water-mediated interactions, which could account for this increase in affinity.

Interestingly, the V379S mutation caused an increase in affinity for all of the inhibitors containing a Trp in the P_2' position - a result that was contrary to that expected with a P_2' decrease in hydrophobicity. Although this result is not readily explained by the crystal structures (Corradi et al., 2006; Corradi et al., 2007; Natesh et al., 2003; Watermeyer et al., 2008), it may be a consequence of a water-mediated hydrogen bond interaction between the Ser and indole N of the P_2' Trp, facilitated by rotation about the RXPA380 χ_1 and χ_2 bonds of the P_2' substituent (figure 4.10). Support for this theory is provided by the fact that no change in affinity is observed for the V379S mutant with the C-domain-selective inhibitor kAF, containing a Phe in this position and therefore lacking a hydrogen-bond acceptor. This idea is further emphasised by the decrease in affinity displayed by the N-domain S357V mutant for RXPA380 (K_i = 320 μM). This N-domain construct lacks a potential hydrogen-bond donor group in this position as a result of the tACE Val substitution.

To further understand the results obtained with the single S_2' mutants (see table 2.1), two multiple S_2' mutant proteins were generated: one containing an N-domain S_2' pocket (TEVVD), where all the unique C-domain residues were substituted by their corresponding

N-domain counterparts, and a similar protein lacking the V379S mutation (TEVD). For RXPA380, the TEVD mutant demonstrated a 32-fold decrease in affinity from tACE, compared to the 16-fold decrease displayed by the full N-domain S_2' pocket construct, TEVVD (table 4.2, figures 4.4 and 4.6). Hence, the introduction of a Ser in the V379 position to the TEVD construct (TEVVD) caused a smaller change in affinity from tACE than that of TEVD, which is not surprising given the result of the single V379S mutation. Therefore, the presence of a Val in position 379 of tACE (or 357 in the N-domain) seems to decrease the affinity for RXPA380, while the presence of a Ser in this position causes the opposite effect.

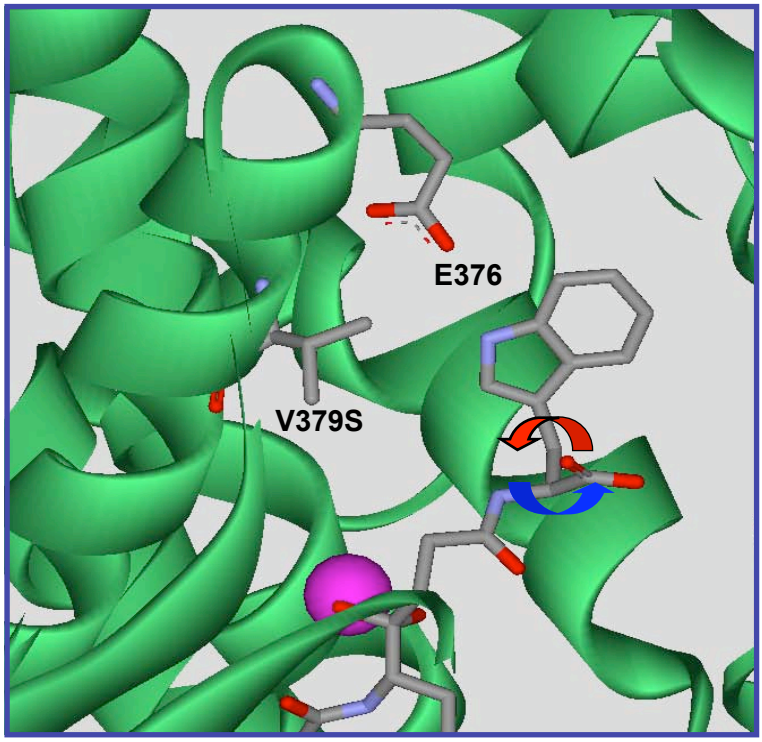

Figure 4.10. **Stick representation of RXPA380 within the active-site of tACE (green cartoon).** The zinc ion is represented as a purple sphere, and residues V379 and E376 are indicated. In the V379S mutant, rearrangement of protein and inhibitor side-chains within the S_2' pocket (indicated by the red and blue arrows) could allow for the formation of water-mediated interactions to occur between the indole N of the inhibitor Trp and the Ser residue. This effect could result in an increased affinity for RXPA380 by this mutant compared to tACE. This image was created in Discovery Studio version 1.6 (Accelrys, Cambridge, UK).

This effect was not displayed by lis-W. A marked increase in K_i was observed for both the TEVD and TEVVD constructs, the more considerable shift being demonstrated by the full S_2' mutant, TEVVD (16-fold from tACE versus 11-fold for that of TEVD) (table 4.4, figure 4.5). Therefore, it is interesting that the V379S mutation alone causes an increase in affinity for lis-

W, as observed with RXPA380, while combined with the N-domain-like S_2' pocket it facilitates a decrease in binding. This could perhaps be explained by a combined effect of the complete N-domain-like S_2' pocket and the different positioning of the P_2' Trp of lis-W compared to that of RXPA380, evident from the two crystal structures, not allowing the rearrangement of residues to facilitate the formation of a water-mediated hydrogen bond interaction (discussed above).

4.3.5.5 Effect of a combined N-domain S_2' pocket and F391Y mutation on RXPA380 binding

The tACE protein S_2'F, containing N-domain S_2' pocket residues (as for mutant TEVVD) as well as the S_2 F391Y mutation (see table 2.1), was used to investigate the combined contribution of these two sub-sites to domain selectivity. S_2'F demonstrated an approximately 80-fold decrease in affinity for RXPA380 over tACE, the largest shift observed among all the mutants (table 4.2, figure 4.6A).

The N-domain K_i for RXPA380 was however approximately 10 times higher than that of the S_2'F construct. This suggests that residues within the other pockets of the active-site might also contribute to the overall selectivity of this inhibitor, for example V518. Furthermore, there may be additional indirect factors that play a role in the marked specificity of RXPA380, such as scaffolding residues affecting the conformation or positioning of conserved residues important for selective binding of inhibitors.

Interestingly, this phenomenon has been demonstrated with cyclic nucleotide phosphodiesterases (PDEs) 4 and 7 (Wang et al., 2005). PDEs contain conserved catalytic domains involved in the hydrolysis of cyclic adenosine monophosphate (cAMP) and cyclic guanosine monophosphate (cGMP) (Antoni, 2000; Carvajal et al., 2000), and although PDE4 and 7 both show a preference for the hydrolysis of cAMP, PDE4-selective inhibitors are not able to block PDE7 hydrolysis (Gardner et al., 2000; Hetman et al., 2000). To elucidate this selectivity, Wang *et al.* mutated key residues within PDE7 and analysed their effect on binding of rolipram, a PDE4-specific inhibitor (Wang et al., 2005). They found that only the combined effect of multiple residues caused a shift in rolipram-selectivity of PDE7 to that of wild-type PDE4. Most interestingly however, this combination included substitution of a

scaffolding residue (Y329 in PDE4, S373 in PDE7) interacting with an amino acid conserved between these enzymes (N369/413 in PDE4/7). The PDE4-rolipram crystal structure revealed that Y329 stabilises the Q369 side-chain via a hydrogen bond interaction (figure 4.11) (Huai et al., 2003). Substitution of this Tyr with S373 in PDE7 results in the hydrogen bond interaction occurring with S377, displayed in the PDE7A1-IBMX structure (PDE7 in complex with a non-selective PDE inhibitor), thus changing the positioning of the Gln side-chain and probably abolishing the hydrogen bond interaction with rolipram (figure 4.12) (Wang et al., 2005). To investigate the potential for this phenomenon contributing to ACE domain selectivity, a detailed analysis of scaffolding residues supporting invariant residues known to be important for inhibitor binding would be required. This would need to be followed by mutational and kinetic studies of constructs containing a combination of active-site substitutions, as well as scaffolding residues identified to potentially play a role in inhibitor selectivity.

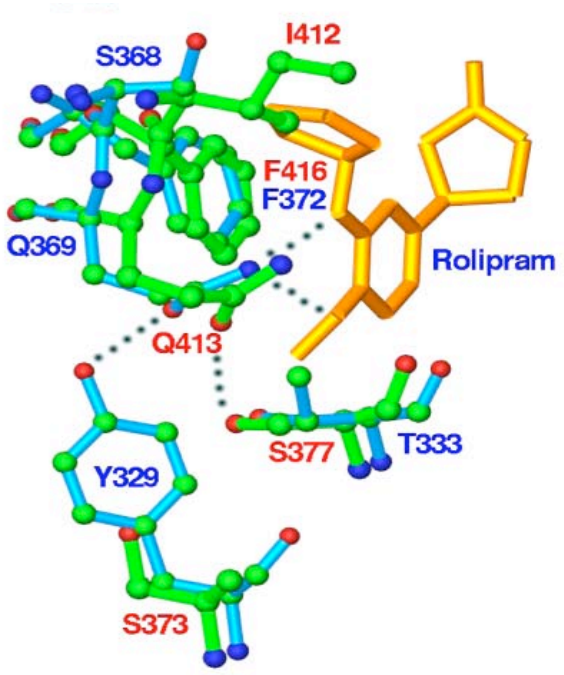

Figure 4.11. **Stick representation of rolipril (yellow) within the active-site of PDE4 (PDB code 1oyn) aligned with PDE7A1 (1zkl)** (taken from (Wang et al., 2005)). PDE4 residues binding rolipril are shown in cyan (blue labels) and corresponding PDE7 residues are represented in green (red labels). Hydrogen bond interactions are indicated by dotted lines.

4.3.6 Roles of tACE active-site residues in binding of the N-domain-selective inhibitor RXP407

RXP407 displays a 538-fold selectivity for the N-domain (figure 4.12). To explore the molecular basis for this specificity, selected single and multiple tACE mutants were tested to analyse the effect of mutations on the affinity of RXP407. The single mutations had little effect on their affinity for this inhibitor compared to wild-type tACE, with the biggest increase (8.5-fold) displayed by V379S (table 4.2, figure 4.12). The V379S conversion would increase the hydrophilicity of the S_2' pocket. This could lead to more favourable binding to the carboxyamide moiety on RXP407's P_2' Ala, believed to play a critical role in RXP407's N-selectivity.

The multiple mutants however, displayed more marked shifts in K_i from that of tACE. The TEVVD construct demonstrated a slight decrease in K_i of approximately 4-fold from that of the C-domain, still 146-fold higher than that of the N-domain (figure 4.12). Interestingly however, this mutant protein combined with the F391Y mutation (which alone only showed a 2-fold shift from tACE), presented with a 175-fold increase in affinity compared to tACE, resulting in a K_i value only 3-fold higher than that of the N-domain (figure 4.12). This marked change in K_i observed for the multiple S_2'F mutant confirms the overall importance of the active-site residues in RXP407 selectivity, and emphasises the co-operative effects of combined active-site residues. Furthermore, factors affecting selectivity may not be limited to the active-site residues interacting directly with the inhibitor (discussed in section 4.3.5.5).

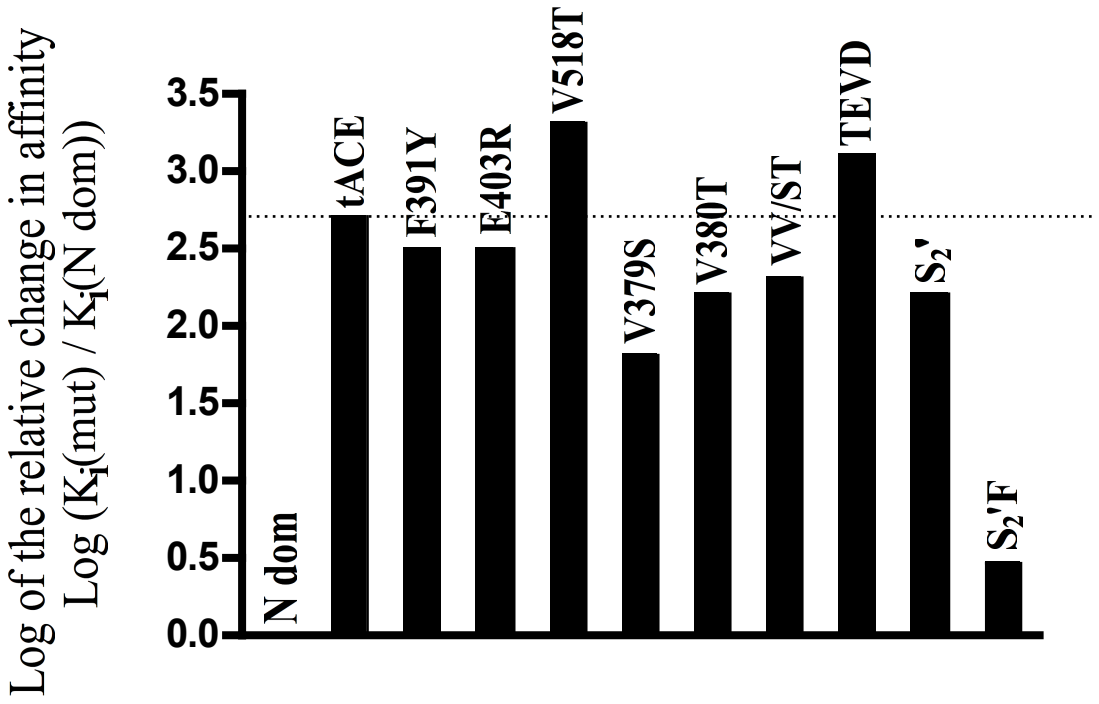

Figure 4.12. **Log scale comparison of the relative binding affinities of tACE active-site mutants for the N-selective RXP407 with that of wild-type N-domain.** Values below the dashed line represent an increase in affinity relative to that of tACE, towards a more N-domain-like K_i.

4.4. Summary

The two single mutations that caused the biggest increase in tACE K_i for RXPA380 and the keto-ACE inhibitors were F391Y and V518T, respectively. Most of the point mutations within the S_2' pocket caused a slight decrease in affinity for these inhibitors, however V379S caused an unexpected increase in affinity relative to wild-type tACE. The combined effect of multiple substitutions within the S_2' and S_2 pockets demonstrated the most notable shift in K_i for all of the inhibitors tested (RXPA380, RXP407 and lis-W). Furthermore, the combined effect of the S_2' pocket alone (TEVVD) displayed an additive effect on the change in affinity, while interestingly, inclusion of the F391Y mutation in this construct resulted in a more co-operative effect on the binding of both the phosphinic inhibitors, where the change in K_i is greater than the sum of the individual changes for the single mutants concerned.

This confirms the overall importance of these residues in the C- and N-specificity of ACE inhibitors, and highlights the fact that domain selectivity is the result of a combination of residues and possibly other factors too, and therefore cannot be attributed to a single amino acid. However, we have shown that residues within the S_2 (F391), S_1 (V518) and S_2' (V379, E367) play a major role in the C-selectivity of ACE.

Conclusions

This study describes an investigation into understanding the molecular determinants of ACE domain selectivity involving a combination of mutational and kinetic approaches. A series of tACE mutants was generated containing specific single and multiple C-domain active-site replacements. These constructs were subsequently used to characterise domain-specific interactions using two fluorogenic peptides, Abz-LFK(Dnp)-OH (C-specific) and Abz-SDK(Dnp)P-OH (N-specific), and a panel of domain-selective inhibitors.

The domain specificity of both Abz-LFK(Dnp)-OH and Abz-SDK(Dnp)P-OH has been attributed to the high catalytic efficiency with which the C-domain and N-domain of ACE cleave these peptides, respectively (Araujo et al., 2000; Bersanetti et al., 2004). This was demonstrated here with the C-selective substrate, but the k_{cat} for the N-domain with Abz-SDK(Dnp)P-OH was only 4-fold higher than that of its C-domain counterpart. The low catalytic rate observed in this study is possibly due to the use of the soluble single N-domain, as opposed to the full-length protein with an inactivated C-domain (Araujo et al., 2000). This result suggests that the marked N-specificity observed by Araujo *et al.* for Abz-SDK(Dnp)P-OH could be due to interactions between the two ACE domains of the full-length protein, which would be absent in single soluble domains.

Modest decreases (3-fold) in the catalytic efficiency of Abz-LFK(Dnp)-OH cleavage were displayed by the two substitutions D377Q and V380T. As these substitutions do not directly affect any of the residues stabilising the transition state (being more than 10 Å away), it is likely that they might introduce unfavourable interactions with the substrate P_1' Phe, which could change the orientation of Abz-LFK(Dnp)-OH within the active-site, resulting in unfavourable interaction with these stabilising residues, thereby reducing the efficiency with which the substrate is cleaved.

None of the mutants tested resulted in acquisition of N-domain-like catalytic efficiencies for either Abz-LFK(Dnp)-OH or Abz-SDK(Dnp)P-OH. This suggests that other residues within the active-site, and perhaps indirect factors such as substrate access and interaction with residues elsewhere in the enzyme, such as the lid region, might contribute to domain

specificity. Unfortunately, due to limited substrate availability, the multiple mutants were not tested with the domain-selective fluorogenic substrates. This phenomenon has, however, been observed with a C-domain construct containing an N-domain-like lid, which displayed a marked shift in k_{cat} for Abz-LFK(Dnp)-OH toward that of the N-domain.

The panel of inhibitors used to characterise the tACE active-site mutants consisted of the highly potent, C- and N-selective phosphinic peptide inhibitors RXPA380 and RXP407 (Dive et al., 1999; Georgiadis et al., 2003); the modestly C-selective keto-ACE and its C-selective derivatives kAW and kAF (Weare et al., 1981; Redelinghuys et al., 2006); and the slightly C-selective lisinopril along with its analogue lis-W, containing a P_2' Trp moiety for improved C-specificity (Nchinda et al., 2006a).

Interestingly, the S_2 F391 residue proved to be critical for the high C-specificity of RXPA380, with the F391Y mutant displaying a 34-fold decrease in affinity for this inhibitor compared to wild-type tACE. This effect is probably due to the loss of an important aromatic interaction between F391 and the P_2 Phe, as well as some potential steric hindrance resulting from the introduction of a Tyr at this position.

In the S_1 pocket, V518 seems to play a crucial role in the 30-fold specificity of keto-ACE, as evidenced by the acquisition of an N-domain-like K_i for this mutant. Both kAW and kAF also demonstrated marked decreases in affinity for this mutant. This substitution causes a reduction in the hydrophobicity of the S_1 pocket, which could lead to less favourable interactions and therefore decreased binding of these inhibitors.

E162 is an S_1' residue believed to play an important role in the C-selectivity of lisinopril and lis-W due to its favourable electrostatic interaction with the P_1' Lys, which seems to be lacking in the N-domain structure. Surprisingly, substitution of E162 with the N-domain Asp, did not cause a change in affinity for either of these inhibitors. This could be due to the scaffolding and/or backbone residues of the C-domain, which may orient the Asp in E162D to maintain favourable interactions with the P_1' side-chain, while the N-domain residues may not cause the same effect.

For most of the single S_2' mutants, only slight decreases in affinity were observed for the inhibitors tested, the most notable of these displayed by V380T and E376D for RXPA380, kAW and kAF. Lis-W also showed a decrease in affinity for the latter mutant, however an increase was observed for V380T. These modest decreases are probably due to the space available within this large pocket, and the increase in affinity displayed by V380T for lis-W is probably due to an interaction with the P_1' moiety rather than interactions within the S_2' pocket.

Intriguingly, V379S, which abrogates hydrophobic interactions with the P_2' group, caused an unexpected decrease in K_i for all of the inhibitors containing a P_2' Trp substituent. This result was supported by a corresponding N-domain mutant (S357V), which displayed an increase in affinity for RXPA380 compared to that of the wild-type N-domain. Furthermore, the full tACE S_2' mutant (TEVVD) displayed less of a decrease in affinity for RXPA380 compared to the similar mutant lacking this V379S substitution (TEVD). Therefore the presence of Val in this position (379 in tACE, 357 in N-domain) seems to decrease the affinity of RXPA380, while exchange of this residue for Ser has the opposite effect. This result could be explained by rotation about the χ_1 and χ_2 bonds of the inhibitor P_2' Trp, enabling the formation of a water-mediated hydrogen bond interaction between the inhibitor-Trp indole N and the hydroxyl of the Ser residue.

Of the single mutant constructs tested with the N-specific RXP407, V379S displayed the highest increase in affinity (8.5-fold). This effect is probably due to the increase in hydrophilicity brought about by the presence of the Ser substituent, resulting in more favourable interactions with the amidated C-terminus of the inhibitor.

The multiple S_2' mutant constructs, TEVD and TEVVD, displayed an additive effect on the change in affinity for the inhibitors tested: RXPA380, RXP407 and lis-W. Interestingly, when the TEVVD construct was combined with the S_2 F391Y substitution (S_2'F), the resulting construct demonstrated a marked decrease and increase in affinity for RXPA380 and RXP407, respectively, indicating a strong co-operative effect on domain specificity. The inhibition constants for the N-domain were, however, 10- and 3-fold higher and lower for RXPA380 and RXP407, respectively, suggesting that there may be additional effects from other active-site

residues (such as V518). Moreover, indirect factors such as scaffolding residues supporting invariant residues critical to inhibitor binding could play a role in conferring domain specificity.

We have identified a number of elements within the active-site of tACE that clearly play a critical role in the C-domain-specificity of this enzyme, namely F391 (S_2), V518 (S_1), E376 (S_2') and V380 (S_2'). We have also shown that multiple residues in the S_2' pocket have an additive effect on affinity for domain-specific inhibitors, while these residues combined with residues in other pockets, such as F391, display a strong co-operative effect on domain-specificity.

Based on this work, a number of suggestions can be made for the development of improved domain-specific ACE inhibitors. Firstly, the space available in the S_2' pocket could be more extensively exploited using moieties that are larger and more rigid than Trp. This could allow stronger and more favourable interactions with unique C-domain S_2' residues, resulting in a higher affinity for this domain. Furthermore, it is important to note that the continuous chamber formed by the S_1' and S_2' sub-site pockets allows even more latitude for the architecture of P_1' and P_2' side-chains. Finally, hydrophobic contacts between the inhibitor P_2 and P_1 substituents and C-domain F391 and V518, respectively, seem to markedly contribute towards the C-domain specificity of the inhibitors tested in this study, particularly in combination with interactions in the C-domain S_2' pocket.

Further elucidation of the molecular basis for the complex domain selectivity of ACE could involve the generation of more multiple mutants incorporating active-site residue substitutions, such as V518T (S_1 pocket) into the S_2'F, in tACE as well as sACE, and analysing the combined effect of these constructs on specificity. Moreover, these multiple mutants could be combined with substitutions of variant scaffolding residues stabilising conserved side-chains important for the binding of C-domain-specific inhibitors. Another approach one could employ would be isothermal titration calorimetry, to directly assess the changes in binding affinities and thermodynamic parameters of inhibitors with these mutant proteins.

This work provides critical and important insight into the molecular determinants of ACE domain specificity. It therefore paves the way for rational design of more efficient domain-specific inhibitors, which could ultimately lead to the development of more efficient therapies for the treatment of cardiovascular disease.

Appendix I

All methods in this appendix were adapted from those in Ausubel et al. (1992), unless otherwise stated.

Cloning and Mutagenesis

Restriction enzyme digests

Digest reaction mixtures (2 µL 10 x restriction buffer, 1-3 µL 1 $\mu g.\mu L^{-1}$ plasmid DNA and 5 units of each restriction enzyme, volumes made up to 20 µL with sterile dH_2O) were incubated at 37°C for 1 hour. Mini-preparation DNA (20 µL) screening digests were stopped with 2.5 µL restriction enzyme STOP buffer (8 parts 6 x loading buffer (0.25 % bromophenol blue, 0.25 % xylene cyanol, 30 % glycerol) and 1 part 0.5 M EDTA, pH 8.0).

Agarose gel electrophoresis

Samples containing 2 µL 6 x loading buffer and 20 µL digest reaction mixtures, or uncut DNA (1-2 µL of 1 $\mu g.\mu L^{-1}$), as well as 8 µL lambda DNA digested with *Eco*RI + *Hind*III (40 µL 553 $\mu g.mL^{-1}$ lambda DNA, 16 µL 10 x restriction buffer, 50 units *Eco*RI, 50 units *Hind*III, volumes made up to 160 µL with sterile dH_2O), were loaded onto a 6 x 10 cm agarose gel (0.8 % agarose in 1 x Tris-borate/EDTA (TBE) buffer (0.045 M Tris-borate, 0.001 M EDTA) with 0.3 $\mu g.mL^{-1}$ ethidium bromide). Electrophoresis was performed at 70 V for approximately 1 hour in 1 x TBE buffer with 0.3 $\mu g.mL^{-1}$ ethidium bromide. DNA bands were visualised using a UV light source, and photographed directly.

Preparation of E. coli JM109 competent cells using RbCl

This method was adapted from that reported in Hanahan (1983). Five mL of Luria-Bertani (LB) broth (10 $g.L^{-1}$ tryptone, 5 $g.L^{-1}$, 172 mM NaCl) was inoculated with a colony of JM109 cells and shaken at 37°C overnight. This starter culture was inoculated into 50 mL LB broth and shaken at 37°C until the cell growth had reached logarithmic phase (OD_{530}=0.35). The culture was then chilled on ice for 15 minutes, and centrifuged at 4000 x g for 5 min at 4°C. The pellet was resuspended in 21 mL ice-cold TF buffer 1 (100 mM RbCl, 50 mM $MnCl_2$, 30 mM KOAc, 10 mM $CaCl_2$, 15% glycerol) and incubated on ice for 90 min. Cells were

harvested by centrifugation at 4000 x g for 5 min at 4°C, and the pellet was resuspended in 3 mL TF buffer 2 (10 mM Morpholinepropanesulphonic acid pH 7.0, 10 mM RbCl, 75 mM $CaCl_2$, 15% glycerol). 200 µL aliquots were frozen in liquid N and stored at –80°C.

Coding sequence of 3' end of pcDNA-tACEΔ36NJ with new stop codon

```
1801      CTCCGCACGGAGAACGAGCTGCATGGGGAGAAGCTGGGCTGGCCGCAGTATAACTGGACG
601        L  R  T  E  N  E  L  H  G  E  K  L  G  W  P  Q  Y  N  W  T

1861      CCGAATTCCTAG
621        P  N  S  *
```

Original primers used for T282S and V380T mutations

Mutant		Primer	RE
T282S	For	5'-CTACTGGGGAACATGTGGGCGCAG**AGT**TGGTCCAACATCTATGAC-3'	
	Rev	5'-GTCATAGATGTTGGACCA**ACT**CTGCGCCCACATGTTCCCCAGTAG-3'	*Bmr*I
V380T	For	5'-GTTAACTTGGAGGACCTGGTG**ACG**GCCCAC-3'	
	Rev	5'-GTGGGC**CGT**CACCAGGTCCTCCAAGTTAAC-3'	*Hpa*I

Figure A1. **Original primers used for T282S and V380T mutations.** Primers produced no positive clones. Complementary mutagenic primers (For, forward; Rev, reverse) were designed containing the mutation of interest, as well as a silent mutation introducing a unique restriction endonuclease site (RE) to facilitate screening. Residues in bold indicate the codon to be mutated, unique restrictions sites are underlined.

Appendix II

Substrate kinetics

Preparation of synthetic substrates

5.7 mM HHL working solution

19.4 mg HHL was added to 1.67 mL 0.28 M NaOH and heated to dissolve the solid. 832 µL 0.5 M HEPES (pH 7.5), 2.498 mL 1 M NaCl and 2.998 mL dH_2O was added to this solution.

1 mM Z-FHL working solution

A 20 mM stock solution of *Z*-FHL was made up by dissolving 220 mg *Z*-FHL in 2 mL 0.28 M NaOH, and making up to 20 mL with dH_2O. This solution was stored in 1 mL aliquots at -20^{o}C.

Working solutions of *Z*-FHL were made up by first adding 15 mL dH_2O to 4 mL 5 x phosphate buffer (0.5 M KPO_4 buffer, pH 8.3, 1.5 M NaCl), then adding 20 µL 10 mM $ZnSO_4$ to this buffer, followed by 1 mL 20 mM *Z*-FHL.

Standard curve for fluorogenic peptide

The change in fluorescence from baseline levels (before addition of ACE) to total hydrolysis of a range of substrate concentrations (0- 2.5 nmoles) was measured at λ_{ex} = 320 nm and λ_{em} = 420 nm. A standard curve was generated by plotting this change in fluorescence versus nmoles of substrate hydrolysed. The slope of the linear regression curve fitted to this plot was determined using GraphPad Prism 4.01.

References

Acharya, K.R., Sturrock, E.D., Riordan, J.F., and Ehlers, M.R. (2003). Ace revisited: a new target for structure-based drug design. *Nat. Rev. Drug Discov.* **2**, 891-902.

Adam, A., Cugno, M., Molinaro, G., Perez, M., Lepage, Y., and Agostoni, A. (2002). Aminopeptidase P in individuals with a history of angio-oedema on ACE inhibitors. *Lancet* **359**, 2088-2089.

Albiston, A.L., McDowall, S.G., Matsacos, D., Sim, P., Clune, E., Mustafa, T., Lee, J., Mendelsohn, F.A., Simpson, R.J., Connolly, L.M., and Chai, S.Y. (2001). Evidence that the angiotensin IV (AT(4)) receptor is the enzyme insulin-regulated aminopeptidase. *J. Biol. Chem.* **276**, 48623-48626.

Aloy, P., Companys, V., Vendrell, J., Aviles, F.X., Fricker, L.D., Coll, M., and Gomis-Rüth, F.X. (2001). The crystal structure of the inhibitor-complexed carboxypeptidase D domain II and the modeling of regulatory carboxypeptidases. *J. Biol. Chem.* **276**, 16177-16184.

Antoni, F.A. (2000). Molecular diversity of cyclic AMP signalling. *Front. Neuroendocrinol.* **21**, 103-132.

Andújar-Sánchez, M., Jara-Pérez, V., and Cámara-Artigas, A. (2007). Thermodynamic determination of the binding constants of angiotensin-converting enzyme inhibitors by a displacement method. *FEBS Lett.* **581**, 3449-3454.

Araujo, M.C., Melo, R.I., Del Nery, E., Alves, M.F., Juliano, M.A., Casarini, D.E., Juliano, L., and Carmona, A.K. (1999). Internally quenched fluorogenic substrates for angiotensin I-converting enzyme. *J. Hypertens.* **17**, 665-672.

Araujo, M.C., Melo, R.L., Cesari, M.H., Juliano, M.A., Juliano, L., and Carmona, A.K. (2000). Peptidase specificity characterization of C- and N-terminal catalytic sites of angiotensin I-converting enzyme. *Biochemistry* **39**, 8519-8525.

Ardaillou, R., and Chansel, D. (1997). Synthesis and effects of active fragments of angiotensin II. *Kidney Int.* **52**, 1458-1468.

Arribas, J.C., Herrero, A.G., Martín-Lomas, M., Cañada, F.J., He, S., and Withers, S.G. (2000). Differential mechanism-based labeling and unequivocal activity assignment of the two active sites of intestinal lactase/phlorizin hydrolase. *Eur. J. Biochem.* **267**, 6996-7005.

F.M. Ausubel, R. Brent, R.E. Kingston, D.D. Moore, J.G. Seidman, J.A. Smith, and K. Struhl, eds. (1992). Short Protocols in Molecular Biology. Second Edition (USA: Greene Publishing Associates and John Wiley & Sons).

Balyasnikova, I.V., Metzger, R, Fanke, F.E., and Danilov, S.M. (2003). Monoclonal antibodies to denatured human ACE (CD 143), broad species specificity, reactivity on paraffin sections, and detection of subtle conformational changes in the C-terminal domain of ACE. *Tissue Antigens* **61**, 49-62.

Barnes, K., Matsas, R., Hooper, N.M., Turner, A.J., and Kenny, A.J. (1988). Endopeptidase-24.11 is striosomally ordered in pig brain and, in contrast to aminopeptidase N and peptidyl dipeptidase A ('angiotensin converting enzyme'), is a marker for a set of striatal efferent fibres. *Neuroscience* **27**, 799-817.

Baudin, B. (2002). New aspects on angiotensin-converting enzyme: from gene to disease. *Clin. Chem. Lab. Med.* **40**, 256-265.

Beau, I., Cotte-Laffitte, J., Géniteau-Legendre, M., Estes, M.K., and Servin, A.L. (2007). An NSP4-dependant mechanism by which rotavirus impairs lactase enzymatic activity in brush border of human enterocyte-like Caco-2 cells. *Cell Microbiol.* **9**, 2254-2266.

Behera, R.K., and Mazumdar, S. (2008). Roles of two surface residues near the access channel in the substrate recognition by cytochrome P450cam. *Biophys. Chem.* **135**, 1-6.

Beneteau, B., Baudin, B., Morgant, G., Giboudeau, J., and Baumann, F.C. (1986). Automated kinetic assay of angiotensin-converting enzyme in serum. *Clin. Chem.* **32**, 884-886.

Bergdoll, M., Eltis, L.D., Cameron, A.D., Dumas, P., and Bolin, J.T. (1998). All in the family: structural and evolutionary relationships among three modular proteins with diverse functions and variable assembly. *Protein Sci.* **7**, 1661-1670.

Bersanetti, P.A., Andrade, M.C., Casarini, D.E., Juliano, M.A., Nchinda, A.T., Sturrock, E.D., Juliano, L., and Carmona, A.K. (2004). Positional-scanning combinatorial libraries of fluorescence resonance energy transfer peptides for defining substrate specificity of the angiotensin I-converting enzyme and development of selective C-domain substrates. *Biochemistry* **43**, 15729-15736.

Bhoola, K.D., Figueroa, C.D., and Worthy, K. (1992). Bioregulation of kinins: kallikreins, kininogens, and kininases. *Pharmacol. Rev.* **44**, 1-80.

Bicket, D.P. (2002). Using ACE inhibitors appropriately. *Am. Fam. Physician* **66**, 461-468.

Bieth, J.G. (1995). Theoretical and practical aspects of proteinase inhibition kinetics. *Methods Enzymol.* **248**, 59-84.

Binevski, P.V., Sizova, E.A., Pozdnev, V.F., and Kost, O.A. (2003). Evidence for the negative cooperativity of the two active sites within bovine somatic angiotensin-converting enzyme. *FEBS Lett.* **550**, 84-88.

Brenner, B.M., Ballermann, B.J., Gunning, M.E., and Zeidel, M.L. (1990). Diverse biological actions of atrial natriuretic peptide. *Physiol. Rev.* **70**, 665-699.

Bradford, M., (1976). A Rapid and Sensitive Method for the Quantification of Protein Utilizing the Principle of Protein-Dye Binding. *Anal. Biochem.* **72**, 248-254.

Byers, L.D., and Wolfenden, R. (1973). Binding of the by-product analog benzylsuccinic acid by carboxypeptidase A. *Biochemistry* **12**, 2070-2078.

Carmona, A.K., Schwager, S.L., Juliano, M.A., Juliano, L., and Sturrock, E.D. (2006). A continuous fluorescence resonance energy transfer angiotensin I-converting enzyme assay. *Nat. Protoc.* **1**, 1971-1976.

Carvajal, J.A., Germain, A.M., Huidobro-Toro, J.P., and Weiner, C.P. (2000). Molecular mechanism of cGMP-mediated smooth muscle relaxation. *J. Cell Physiol.* **184**, 409-420.

Chai, S.Y., McKinley, M.J., and Mendelsohn, F.A. (1987). Distribution of angiotensin converting enzyme in sheep hypothalamus and medulla oblongata visualized by in vitro autoradiography. *Clin. Exp. Hypertens. A* **9**, 449-460.

Chen, X., Li, W., Yoshida, H., Tsuchida, S., Nishimura, H., Takemoto, F., Okubo, S., Fogo, A., Matsusaka, T., and Ichikawa, I. (1997). Targeting deletion of angiotensin type 1B receptor gene in the mouse. *Am. J. Physiol.* **272**, F299-F304.

Cole, J., Ertoy, D., Lin, H., Sutliff, R.L., Ezan, E., Guyene, T.T., Capecchi, M., Corvol, P., and Bernstein, K.E. (2000). Lack of angiotensin II-facilitated erythropoiesis causes anemia in angiotensin-converting enzyme-deficient mice. *J. Clin. Invest.* **106**, 1391-1398.

Colombo, V., Lorenz-Meyer, H., and Semenza, G. (1973). Small intestinal phlorizin hydrolase: the "beta-glycosidase complex". *Biochim. Biophys. Acta.* **327**, 412-424.

Corradi, H.R., Chitapi, I., Sewell, B.T., Georgiadis, D., Dive, V., Sturrock, E.D., and Acharya, K.R. (2007). The structure of testis angiotensin-converting enzyme in complex with the C domain-specific inhibitor RXPA380. *Biochemistry* **46**, 5473-5478.

Corradi, H.R., Schwager, S.L., Nchinda, A.T., Sturrock, E.D., and Acharya, K.R. (2006). Crystal structure of the N domain of human somatic angiotensin I-converting enzyme provides a structural basis for domain-specific inhibitor design. *J. Mol. Biol.* **357**, 964-974.

Corvol, P., and Williams, T.A. (1998). in Handbook of Proteolytic Enzymes, A.J. Barret, N.D. Rawlings, and J.F. Woessner, eds. (London: Academic Press).

Csikós, T., Chung, O., and Unger, T. (1998). Receptors and their classification: focus on angiotensin II and the AT2 receptor. *J. Hum. Hypertens.* **12**, 311-318.

Cushman, D.W., and Cheung, H.S. (1971). Spectrophotometric assay and properties of the angiotensin-converting enzyme of rabbit lung. *Biochem. Pharmacol.* **20**, 1637-1648.

Cushman, D.W., Cheung, H.S., Sabo, E.F., and Ondetti, M.A. (1977). Design of potent competitive inhibitors of angiotensin-converting enzyme. Carboxyalkanoyl and mercaptoalkanoyl amino acids. *Biochemistry* **16**, 5484-5491.

Cushman, W.C. (2003). Are there benefits to specific antihypertensive drug therapy? *Am. J. Hypertens.* **16**, 31S-35S.

Damas, J. (1996). The brown Norway rats and the kinin system. *Peptides* **17**, 859-872.

Danilov, S., Jaspard, E., Churakova, T., Towbin, H., Savoie, F., Wei, L., and Alhenc-Gelas, F. (1994). Structure-function analysis of angiotensin I-converting enzyme using monoclonal antibodies. Selective inhibition of the amino-terminal active site. *J. Biol. Chem.* **269**, 26806-26814.

Das, M., and Soffer, R.L. (1975). Pulmonary angiotensin-converting enzyme. Structural and catalytic properties. *J. Biol. Chem.* **250**, 6762-6768.

Deddish, P.A., Marcic, B., Jackman, H.L., Wang, H.Z., Skidgel, R.A., and Erdös, E.G. (1998). N-domain-specific substrate and C-domain inhibitors of angiotensin-converting enzyme: angiotensin-(1-7) and keto-ACE. *Hypertension* **31**, 912-917.

Deddish, P.A., Wang, J., Michel, B., Morris, P.W., Davidson, N.O., Skidgel, R.A., and Erdös, E.G. (1994). Naturally occurring active N-domain of human angiotensin I-converting enzyme. *Proc. Natl. Acad. Sci. U S A* **91**, 7807-7811.

Defendini, R., Zimmerman, E.A., Weare, J.A., Alhenc-Gelas, F., and Erdös, E.G. (1983). Angiotensin-converting enzyme in epithelial and neuroepithelial cells. *Neuroendocrinology* **37**, 32-40.

Dickerson, I.M., and Noel, G. (1991). In Peptide Biosynthesis and Processing, L.D. Fricker, ed. (Boca Raton, Florida: CRC Press).

Dickstein, K., Kjekshus, J., and OPTIMAAL Steering Committee of the OPTIMAAL Study Group (2002). Effects of losartan and captopril on mortality and morbidity in high-risk patients after acute myocardial infarction: the OPTIMAAL randomised trial. Optimal Trial in Myocardial Infarction with Angiotensin II Antagonist Losartan. *Lancet* **360**, 752-760.

Dive, V., Cotton, J., Yiotakis, A., Michaud, A., Vassiliou, S., Jiracek, J., Vazeux, G., Chauvet, M.T., Cuniasse, P., and Corvol, P. (1999). RXP 407, a phosphinic peptide, is a potent inhibitor of angiotensin I converting enzyme able to differentiate between its two active sites. *Proc. Natl. Acad. Sci. U S A* **96**, 4330-4335.

Dixon, M. (1953). The determination of enzyme inhibitor constants. *Biochem. J.* **55**, 170-171.

Díaz-Mejía, J.J., Pérez-Rueda, E., and Segovia, L. (2007). A network perspective on the evolution of metabolism by gene duplication. *Genome Biol.* **8**, R26.

Donoghue, M., Hsieh, F., Baronas, E., Godbout, K., Gosselin, M., Stagliano, N., Donovan, M., Woolf, B., Robison, K., Jeyaseelan, R., Breitbart, R.E., and Acton, S. (2000). A novel angiotensin-converting enzyme-related carboxypeptidase (ACE2) converts angiotensin I to angiotensin 1-9. *Circ. Res.* **87**, E1-E9.

Ehlers, M.R., and Riordan, J.F. (1991). Angiotensin-converting enzyme: zinc- and inhibitor-binding stoichiometries of the somatic and testis isozymes. *Biochemistry* **30**, 7118-7126.

Ehlers, M.R., Chen, Y.N., and Riordan, J.F. (1991). Purification and characterization of recombinant human testis angiotensin-converting enzyme expressed in Chinese hamster ovary cells. *Protein Expr. Purif.* **2**, 1-9.

Ehlers, M.R., Fox, E.A., Strydom, D.J., and Riordan, J.F. (1989). Molecular cloning of human testicular angiotensin-converting enzyme: the testis isozyme is identical to the C-terminal half of endothelial angiotensin-converting enzyme. *Proc. Natl. Acad. Sci. U S A* **86**, 7741-7745.

Ehlers, M.R., Schwager, S.L., Scholle, R.R., Manji, G.A., Brandt, W.F., and Riordan, J.F. (1996). Proteolytic release of membrane-bound angiotensin-converting enzyme: role of the juxtamembrane stalk sequence. *Biochemistry* **35**, 9549-9559.

Eipper, B.A., Stoffers, D.A., and Mains, R.E. (1992). The biosynthesis of neuropeptides: peptide alpha-amidation. *Annu. Rev. Neurosci.* **15**, 57-85.

Eisenthal, R., and Cornish-Bowden, A. (1974). The direct linear plot. A new graphical procedure for estimating enzyme kinetic parameters. *Biochem. J.* **139**, 715-720.

Eng, F.J., Novikova, E.G., Kuroki, K., Ganem, D., and Fricker, L.D. (1998). gp180, a protein that binds duck hepatitis B virus particles, has metallocarboxypeptidase D-like enzymatic activity. *J. Biol. Chem.* **273**, 8382-8388.

Erdos, E.G., and Yang, H.Y. (1967). An enzyme in microsomal fraction of kidney that inactivates bradykinin. *Life Sci.* **6**, 569-574.

Esther, C.R., Howard, T.E., Marino, E.M., Goddard, J.M., Capecchi, M.R., and Bernstein, K.E. (1996). Mice lacking angiotensin-converting enzyme have low blood pressure, renal pathology, and reduced male fertility. *Lab. Invest.* **74**, 953-965.

Fernandez, M., Liu, X., Wouters, M.A., Heyberger, S., and Husain, A. (2001). Angiotensin I-converting enzyme transition state stabilization by HIS1089: evidence for a catalytic mechanism distinct from other gluzincin metalloproteinases. *J. Biol. Chem.* **276**, 4998-5004.

Ferreira, S.H., Greene, L.H., Alabaster, V.A., Bakhle, Y.S., and Vane, J.R. (1970). Activity of various fractions of bradykinin potentiating factor against angiotensin I converting enzyme. *Nature* **25**, 379-380.

Friedland, J., and Silverstein, E. (1976). A sensitive fluorimetric assay for serum angiotensin-converting enzyme. *Am. J. Clin. Pathol.* **66**, 416-424.

Fuchs, S., Xiao, H.D., Cole, J.M., Adams, J.W., Frenzel, K., Michaud, A., Zhao, H., Keshelava, G., Capecchi, M.R., Corvol, P., and Bernstein, K.E. (2004). Role of the N-terminal catalytic domain of angiotensin-converting enzyme investigated by targeted inactivation in mice. *J. Biol. Chem.* **279**, 15946-15953.

Fuchs, S., Xiao, H.D., Hubert, C., Michaud, A., Campbell, D.J., Adams, J.W., Capecchi, M.R., Corvol, P., and Bernstein, K.E. (2008). Angiotensin-converting enzyme C-terminal catalytic domain is the main site of angiotensin I cleavage in vivo. *Hypertension* **51**, 267-274.

Fyhrquist, F., and Saijonmaa, O. (2008). Renin-angiotensin system revisited. *J. Intern. Med.* **264**, 224-236.

Gardner, C., Robas, N., Cawkill, D., and Fidock, M. (2000). Cloning and characterization of the human and mouse PDE7B, a novel cAMP-specific cyclic nucleotide phosphodiesterase. *Biochem. Biophys. Res. Commun.* **272**, 186-192.

de Gasparo, M., Husain, A., Alexander, W., Catt, K.J., Chiu, A.T., Drew, M., Goodfriend, T., Harding, J.W., Inagami, T., and Timmermans, P.B. (1995). Proposed update of angiotensin receptor nomenclature. *Hypertension* **25**, 924-927.

Georgiadis, D., Beau, F., Czarny, B., Cotton, J., Yiotakis, A., and Dive, V. (2003). Roles of the two active sites of somatic angiotensin-converting enzyme in the cleavage of angiotensin I and bradykinin: insights from selective inhibitors. *Circ. Res.* **93**, 148-154.

Georgiadis, D., Cuniasse, P., Cotton, J., Yiotakis, A., and Dive, V. (2004). Structural determinants of RXPA380, a potent and highly selective inhibitor of the angiotensin-converting enzyme C-domain. *Biochemistry* **43**, 8048-8054.

Goldblatt, H., Lynch, J., Hanzal, R.F., and Summerville, W.N. (1934). Studies on experimental hypertension.I. The production of persistent elevation of systolic blood pressure by means of renal ischemia. *J. Exp. Med.* **59**, 347-379.

Gomis-Rüth, F.X., Companys, V., Qian, Y., Fricker, L.D., Vendrell, J., Avilés, F.X., and Coll, M. (1999). Crystal structure of avian carboxypeptidase D domain II: a prototype for the regulatory metallocarboxypeptidase subfamily. *EMBO J.* **18**, 5817-5826.

Hagaman, J.R., Moyer, J.S., Bachman, E.S., Sibony, M., Magyar, P.L., Welch, J.E., Smithies, O., Krege, J.H., and O'Brien, D.A. (1998). Angiotensin-converting enzyme and male fertility. *Proc. Natl. Acad. Sci. U S A* **95**, 2552-2557.

Hanahan, D. (1983). Studies on transformation of Escherichia coli with plasmids. *J. Mol. Biol.* **166**, 557-580.

Henegariu, O., Heerema, N.A., Dlouhy, S.R., Vance, G.H., and Vogt, P.H. (1997). Multiplex PCR: critical parameters and step-by-step protocol. *Biotechniques* **23**, 504-511.

Hetman, J.M., Soderling, S.H., Glavas, N.A., and Beavo, J.A. (2000). Cloning and characterization of PDE7B, a cAMP-specific phosphodiesterase. *Proc. Natl. Acad. Sci. U S A* **97**, 472-476.

Holmquist, B., Bünning, P., and Riordan, J.F. (1979). A continuous spectrophotometric assay for angiotensin converting enzyme. *Anal. Biochem.* **95**, 540-548.

Horiuchi, M. (1996). Functional aspects of angiotensin type 2 receptor. *Adv. Exp. Med. Biol.* **396**, 217-224.

Houssay., B.A., and Fasciolo, J.C. (1937). Secretion hipertensora del rinon isquemaido. *Rev. Soc. Argent. Biol.* **13**, 284-294.

Howard, T.E., Shai, S.Y., Langford, K.G., Martin, B.M., and Bernstein, K.E. (1990). Transcription of testicular angiotensin-converting enzyme (ACE) is initiated within the 12th intron of the somatic ACE gene. *Mol. Cell Biol.* **10**, 4294-4302.

Huai, Q., Wang, H., Sun, Y., Kim, H.Y., Liu, Y., and Ke, H. (2003). Three-dimensional structures of PDE4D in complex with roliprams and implication on inhibitor selectivity. *Structure* **11**, 865-873.

Huang, P.J., Chien, K.L., Chen, M.F., Lai, L.P., and Chiang, F.T. (2001). Efficacy and safety of imidapril in patients with essential hypertension: a double-blind comparison with captopril. *Cardiology* **95**, 146-150.

Hubert, C., Houot, A.M., Corvol, P., and Soubrier, F. (1991). Structure of the angiotensin I-converting enzyme gene. Two alternate promoters correspond to evolutionary steps of a duplicated gene. *J. Biol. Chem.* **266**, 15377-15383.

Hunziker, W., Spiess, M., Semenza, G., and Lodish, H.F. (1986). The sucrase-isomaltase complex: primary structure, membrane-orientation, and evolution of a stalked, intrinsic brush border protein. *Cell* **46**, 227-234.

Inagami, T. (1994). The renin-angiotensin system. *Essays Biochem.* **28**, 147-164.

Innis, M.A., and Gelfand, D.H. (1990). PCR Protocols: A Guide to Methods and Applications, M.A. Innis, D.H. Gelfand, J.J. Sninsky, and T.J. White, eds. (San Diego: Academic Press).

Ito, M., Oliverio, M.I., Mannon, P.J., Best, C.F., Maeda, N., Smithies, O., and Coffman, T.M. (1995). Regulation of blood pressure by the type 1A angiotensin II receptor gene. *Proc. Natl. Acad. Sci. U S A* **92**, 3521-3525.

Iyer, S.N., Averill, D.B., Chappell, M.C., Yamada, K., Allred, A.J., and Ferrario, C.M. (2000). Contribution of angiotensin-(1-7) to blood pressure regulation in salt-depleted hypertensive rats. *Hypertension* **36**, 417-422.

Jacob, R., Pürschel, B., and Naim, H.Y. (2002). Sucrase is an intramolecular chaperone located at the C-terminal end of the sucrase-isomaltase enzyme complex. *J. Biol. Chem.* **277**, 32141-32148.

Jaspard, E., Wei, L., and Alhenc-Gelas, F. (1993). Differences in the properties and enzymatic specificities of the two active sites of angiotensin I-converting enzyme (kininase II). Studies with bradykinin and other natural peptides. *J. Biol. Chem.* **268**, 9496-9503.

Johnson, R.G., and Scarpa, A. (1976). Internal pH of isolated chromaffin vesicles. *J. Biol. Chem.* **251**, 2189-2191.

Jullien, N.D., Cuniasse, P., Georgiadis, D., Yiotakis, A., and Dive, V. (2006). Combined use of selective inhibitors and fluorogenic substrates to study the specificity of somatic wild-type angiotensin-converting enzyme. *FEBS J.* **273**, 1772-1781.

Jung, L.J., and Scheller, R.H. (1991). Peptide processing and targeting in the neuronal secretory pathway. *Science* **251**, 1330-1335.

Junot, C., Gonzales, M.F., Ezan, E., Cotton, J., Vazeux, G., Michaud, A., Azizi, M., Vassiliou, S., Yiotakis, A., Corvol, P., and Dive, V. (2001). RXP 407, a selective inhibitor of the N-domain of angiotensin I-converting enzyme, blocks in vivo the degradation of hemoregulatory peptide acetyl-Ser-Asp-Lys-Pro with no effect on angiotensin I hydrolysis. *J. Pharmacol. Exp. Ther.* **297**, 606-611.

Kato, I., Yonekura, H., Yamamoto, H., and Okamoto, H. (1990). Isolation and functional expression of pituitary peptidylglycine alpha-amidating enzyme mRNA. A variant lacking the transmembrane domain. *FEBS Lett.* **269**, 319-323.

Katopodis, A.G., Ping, D., and May, S.W. (1990). A novel enzyme from bovine neurointermediate pituitary catalyzes dealkylation of alpha-hydroxyglycine derivatives, thereby functioning sequentially with peptidylglycine alpha-amidating monooxygenase in peptide amidation. *Biochemistry* **29**, 6115-6120.

Katopodis, A.G., Ping, D.S., Smith, C.E., and May, S.W. (1991). Functional and structural characterization of peptidylamidoglycolate lyase, the enzyme catalyzing the second step in peptide amidation. *Biochemistry* **30**, 6189-6194.

Katori, M., and Majima, M. (1996). Pivotal role of renal kallikrein-kinin system in the development of hypertension and approaches to new drugs based on this relationship. *Jpn. J. Pharmacol.* **70**, 95-128.

Kim, H.S., Krege, J.H., Kluckman, K.D., Hagaman, J.R., Hodgin, J.B., Best, C.F., Jennette, J.C., Coffman, T.M., Maeda, N., and Smithies, O. (1995). Genetic control of blood pressure and the angiotensinogen locus. *Proc. Natl. Acad. Sci. U S A* **92**, 2735-2739.

Knight, C.G. (1995). Active-site titration of peptidases. *Methods Enzymol.* **248**, 85-101.

Kraml, J., Kolínská, J., Eddederová, D., and Hirsová, D. (1972). -Glucosidase (phlorizin hydrolase) activity of the lactase fraction isolated from the small intestinal mucosa of infant rats, and the relationship between -glucosidases and -galactosidases. *Biochim. Biophys. Acta.* **258**, 520-530.

Krege, J.H., John, S.W., Langenbach, L.L., Hodgin, J.B., Hagaman, J.R., Bachman, E.S., Jennette, J.C., O'Brien, D.A., and Smithies, O. (1995). Male-female differences in fertility and blood pressure in ACE-deficient mice. *Nature* **375**, 146-148.

Kuroki, K., Eng, F., Ishikawa, T., Turck, C., Harada, F., and Ganem, D. (1995). gp180, a host cell glycoprotein that binds duck hepatitis B virus particles, is encoded by a member of the carboxypeptidase gene family. *J. Biol. Chem.* **270**, 15022-15028.

Laemmli, U.K. (1970). Cleavage of structural proteins during the assembly of the head of bacteriophage T4. *Nature* **227**, 680-685.

Lalloo, U.G., Barnes, P.J., and Chung, K.F. (1996). Pathophysiology and clinical presentations of cough. *J. Allergy Clin. Immunol.* **98**, S91-6; discussion S96-7.

Langford, K.G., Zhou, Y., Russell, L.D., Wilcox, J.N., and Bernstein, K.E. (1993). Regulated expression of testis angiotensin-converting enzyme during spermatogenesis in mice. *Biol. Reprod.* **48**, 1210-1218.

Lazard, D., Briend-Sutren, M.M., Villageois, P., Mattei, M.G., Strosberg, A.D., and Nahmias, C. (1994). Molecular characterization and chromosome localization of a human angiotensin II AT2 receptor gene highly expressed in fetal tissues. *Receptors Channels* **2**, 271-280.

Mains, R.E., Dickerson, I.M., May, V., Stoffers, D.A., Perkins, S.N., Ouafik, L.'.H., Husten, E.J., and Eipper, B.A. (1990). Cellular and molecular aspects of peptide hormone biosynthesis. *Front. Neuroendocrinol.* **11**, 52-89.

Mantei, N., Villa, M., Enzler, T., Wacker, H., Boll, W., James, P., Hunziker, W., and Semenza, G. (1988). Complete primary structure of human and rabbit lactase-phlorizin hydrolase: implications for biosynthesis, membrane anchoring and evolution of the enzyme. *EMBO J.* **7**, 2705-2713.

Marcic, B.M., and Erdös, E.G. (2000). Protein kinase C and phosphatase inhibitors block the ability of angiotensin I-converting enzyme inhibitors to resensitize the receptor to bradykinin without altering the primary effects of bradykinin. *J. Pharmacol. Exp. Ther.* **294**, 605-612.

Matsas, R., Kenny, A.J., and Turner, A.J. (1984). The metabolism of neuropeptides. The hydrolysis of peptides, including enkephalins, tachykinins and their analogues, by endopeptidase-24.11. *Biochem. J.* **223**, 433-440.

Matthews, B.W. (1988). Structural basis of the action of thermolysin and related zinc peptidases. *Acc. Chem. Res.* **21**, 333-340.

McNeil, J.J., Anderson, A., Christophidis, N., Jarrott, B., and Louis, W.J. (1979). Taste loss associated with captopril treatment. *Br. Med. J.* **6204**, 1555-1556.

Menard, J., and Patchett, A.A. (2001). Angiotensin-converting enzyme inhibitors. *Adv. Protein Chem.* **56**, 13-75.

Ménard, J. (2004). The 45-year story of the development of an anti-aldosterone more specific than spironolactone. *Mol. Cell Endocrinol.* **217**, 45-52.

Michaud, A., Chauvet, M.T., and Corvol, P. (1999). N-domain selectivity of angiotensin I-converting enzyme as assessed by structure-function studies of its highly selective substrate, N-acetyl-seryl-aspartyl-lysyl-proline. *Biochem. Pharmacol.* **57**, 611-618.

Michaud, A., Williams, T.A., Chauvet, M.T., and Corvol, P. (1997). Substrate dependence of angiotensin I-converting enzyme inhibition: captopril displays a partial selectivity for inhibition of N-acetyl-seryl-aspartyl-lysyl-proline hydrolysis compared with that of angiotensin I. *Mol. Pharmacol.* **51**, 1070-1076.

Morimoto, T., Gandhi, T.K., Fiskio, J.M., Seger, A.C., So, J.W., Cook, E.F., Fukui, T., and Bates, D.W. (2004). An evaluation of risk factors for adverse drug events associated with angiotensin-converting enzyme inhibitors. *J. Eval. Clin. Pract.* **10**, 499-509.

Nakamoto, H., Ferrario, C.M., Fuller, S.B., Robaczewski, D.L., Winicov, E., and Dean, R.H. (1995). Angiotensin-(1-7) and nitric oxide interaction in renovascular hypertension. *Hypertension* **25**, 796-802.

Nakamura, S., Averill, D.B., Chappell, M.C., Diz, D.I., Brosnihan, K.B., and Ferrario, C.M. (2003). Angiotensin receptors contribute to blood pressure homeostasis in salt-depleted SHR. *Am. J. Physiol. Regul. Integr. Comp. Physiol.* **284**, R164-R173.

Natesh, R., Schwager, S.L., Evans, H.R., Sturrock, E.D., and Acharya, K.R. (2004). Structural details on the binding of antihypertensive drugs captopril and enalaprilat to human testicular angiotensin I-converting enzyme. *Biochemistry* **43**, 8718-8724.

Natesh, R., Schwager, S.L., Sturrock, E.D., and Acharya, K.R. (2003). Crystal structure of the human angiotensin-converting enzyme-lisinopril complex. *Nature* **421**, 551-554.

Nchinda, A.T., Chibale, K., Redelinghuys, P., and Sturrock, E.D. (2006a). Synthesis and molecular modeling of a lisinopril-tryptophan analogue inhibitor of angiotensin I-converting enzyme. *Bioorg. Med. Chem. Lett.* **16**, 4616-4619.

Nchinda, A.T., Chibale, K., Redelinghuys, P., and Sturrock, E.D. (2006b). Synthesis of novel keto-ACE analogues as domain-selective angiotensin I-converting enzyme inhibitors. *Bioorg. Med. Chem. Lett.* **16**, 4612-4615.

Novikova, E.G., Eng, F.J., Yan, L., Qian, Y., and Fricker, L.D. (1999). Characterization of the enzymatic properties of the first and second domains of metallocarboxypeptidase D. *J. Biol. Chem.* **274**, 28887-28892.

O'Neill, H.G., Redelinghuys, P., Schwager, S.L., and Sturrock, E.D. (2008). The role of glycosylation and domain interactions in the thermal stability of human angiotensin-converting enzyme. *Biol. Chem.* **389**, 1153-1161.

Oblin, A., Danse, M.J., and Zivkovic, B. (1988). Degradation of substance P by membrane peptidases in the rat substantia nigra: effect of selective inhibitors. *Neurosci. Lett.* **84**, 91-96.

Oliverio, M.I., Kim, H.S., Ito, M., Le, T., Audoly, L., Best, C.F., Hiller, S., Kluckman, K., Maeda, N., Smithies, O., and Coffman, T.M. (1998). Reduced growth, abnormal kidney structure, and type 2 (AT2) angiotensin receptor-mediated blood pressure regulation in mice lacking both AT1A and AT1B receptors for angiotensin II. *Proc. Natl. Acad. Sci. U S A* **95**, 15496-15501.

Ondetti, M.A., Rubin, B., and Cushman, D.W. (1977). Design of specific inhibitors of angiotensin-converting enzyme: new class of orally active antihypertensive agents. *Science* **196**, 441-444.

Ondetti, M.A., Williams, N.J., Sabo, E.F., Pluscec, J., Weaver, E.R., and Kocy, O. (1971). Angiotensin-converting enzyme inhibitors from the venom of Bothrops jararaca. Isolation, elucidation of structure, and synthesis. *Biochemistry* **10**, 4033-4039.

Ouafik, L.H., Stoffers, D.A., Campbell, T.A., Johnson, R.C., Bloomquist, B.T., Mains, R.E., and Eipper, B.A. (1992). The multifunctional peptidylglycine alpha-amidating monooxygenase gene: exon/intron organization of catalytic, processing, and routing domains. *Mol. Endocrinol.* **6**, 1571-1584.

Page, I.H., and Helmer, O.M. (1940). A crystalline pressor substance (angiotonin) resulting from the interaction between renin and renin activator. *J. Exp. Med.* **71**, 29.

Papworth, C., Braman, J., and Wright, D.A. (1996). Site-directed mutagenesis in One Day with 80 % efficiency. *Strategies* **9**, 3-4.

Patchett, A.A., Harris, E., Tristram, E.W., Wyvratt, M.J., Wu, M.T., Taub, D., Peterson, E.R., Ikeler, T.J., ten Broeke, J., Payne, L.G., Ondeyka, D.L., Thorsett, E.D., Greenlee, W.J., Lohr, N.S., Hoffsommer, R.D., Joshua, H., Ruyle, W.V., Rothrock, J.W., Aster, S.D., Maycock, A.L., Robinson, F.M., Hirschmann, R., Sweet, C.S., Ulm, E.H., Gross, D.M., Vassil, T.C., and Stone, C.A. (1980). A new class of angiotensin-converting enzyme inhibitors. *Nature* **288**, 280-283.

Pelmenschikov, V., Blomberg, M.R., and Siegbahn, P.E. (2002). A theoretical study of the mechanism for peptide hydrolysis by thermolysin. *J. Biol. Inorg. Chem.* **7**, 284-298.

Redelinghuys, P., Nchinda, A.T., and Sturrock, E.D. (2005). Development of domain-selective angiotensin I-converting enzyme inhibitors. *Ann. N. Y. Acad. Sci.* **1056**, 160-175.

Redelinghuys, P., Nchinda, A.T., Chibale, K., and Sturrock, E.D. (2006). Novel ketomethylene inhibitors of angiotensin I-converting enzyme (ACE): inhibition and molecular modelling. *Biol. Chem.* **387**, 461-466.

Regoli, D., Rhaleb, N.E., Drapeau, G., Dion, S., Tousignant, C., D'Orléans-Juste, P., and Devillier, P. (1989). Basic pharmacology of kinins: pharmacologic receptors and other mechanisms. *Adv. Exp. Med. Biol.* **247A**, 399-407.

Rousseau, A., Michaud, A., Chauvet, M.T., Lenfant, M., and Corvol, P. (1995). The hemoregulatory peptide N-acetyl-Ser-Asp-Lys-Pro is a natural and specific substrate of the N-terminal active site of human angiotensin-converting enzyme. *J. Biol. Chem.* **270**, 3656-3661.

Ruilope, L.M., Rosei, E.A., Bakris, G.L., Mancia, G., Poulter, N.R., Taddei, S., Unger, T., Volpe, M., Waeber, B., and Zannad, F. (2005). Angiotensin receptor blockers: therapeutic targets and cardiovascular protection. *Blood Press.* **14**, 196-209.

Rushworth, C.A., Guy, J.L., and Turner, A.J. (2008). Residues affecting the chloride regulation and substrate selectivity of the angiotensin-converting enzymes (ACE and ACE2) identified by site-directed mutagenesis. *FEBS J.* **275**, 6033-6042.

Russell, J.T. (1984). Delta pH, H+ diffusion potentials, and Mg2+ ATPase in neurosecretory vesicles isolated from bovine neurohypophyses. *J. Biol. Chem.* **259**, 9496-9507.

J. Sambrook, and D.W. Russel, eds. (2001). Molecular Cloning Volume 1, 3rd edition (Cold Spring Harbor, New York: Cold Spring Harbor Latoratory Press).

Santos, R.A., Simoes e Silva, A.C., Maric, C., Silva, D.M., Machado, R.P., de Buhr, I., Heringer-Walther, S., Pinheiro, S.V., Lopes, M.T., Bader, M., Mendes, E.P., Lemos, V.S., Campagnole-Santos, M.J., Schultheiss, H.P., Speth, R., and Walther, T. (2003). Angiotensin-(1-7) is an endogenous ligand for the G protein-coupled receptor Mas. *Proc. Natl. Acad. Sci. U S A* **100**, 8258-8263.

Saruta, T., Arakawa, K., Iimura, O., Abe, K., Matsuoka, H., Nakano, T., Nakagawa, M., Ogihara, T., Kajiyama, G., Hiwada, K., Fujishima, M., and Nakajima, M. (1999). Difference in the incidence of cough induced by angiotensin converting enzyme inhibitors: a comparative study using imidapril hydrochloride and enalapril maleate. *Hypertens. Res.* **22**, 197-202.

Sasaguri, M., Ideishi, M., Ogata, S., Miura, S., Ikeda, M., and Arakawa, K. (1995). Human urinary kallikrein can generate angiotensin II from homologous renin substrates. *Hypertens. Res.* **18**, 33-37.

Schäfer, M.K., Day, R., Cullinan, W.E., Chrétien, M., Seidah, N.G., and Watson, S.J. (1993). Gene expression of prohormone and proprotein convertases in the rat CNS: a comparative in situ hybridization analysis. *J. Neurosci.* **13**, 1258-1279.

Schechter, I., and Berger, A. (1967). On the size of the active site in proteases. I. Papain. *Biochem. Biophys. Res. Commun.* **27**, 157-162.

Schlegel-Haueter, S., Hore, P., Kerry, K.R., and Semenza, G. (1972). The preparation of lactase and glucoamylase of rat small intestine. *Biochim. Biophys. Acta.* **258**, 506-519.

Schmaier, A.H. (2002). The plasma kallikrein-kinin system counterbalances the renin-angiotensin system. *J. Clin. Invest.* **109**, 1007-1009.

Sealey, J.E., Atlas, S.A., Laragh, J.H., Silverberg, M., and Kaplan, A.P. (1979). Initiation of plasma prorenin activation by Hageman factor-dependent conversion of plasma prekallikrein to kallikrein. *Proc. Natl. Acad. Sci. U S A* **76**, 5914-5918.

Seidah, N.G., Chrétien, M., and Day, R. (1994). The family of subtilisin/kexin like pro-protein and pro-hormone convertases: divergent or shared functions. *Biochimie* **76**, 197-209.

Seidah, N.G., Day, R., Hamelin, J., Gaspar, A., Collard, M.W., and Chrétien, M. (1992). Testicular expression of PC4 in the rat: molecular diversity of a novel germ cell-specific Kex2/subtilisin-like proprotein convertase. *Mol. Endocrinol.* **6**, 1559-1570.

Seidah, N.G., Hamelin, J., Mamarbachi, M., Dong, W., Tardos, H., Mbikay, M., Chretien, M., and Day, R. (1996). cDNA structure, tissue distribution, and chromosomal localization of rat PC7, a novel mammalian proprotein convertase closest to yeast kexin-like proteinases. *Proc. Natl. Acad. Sci. U S A* **93**, 3388-3393.

Semple, P.F. (1995). Putative mechanisms of cough after treatment with angiotensin converting enzyme inhibitors. *J. Hypertens. Suppl.* **13**, S17-S21.

Shanmugam, S., and Sandberg, K. (1996). Ontogeny of angiotensin II receptors. *Cell Biol. Int.* **20**, 169-176.

Sibony, M., Gasc, J.M., Soubrier, F., Alhenc-Gelas, F., and Corvol, P. (1993). Gene expression and tissue localization of the two isoforms of angiotensin I converting enzyme. *Hypertension* **21**, 827-835.

Sjöbring, U., Mecklenburg, M., Andersen, A.B., and Miörner, H. (1990). Polymerase chain reaction for detection of Mycobacterium tuberculosis. *J. Clin. Microbiol.* **28**, 2200-2204.

Skeggs, L.T., Kahn, J.R., and Shumway, N.P. (1956). The preparation and function of the hypertensin-converting enzyme. *J. Exp. Med.* **103**, 295-299.

Skeggs, L.T., Marsh, W.H., Kahn, J.R., and Shumway, N.P. (1954). The purification of hypertensin I. *J. Exp. Med.* **100**, 363-370.

Skidgel, R.A., and Erdös, E.G. (1985). Novel activity of human angiotensin I converting enzyme: release of the NH2- and COOH-terminal tripeptides from the luteinizing hormone-releasing hormone. *Proc. Natl. Acad. Sci. U S A* **82**, 1025-1029.

Skirgello, O.E., Binevski, P.V., Pozdnev, V.F., and Kost, O.A. (2005). Kinetic probes for inter-domain co-operation in human somatic angiotensin-converting enzyme. *Biochem. J.* **391**, 641-647.

Skovbjerg, H., Sjöström, H., and Norén, O. (1981). Purification and characterisation of amphiphilic lactase/phlorizin hydrolase from human small intestine. *Eur. J. Biochem.* **114**, 653-661.

Sleight, P. (2002). The renin-angiotensin system: a review of trials with angiotensin-converting enzyme inhibitors and angiotensin receptor blocking agents. *Eur. Heart J.* **4**, (Suppl. A), A53-(Suppl. A), A57.

Song, L., and Fricker, L.D. (1995). Purification and characterization of carboxypeptidase D, a novel carboxypeptidase E-like enzyme, from bovine pituitary. *J. Biol. Chem.* **270**, 25007-25013.

Song, L., and Fricker, L.D. (1996). Tissue distribution and characterization of soluble and membrane-bound forms of metallocarboxypeptidase D. *J. Biol. Chem.* **271**, 28884-28889.

Soubrier, F., Alhenc-Gelas, F., Hubert, C., Allegrini, J., John, M., Tregear, G., and Corvol, P. (1988). Two putative active centers in human angiotensin I-converting enzyme revealed by molecular cloning. *Proc. Natl. Acad. Sci. U S A* **85**, 9386-9390.

Stefan, R.I., Aboul-Enein, H.Y., and Radu, G.L. (1998). Biosensors for the enantioselective analysis of S-enalapril and S-ramipril. *Prep. Biochem. Biotechnol.* **28**, 305-312.

Steiner, D.F. (1991). In Peptide Biosynthesis and Processing, L.D. Fricker, eds. (CRC Press).

Steitz, T.A., Ludwig, M.L., Quiocho, F.A., and Lipscomb, W.N. (1967). The structure of carboxypeptidase A. V. Studies of enzyme-substrate and enzyme-inhibitor complexes at 6 Å resoultion. *J. Biol. Chem.* **242**, 4662-4668.

Strittmatter, S.M., Lo, M.M., Javitch, J.A., and Snyder, S.H. (1984). Autoradiographic visualization of angiotensin-converting enzyme in rat brain with [3H]captopril: localization to a striatonigral pathway. *Proc. Natl. Acad. Sci. U S A* **81**, 1599-1603.

Suzuki, K., Shimoi, H., Iwasaki, Y., Kawahara, T., Matsuura, Y., and Nishikawa, Y. (1990). Elucidation of amidating reaction mechanism by frog amidating enzyme, peptidylglycine alpha-hydroxylating monooxygenase, expressed in insect cell culture. *EMBO J.* **9**, 4259-4265.

Swanson, G.N., Hanesworth, J.M., Sardinia, M.F., Coleman, J.K., Wright, J.W., Hall, K.L., Miller-Wing, A.V., Stobb, J.W., Cook, V.I., and Harding, E.C. (1992). Discovery of a distinct binding site for angiotensin II (3-8), a putative angiotensin IV receptor. *Regul. Pept.* **40**, 409-419.

Takada, Y., Hiwada, K., Akutsu, H., Hashimoto, A., and Kokubu, T. (1984). The immunocytochemical detection of angiotensin-converting enzyme in alveolar macrophages from patients with sarcoidosis. *Lung* **162**, 317-323.

Tan, F., Rehli, M., Krause, S.W., and Skidgel, R.A. (1997). Sequence of human carboxypeptidase D reveals it to be a member of the regulatory carboxypeptidase family with three tandem active site domains. *Biochem. J.* **327** (Pt 1), 81-87.

Tian, B., Meng, Q.C., Chen, Y.F., Krege, J.H., Smithies, O., and Oparil, S. (1997). Blood pressures and cardiovascular homeostasis in mice having reduced or absent angiotensin-converting enzyme gene function. *Hypertension* **30**, 128-133.

Timmermans, P.B., Benfield, P., Chiu, A.T., Herblin, W.F., Wong, P.C., and Smith, R.D. (1992). Angiotensin II receptors and functional correlates. *Am. J. Hypertens.* **5**, 221S-235S.

Timmermans, P.B., Wong, P.C., Chiu, A.T., Herblin, W.F., Benfield, P., Carini, D.J., Lee, R.J., Wexler, R.R., Saye, J.A., and Smith, R.D. (1993). Angiotensin II receptors and angiotensin II receptor antagonists. *Pharmacol. Rev.* **45**, 205-251.

Tsuchida, S., Matsusaka, T., Chen, X., Okubo, S., Niimura, F., Nishimura, H., Fogo, A., Utsunomiya, H., Inagami, T., and Ichikawa, I. (1998). Murine double nullizygotes of the angiotensin type 1A and 1B receptor genes duplicate severe abnormal phenotypes of angiotensinogen nullizygotes. *J. Clin. Invest.* **101**, 755-760.

Tumanan-Mendoza, B.A., Dans, A.L., Villacin, L.L., Mendoza, V.L., Rellama-Black, S., Bartolome, M., Ragual, J., Flor, B., and Valdez, J. (2007). Dechallenge and rechallenge method showed different incidences of cough among four ACE-Is. *J. Clin. Epidemiol.* **60**, 547-553.

Turner, A.J., Tipnis, S.R., Guy, J.L., Rice, G., and Hooper, N.M. (2002). ACEH/ACE2 is a novel mammalian metallocarboxypeptidase and a homologue of angiotensin-converting enzyme insensitive to ACE inhibitors. *Can J. Physiol. Pharmacol.* **80**, 346-353.

Tzakos, A.G., and Gerothanassis, I.P. (2005). Domain-selective ligand-binding modes and atomic level pharmacophore refinement in angiotensin I converting enzyme (ACE) inhibitors. *Chembiochem* **6**, 1089-1103.

Tzakos, A.G., Galanis, A.S., Spyroulias, G.A., Cordopatis, P., Manessi-Zoupa, E., and Gerothanassis, I.P. (2003). Structure-function discrimination of the N- and C- catalytic domains of human angiotensin-converting enzyme: implications for Cl- activation and peptide hydrolysis mechanisms. *Protein Eng.* **16**, 993-1003.

van Esch, J.H., Tom, B., Dive, V., Batenburg, W.W., Georgiadis, D., Yiotakis, A., van Gool, J.M., de Bruijn, R.J., de Vries, R., and Danser, A.H. (2005). Selective angiotensin-converting enzyme C-domain inhibition is sufficient to prevent angiotensin I-induced vasoconstriction. *Hypertension* **45**, 120-125.

Voronov, S., Zueva, N., Orlov, V., Arutyunyan, A., and Kost, O. (2002). Temperature-induced selective death of the C-domain within angiotensin-converting enzyme molecule. *FEBS Lett.* **522**, 77-82.

Waeber, B., Gavras, I., Brunner, H.R., Cook, C.A., Charocopos, F., and Gavras, H.P. (1982). Prediction of sustained antihypertensive efficacy of chronic captopril therapy: relationships to immediate blood pressure response and control plasma renin activity. *Am. Heart. J.* **103**, 384-390.

Wang, H., Liu, Y., Chen, Y., Robinson, H., and Ke, H. (2005). Multiple elements jointly determine inhibitor selectivity of cyclic nucleotide phosphodiesterases 4 and 7. *J. Biol. Chem.* **280**, 30949-30955.

Watermeyer, J.M. (2008). PhD Thesis Title: Structural Determinants of the Domain-Selectivity of Novel Inhibitors of Human Testis Angiotensin-Converting Enzyme (University of Cape Town, South Africa).

Watermeyer, J.M., Kröger, W.L., O'Neill, H.G., Sewell, B.T., and Sturrock, E.D. (2008). Probing the basis of domain-dependent inhibition using novel ketone inhibitors of Angiotensin-converting enzyme. *Biochemistry* **47**, 5942-5950.

Weare, J.A., Stewart, T.A., Gafford, J.T., and Erdös, E.G. (1981). Inhibition of human converting enzyme in vitro by a novel tripeptide analog. *Hypertension* **3**, I50-I53.

Wei, L., Alhenc-Gelas, F., Corvol, P., and Clauser, E. (1991). The two homologous domains of human angiotensin I-converting enzyme are both catalytically active. *J. Biol. Chem.* **266**, 9002-9008.

Wei, L., Clauser, E., Alhenc-Gelas, F., and Corvol, P. (1992). The two homologous domains of human angiotensin I-converting enzyme interact differently with competitive inhibitors. *J. Biol. Chem.* **267**, 13398-13405.

Williams, T.A., Corvol, P., and Soubrier, F. (1994). Identification of two active site residues in human angiotensin I-converting enzyme. *J. Biol. Chem.* **269**, 29430-29434.

Wood, J.M., Maibaum, J., Rahuel, J., Grütter, M.G., Cohen, N.C., Rasetti, V., Rüger, H., Göschke, R., Stutz, S., Fuhrer, W., Schilling, W., Rigollier, P., Yamaguchi, Y., Cumin, F., Baum, H.P., Schnell, C.R., Herold, P., Mah, R., Jensen, C., O'Brien, E., Stanton, A., and Bedigian, M.P. (2003). Structure-based design of aliskiren, a novel orally effective renin inhibitor. *Biochem. Biophys. Res. Commun.* **308**, 698-705.

Woodman, Z.L., Oppong, S.Y., Cook, S., Hooper, N.M., Schwager, S.L., Brandt, W.F., Ehlers, M.R., and Sturrock, E.D. (2000). Shedding of somatic angiotensin-converting enzyme (ACE) is inefficient compared with testis ACE despite cleavage at identical stalk sites. *Biochem. J.* **347 (**Pt 3), 711-718.

Woodman, Z.L., Schwager, S.L., Redelinghuys, P., Carmona, A.K., Ehlers, M.R., and Sturrock, E.D. (2005). The N domain of somatic angiotensin-converting enzyme negatively regulates ectodomain shedding and catalytic activity. *Biochem. J.* **389**, 739-744.

Woodman, Z.L., Schwager, S.L., Redelinghuys, P., Chubb, A.J., van der Merwe, E.L., Ehlers, M.R., and Sturrock, E.D. (2006). Homologous substitution of ACE C-domain regions with N-domain sequences: effect on processing, shedding, and catalytic properties. *Biol. Chem.* **387**, 1043-1051.

Wright, J.W., and Harding, J.W. (1997). Important role for angiotensin III and IV in the brain renin-angiotensin system. *Brain Res. Brain Res. Rev.* **25**, 96-124.

Xiao, H.D., Fuchs, S., Cole, J.M., Disher, K.M., Sutliff, R.L., and Bernstein, K.E. (2003). Role of bradykinin in angiotensin-converting enzyme knockout mice. *Am. J. Physiol. Heart Circ. Physiol.* **284**, H1969-H1977.

Yamaguchi, T., Carretero, O.A., and Scicli, A.G. (1991). A novel serine protease with vasoconstrictor activity coded by the kallikrein gene S3. *J. Biol. Chem.* **266**, 5011-5017.

Yanai, K., Saito, T., Kakinuma, Y., Kon, Y., Hirota, K., Taniguchi-Yanai, K., Nishijo, N., Shigematsu, Y., Horiguchi, H., Kasuya, Y., Sugiyama, F., Yagami, K., Murakami, K., and Fukamizu, A. (2000). Renin-dependent cardiovascular functions and renin-independent blood-brain barrier functions revealed by renin-deficient mice. *J. Biol. Chem.* **275**, 5-8.

Yang, H.Y., Erdös, E.G., and Levin, Y. (1970). A dipeptidyl carboxypeptidase that converts angiotensin I and inactivates bradykinin. *Biochim Biophys Acta* **214**, 374-376.

Yang, H.Y., Erdös, E.G., and Levin, Y. (1971). Characterization of a dipeptide hydrolase (kininase II: angiotensin I converting enzyme). *J. Pharmacol. Exp. Ther.* **177**, 291-300.

Yang, X.P., Liu, Y.H., Scicli, G.M., Webb, C.R., and Carretero, O.A. (1997). Role of kinins in the cardioprotective effect of preconditioning: study of myocardial ischemia/reperfusion injury in B2 kinin receptor knockout mice and kininogen-deficient rats. *Hypertension* **30**, 735-740.

Yaron, A., Carmel, A., and Katchalski-Katzir, E. (1979). Intramolecularly quenched fluorogenic substrates for hydrolytic enzymes. *Anal. Biochem.* **95**, 228-235.

Yu, X.C., Sturrock, E.D., Wu, Z., Biemann, K., Ehlers, M.R., and Riordan, J.F. (1997). Identification of N-linked glycosylation sites in human testis angiotensin-converting enzyme and expression of an active deglycosylated form. *J. Biol. Chem.* **272**, 3511-3519.

Zaman, M.A., Oparil, S., and Calhoun, D.A. (2002). Drugs targeting the renin-angiotensin-aldosterone system. *Nat. Rev. Drug Discov.* **1**, 621-636.

Zecca, L., Mesonero, J.E., Stutz, A., Poirée, J.C., Giudicelli, J., Cursio, R., Gloor, S.M., and Semenza, G. (1998). Intestinal lactase-phlorizin hydrolase (LPH): the two catalytic sites; the role of the pancreas in pro-LPH maturation. *FEBS Lett.* **435**, 225-228.

Zheng, M., Streck, R.D., Scott, R.E., Seidah, N.G., and Pintar, J.E. (1994). The developmental expression in rat of proteases furin, PC1, PC2, and carboxypeptidase E: implications for early maturation of proteolytic processing capacity. *J. Neurosci.* **14**, 4656-4673.